AD-A154 685 THE DEVELOPMENT AND EVALUATION OF POINT DEFECT MODELS FOR THE GROWTH OF P.. (U) OHIO STATE UNIV COLUMBUS FONTANA CORROSION CENTER D D MACDONALD ET AL. 1/2

UNCLASSIFIED 30 APR 85 FCC-4445-4 N00014-82-K-0265 F/G 20/2 NL

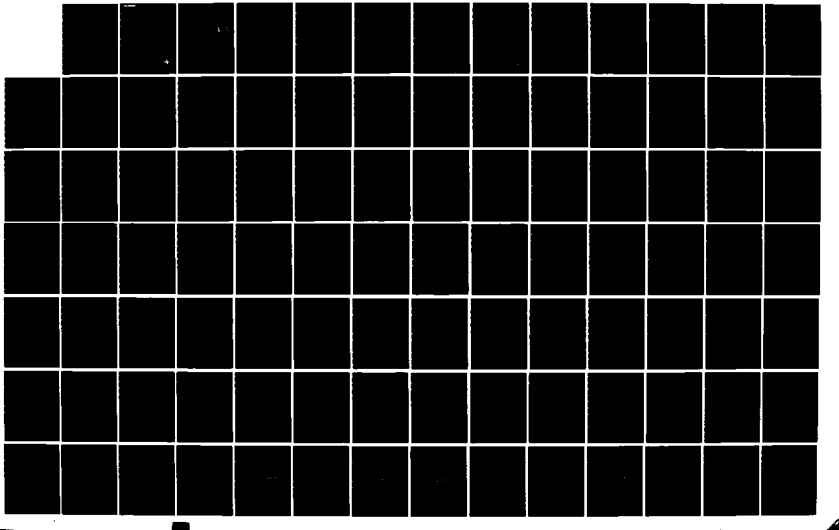

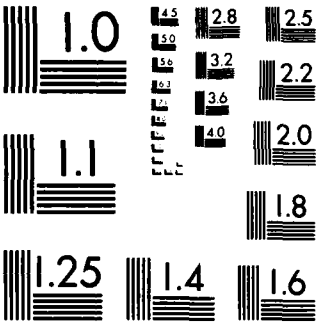

FCC 8505-4
FINAL REPORT
APRIL 30, 1985

THE DEVELOPMENT AND EVALUATION OF POINT DEFECT MODELS FOR THE GROWTH OF PASSIVE FILMS ON SINGLE CRYSTAL, POLYCRYSTALLINE, AND AMORPHOUS METAL SURFACES

OFFICE OF NAVAL RESEARCH
CONTRACT N00014-82-K-0255

D.D. MACDONALD
S.S. POWER
P. MORRISON
B.E. WILDE

The Ohio State University
Columbus, Ohio
FONTANA CORROSION CENTER

SECURITY CLASSIFICATION OF THIS PAGE AD-A154 625

REPORT DOCUMENTATION PAGE

1a. REPORT SECURITY CLASSIFICATION: Unclassified	1b. RESTRICTIVE MARKINGS
2a. SECURITY CLASSIFICATION AUTHORITY	3. DISTRIBUTION/AVAILABILITY OF REPORT: Approved for public release: distribution unlimited
2b. DECLASSIFICATION/DOWNGRADING SCHEDULE	
4. PERFORMING ORGANIZATION REPORT NUMBER(S): OSURF MPN 763048/714445	5. MONITORING ORGANIZATION REPORT NUMBER(S)
6a. NAME OF PERFORMING ORGANIZATION: The Ohio State University Research Foundation; 6b. OFFICE SYMBOL (If applicable): OSURF	7a. NAME OF MONITORING ORGANIZATION
6c. ADDRESS (City, State and ZIP Code): 1314 Kinnear Road, Columbus, OH 43212	7b. ADDRESS (City, State and ZIP Code)
8a. NAME OF FUNDING/SPONSORING ORGANIZATION: Office of Naval Research; 8b. OFFICE SYMBOL (If applicable): ONR	9. PROCUREMENT INSTRUMENT IDENTIFICATION NUMBER: N00014-82-K-0265 A
8c. ADDRESS (City, State and ZIP Code): Engineering Sciences Directorate, Materials Division, 800 N. Quincy St., Arlington, VA 22217	10. SOURCE OF FUNDING NOS.
11. TITLE (Include Security Classification): *	PROGRAM ELEMENT NO.: — ; PROJECT NO.: NR036-156/ 12-23-81 (430) ; TASK NO.: — ; WORK UNIT NO.: —

DTIC ELECTE JUN 10 1985 D

12. PERSONAL AUTHOR(S): D.D. Macdonald, M. Urquidi, B.W. Wilde

13a. TYPE OF REPORT	13b. TIME COVERED	14. DATE OF REPORT (Yr., Mo., Day)	15. PAGE COUNT
Final-Technical	FROM 82Mar01 TO 85Apr30	85 April 30	102

16. SUPPLEMENTARY NOTATION: (Fr-p iii)

17 COSATI CODES			18. SUBJECT TERMS (Continue on reverse if necessary and identify by block number)
FIELD	GROUP	SUB. GR.	Pitting potentials, passivity, single crystal nickel, polycrystalline nickel, point defect model, space-charge.

19. ABSTRACT (Continue on reverse if necessary and identify by block number)

*THE DEVELOPMENT AND EVALUATION OF POINT DEFECT MODELS FOR THE GROWTH OF PASSIVE FILMS ON SINGLE CRYSTAL, POLYCRYSTALLINE, AND AMORPHOUS METAL SURFACES

The principal task of this program was to develop a better understanding of:

i) the mechanisms of the growth of passive films on metal surfaces,
ii) the role of space charge in determining the properties of the film,
and iii) passivity breakdown phenomena.

Experimental data for the ac impedance and passivity breakdown properties of passive films on nickel are presented in Sections 2 and 3. Also a theoretical development of the point defect model is presented in Section 4. A comparison between the theoretical and experimental data for the growth of passive films on nickel and iron is included. In addition, the role of minor alloying elements (such as molybdenum) on pitting and passivity breakdown is considered theoretically, and the model is compared with (cont.

20 DISTRIBUTION/AVAILABILITY OF ABSTRACT	21. ABSTRACT SECURITY CLASSIFICATION	
UNCLASSIFIED/UNLIMITED ☒ SAME AS RPT ☐ DTIC USERS ☐	Unclassified	
22a. NAME OF RESPONSIBLE INDIVIDUA	22b. TELEPHONE NUMBER (Include Area Code)	22c. OFFICE SYMBOL

DD FORM 1473, 83 APR EDITION OF 1 JAN 73 IS OBSOLETE

SECURITY CLASSIFICATION OF THIS PAGE

19.
experimental data for 18% Cr ferritic stainless steel.

The results of this study indicate that the point defect model, although at present in a crude state of development, is a reasonable first-approximation theory for explaining some of the basic phenomena related to the growth and breakdown of anodic passive films on metal surfaces. On the basis of data developed in this program, it is recommended that further experiments be conducted to further refine the model.

REPORT DISTRIBUTION

Scientific Officer (Code N00014)

ACO (Code N66015)

Director, Naval Research Laboratory (Code N00173)

Defense Technical Information Center (Code S47031)

Office of Naval Research Branch Office (Code N62880)

SUPPLEMENTAL DISTRIBUTION (036 Contractors)

Prof. I.M. Bernstein
Dept. of Metallurgy and Materials Science
Carnegie-Mellon University
Pittsburgh, PA 15213

Prof. H.K. Birnbaum
Dept. of Metallurgy and Mining Engineering
University of Illinois
Urbana, IL 61801

Dr. D.H. Boone
Department of Mechanical Engineering
Naval Postgraduate School
Monterey, CA 93943

Dr. C.R. Clayton
Department of Materials Science and Engineering
State University of New York
Stony Brook
Long Island, NY 11794

Dr. C.R. Crowe
Code 6372
Naval Research Laboratory
Washington, D.C. 20375

Prof. D.J. Duquette
Dept. of Metallurgical Engineering
Rensselaer Polytechnic Inst.
Troy NY 12181

Prof. J.P. Hirth
Dept. of Metallurgical Engineering
The Ohio State University
116 West 19th Avenue
Columbus, OH 43210

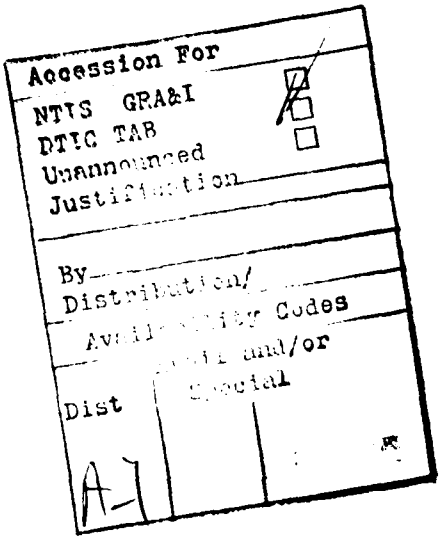

Dr. R.G. Kasper
Code 4493
Naval Underwater Systems Center
New London, CT 06320

Prof. H. Leidheiser, Jr.
Center for Coatings and Surface Research
Sinclair Laboratory, Bldg. No. 7
Lehigh University
Bethlehem, PA 18015

Dr. F. Mansfeld
Rockwell International-Science Center
1049 Camino Dos Rios
P.O. Box 1085
Thousand Oaks, CA 91360

Profs. G.H. Meir and F.S. Pettit
Dept. of Metallurgical and Materials Engineering
University of Pittsburgh
Pittsburgh, PA 15261

Dr. J.R. Pickens
Martin Marietta Laboratories
1450 South Rolling Road
Baltimore, MD 21227-3898

Prof. H.W. Pickering
Dept. of Materials Science and Engineering
The Pennsylvania State University
University Park, PA 16802

Prof. R. Summit
Dept. of Metallurgy Mechanics and Materials Science
Michigan State University
East Lansing, MI 48824

Prof. R.P. Wei
Dept. of Mechanical Engineering and Mechanics
Lehigh University
Bethlemen, PA 18015

Prof. A.J. Ardell
Dept. of Materials Science and Engineering
School of Engineering and Applied Sciences
University of California at Los Angeles
Los Angeles, CA 90024

Prof. B.E. Wilde
Fontana Corrosion Center
Department of Metallurgical Engineering
The Ohio State University
116 West 19th Avenue
Columbus, Ohio 43210

THE DEVELOPMENT AND EVALUATION OF POINT DEFECT MODELS FOR THE GROWTH OF PASSIVE FILMS ON SINGLE CRYSTAL, POLYCRYSTALLINE, AND AMORPHOUS METAL SURFACES

Final Report

Office of Naval Research
Contract N00014-82-K-0265

Principal Investigators:

D.D. Macdonald, March 1, 1982 - March 31, 1984
B.E. Wilde (Administrative), April 1, 1984 - April 30, 1985

Fontana Corrosion Center
Department of Metallurgical Engineering
The Ohio State University
116 West 19th Avenue
Columbus, Ohio 43210

ABSTRACT

The principal task of this program was to develop a better understanding of:

i) the mechanisms of the growth of passive films on metal surfaces,

ii) the role of space charge in determining the properties of the film, and

iii) passivity breakdown phenomena.

Experimental data for the ac impedance and passivity breakdown properties of passive films on nickel are presented in Sections 2 and 3. Also a theoretical development of the point defect model is presented in Section 4. A comparison between the theoretical and experimental data for the growth of passive films on nickel and iron is included. In addition, the role of minor alloying elements (such as molybdenum) on pitting and passivity breakdown is considered theoretically, and the model is compared with experimental data for 18% Cr ferritic stainless steel.

The results of this study indicate that the point defect model although at present in a crude state of development, is a reasonable first-approximation theory for explaining some of the basic phenomena related to the growth and breakdown of anodic passive films on metal surfaces. On the basis of data developed in this program it is recommended that further experiments be conducted to further refine the model.

FORWARD

The following personnel have technically contributed to the completion of this project:

Dr. D. D. Macdonald
Dr. Bruce Pound
K.S. Lei*
Mirna Urquidi
J.D. Willis

Dr. B. E. Wilde has administered the program for the final 12 month phase.

* The data developed on this project will be used for a thesis for partial fulfillment of the requirements for a Ph.D. degree in Summer 1985.

TABLE OF CONTENTS

	Page
Abstract	iii
Forward	v
Table of Contents	vii
List of Figures	ix
List of Tables	xiii
Section 1 Introduction	1
Section 2	2
Analysis	3
Discussion	3
Summary	11
Section 3	12
General Objective	12
Previous Work	12
Results and Discussion	14
Summary	28
Section 4	30
4.1 First Order Point Defect Model	30
Introduction	30
Assumption	30
Solution of Diffusion Equations	36
Results	41
Sensitivity Study	50
Kinetics of Film Growth	53
Logarithmic Law	57
Inverse Logarithmic Law	57
Discussion	59

		Page
4.2	Role of Space Charge in Passive Films	62
	Introduction	62
	Numerical Analysis	64
	Results	69
	Sensitivity Study	72
	Discussion	81
4.3	Breakdown of Passive Films	82
	Introduction	82
	Theoretical Basis	83
	Solute/Vacancy Interaction Model	86
	Results and Discussion	89
References		96
Appendix		98

LIST OF FIGURES

Figure No.		Page
1	Nyquist plot of impedance data for single crystal nickel in phosphate solution. E = 0.3V(SCE), pH = 9	5
2	Nyquist plot of impedance data for single crystal nickel in phosphate solution. E = 0.1V(SCE), pH = 10	6
3	Nyquist plot of impedence data for single crystal nickel in phosphate solution. E = 0.2V(SCE), pH = 11	7
4	Nyquist plot of impedance data for single crystal nickel in phosphate solution. E = 0.4V(SCE), pH = 11	8
5	Experimental set-up for pitting corrosion studies.	13
6	Shield design for reducing crevice corrosion.	15
7	(a) Potential-time profile in film breakdown studies, (b) Current-potential curve in film breakdown studies.	16
8	(a) Potential-time profile in induction time studies, (b) Current-time curve in induction time studies.	17
9	Comparison of film breakdown potential experiments for films grown in chloride-containing and chloride-free solutions.	18
10	The current-potential curves in buffered borate solution with 0.2N chloride concentration at different sweep rates.	20
11	The effect of sweep rate on the film breakdown potential of pure nickel (100).	21
12a	Relation between the critical pitting potential and the chloride concentration.	23
12b	Plot of the logarithm of induction time (lot t) versus the inverse of overpotential (1/ΔV).	24
12c	Plot of the logarithm of induction time (lot t) versus overpotential (ΔV) according to the point defect model.	25
13	Schematic of the working and reference electrodes in a typical electrochemical cell (upper figure) and the corresponding potential-distance relationships (lower figure).	33
14	Film thickness as a function of external potential for the passive film on iron in borate buffer solution. Film thickness calculated after one hour of polarization.	43

Figure No.		Page
15	Theoretical growth of the passive film Fe_2O_3 as a function of time, for iron in borate buffer solution. Condition as in Figure 14.	45
16	Concentration of oxygen vacancies at the metal/film interface as a function of film thickness according to the first order point defect model. The calculations are for an Fe_2O_3 film on iron in borate buffer solution under the condition stated in Figure 14.	46
17	Theoretical and experimental data for the growth of passive films on nickel in 0.1 N $Na_2H_2PO_4$ (pH = 4.85) solution at 25°C and at an applied voltage of 1.24 (V vs SCE).	49
18	Variation of film thickness and oxygen ion vacancy concentration as a function of time, for different values of the vacancy diffusion coefficient.	51
19	Calculated thickness of the passive film on nickel as a function of the diffusion coefficient. Polarization time = 30 min, other parameters as indicated in the text.	52
20	Calculated film thickness for $Ni(OH)_2$ on nickel as a function of time, for different values of concentration of vacancies at the metal/film interface other parameters as indicated in the text.	54
21	Schematic film thickness versus time, as predicted by the first order point defect model [Equation (22)].	56
22	Schematic of film thickness versus time, as predicted by the l arithmic growth law.	58
23	Schematic of thickness versus time, as predicted by the inverse rithmic growth law.	60
24	Calculated electric field strength vs film thickness. Note that the poionts designated D obey the electro-neutrality condition.	70
25	Potential function $\Delta\phi(x)$ vs film thickness. Note that the points designed D obey the electro-neutrality condition.	71
26	Calculated electric field strength versus film thickness. Increasing deviation from electrical neutrality ● < ○ < □.	73

the increase in the measured capacitance with potential probably arises from a corresponding increase in the space charge capacitance of the p-type β-$Ni(OH)_2$. Nevertheless, a typical double layer capacitance also exhibits a potential-dependence, and part of the observed increase in C_p may reflect this factor. In addition, the relative contribution of the double layer capacitance to the measured capacitance could well increase at higher potentials where the space charge capacitance is larger.

Summary

Impedance data for single crystal nickel in phosphate solutions have been analyzed in terms of an equivalent circuit model to provide a parallel capacitance, charge transfer resistance, and Warburg coefficient, σ. The value of σ was found to be independent of potential within experimental error at pH values of 9, 11, and 12. At other values of pH in the range studied (7 to 12), the lack of a true steady state for film growth and a non-uniform composition of the film may have been the cause for relatively large changes in σ with potential.

The presence of a large charge transfer resistance indicates that the thickness of the surface film is small enough to allow both an interfacial electrochemical reaction and solid state mass transport processes to control the film growth kinetics.

The capacitance appears to originate largely from the double layer in solution, although the space charge layer in the β-$Ni(OH)_2$ film might provide an important contribution depending on the potential.

case, a rotating ring disk electrode study (12) of nickel has shown that, despite the predicted thermodynamic stability of the $Ni(OH)_3^-$ ion, there is no significant dissolution of the electrode. Nevertheless, significant dissolution at pH values of 7, and possibly 8, may substantially reduce the influence of solid state mass transport in controlling the overall rate of film growth.

It is difficult to determine the extent to which the lack of a true steady state and a non-uniform composition affect the film growth kinetics, particularly solid state mass transport processes. Nevertheless, based on the drift in the "steady-state" current, the overall uncertainty in R_t and σ is estimated to be ±5%. It is of significance to the point defect model that, when this uncertainty is taken into account, σ is found to be approximately constant for several pH values.

The presence of a large charge transfer resistance indicates that the rate of film growth is partly controlled by an interfacial electrochemical reaction. At this stage, it is possible to only speculate whether this reaction occurs at the metal/film or film/solution interface. Although it appears from Table 1, that R_t does not exhibit a well-defined dependence on pH, there is some evidence from another study (8) that the rate-determining reaction may occur at the film/solution interface.

Clearly, the film does not become sufficiently thick to allow solid state mass transport processes to dominate control of the film growth rate. This is consistent with previous work (9) which has shown that the thickness of films grown potentiostatically, or galvanostatically, on nickel is usually less than several hundred Angstroms.

The capacitance measured for $Ni(OH)_2$ films in phosphate solutions appears to mainly involve the space charge layer. Nevertheless, the double layer would be expected to provide some contribution to the capacitance. Normally, the space charge capacitance is smaller than the double layer capacitance, and so dominates the overall capacitance (10). However, the Mott-Schottky relationship for a p-type semi-conductor predicts that the space charge capacitance increases as the potential is made more positive. Accordingly,

work, I_{dc} was found to be in general independent of potential within experimental error. In addition, the analysis of the impedance data showed that σ was independent of potential within experimental error for several pH values.

The uncertainty in both σ and R_t arises from several sources. The only direct contribution is from the calculation of these parameters which are obtained essentially as best-fit values and accordingly, have a given error for each set of impedance data.

Various other factors contribute indirectly to the uncertainty. The major one is the difficulty in attaining a true steady state for the growth of the films and this may have been at least partly responsible for the larger variation in σ with potential for pH values of 7, 8, and 10. Although the impedance measurements were commenced when the rate of change of the dc current was negligible, the dc "steady state" current (typically 0.5 $\mu A/cm^2$) generally showed some decrease over extended times. Usually, this decrease was only 0.1-0.2 $\mu A/cm^2$ but it did indicate an inherent problem in measuring the impedance of a film at various potentials when the film thickness is not in a true steady state.

A further factor is the nature and composition of the film formed at each potential and pH. It was found in previous work (4) that a partially dehydrated film is formed on nickel in a Na_2HPO_4 solution at pH=9.1. This film is unlikely to be uniform in composition, but probably becomes more hydrated towards the film/solution interface. Such a change in the composition would be expected to affect the diffusion characteristics of the film, thereby resulting in a poorly-defined diffusion coefficient for the mobile species. In addition, the degree of hydration of the film may well vary quite significantly over the pH range studied.

The final aspect to be considered is the solubility of the surface film. Previously published thermodynamic data (11) for the nickel/water system at 25°C show that at a pH slightly greater than 8, $Ni(OH)_2$ is in equilibrium with dissolved Ni^{2+} at an activity of 10^{-6} mol kg^{-1}. Similarly, at a pH of approximately 12.5, $Ni(OH)_2$ and $Ni(OH)_3^-$ are in equilibrium. However, in this

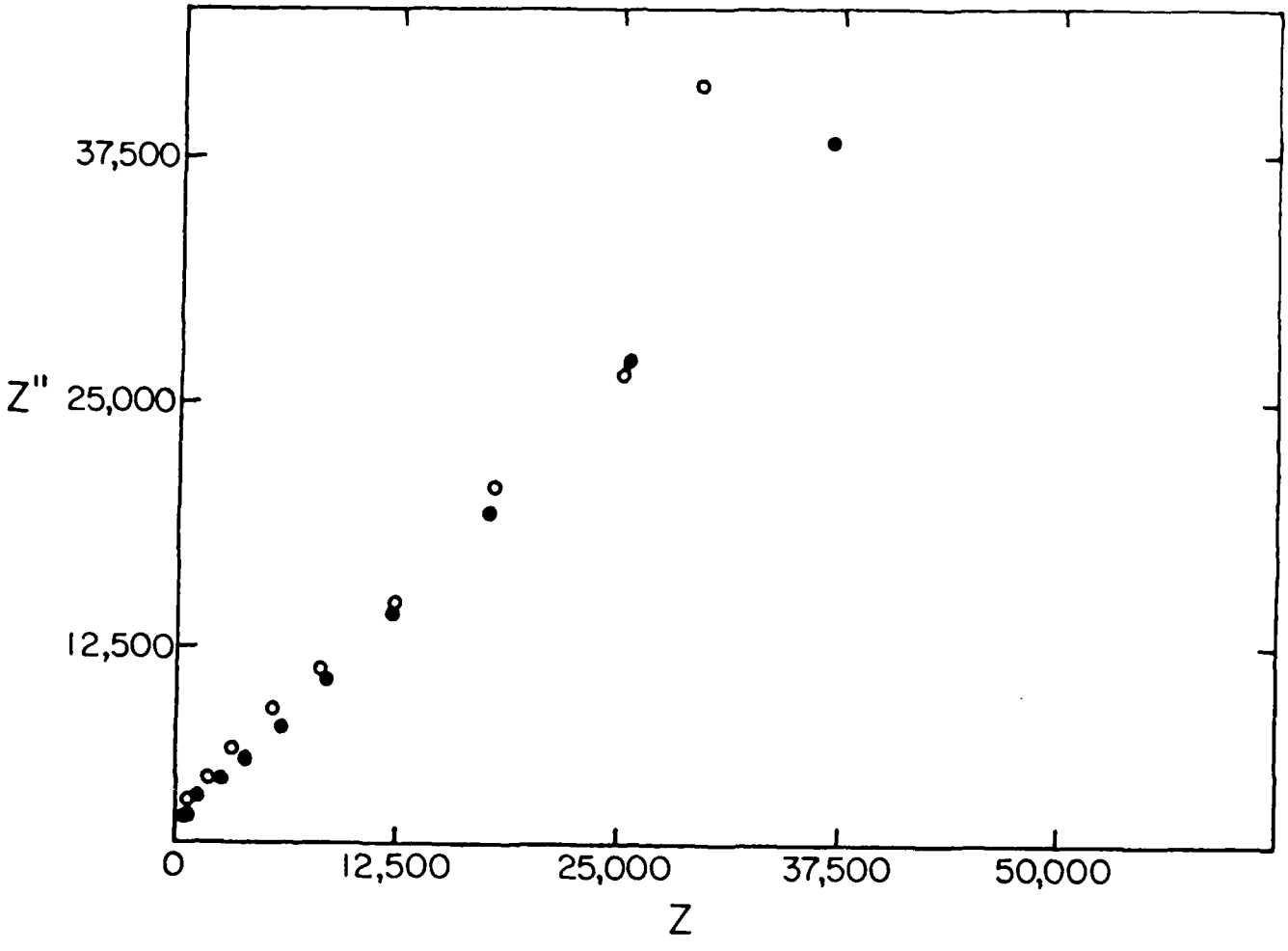

Figure 4. Nyquist plot of impedance data for single crystal nickel in phosphate solution. E = 0.4V(SCE), pH = 11

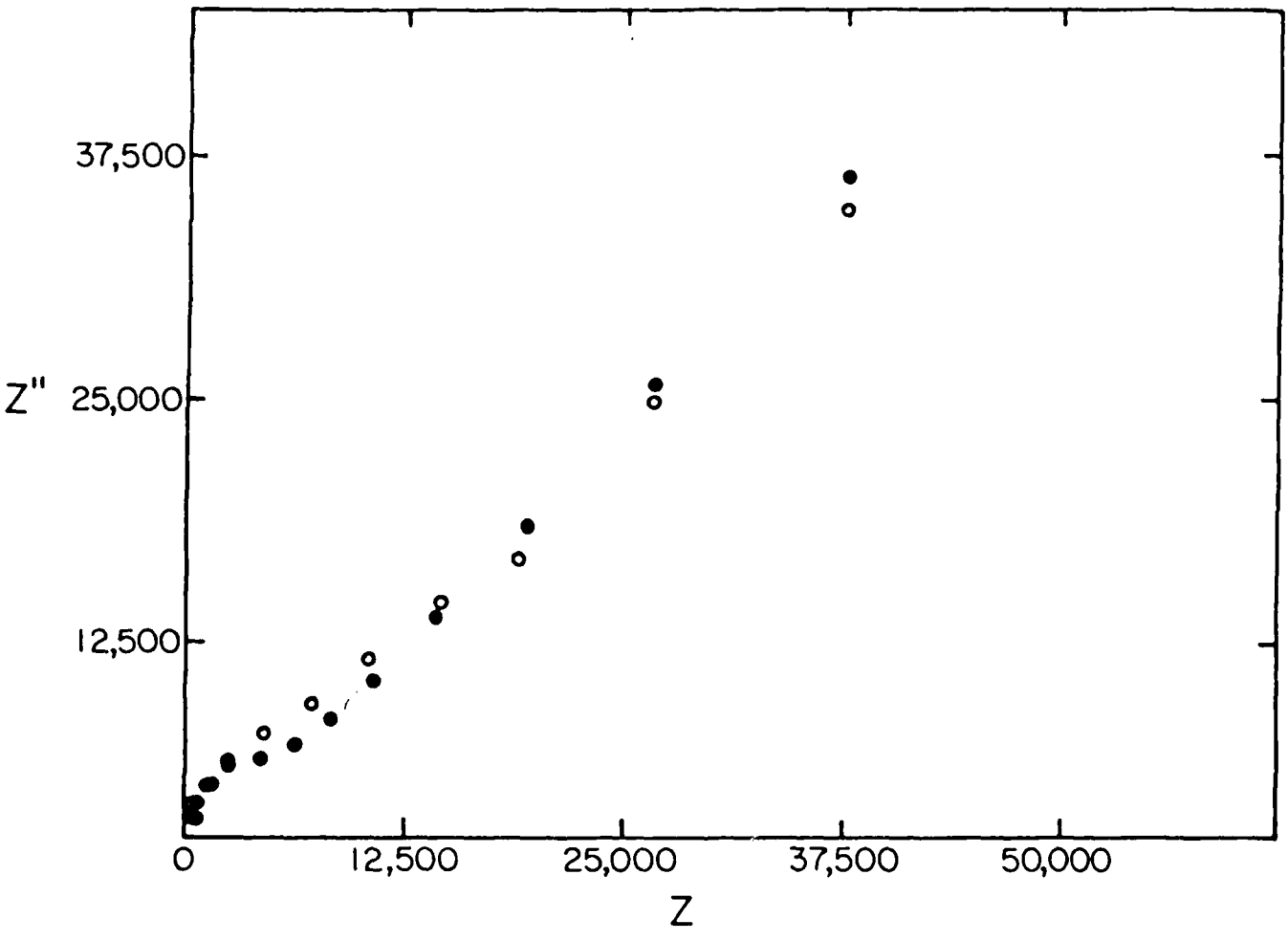

Figure 3. Nyquist plot of impedence data for single crystal nickel in phosphate solution. E = 0.2V(SCE), pH = 11

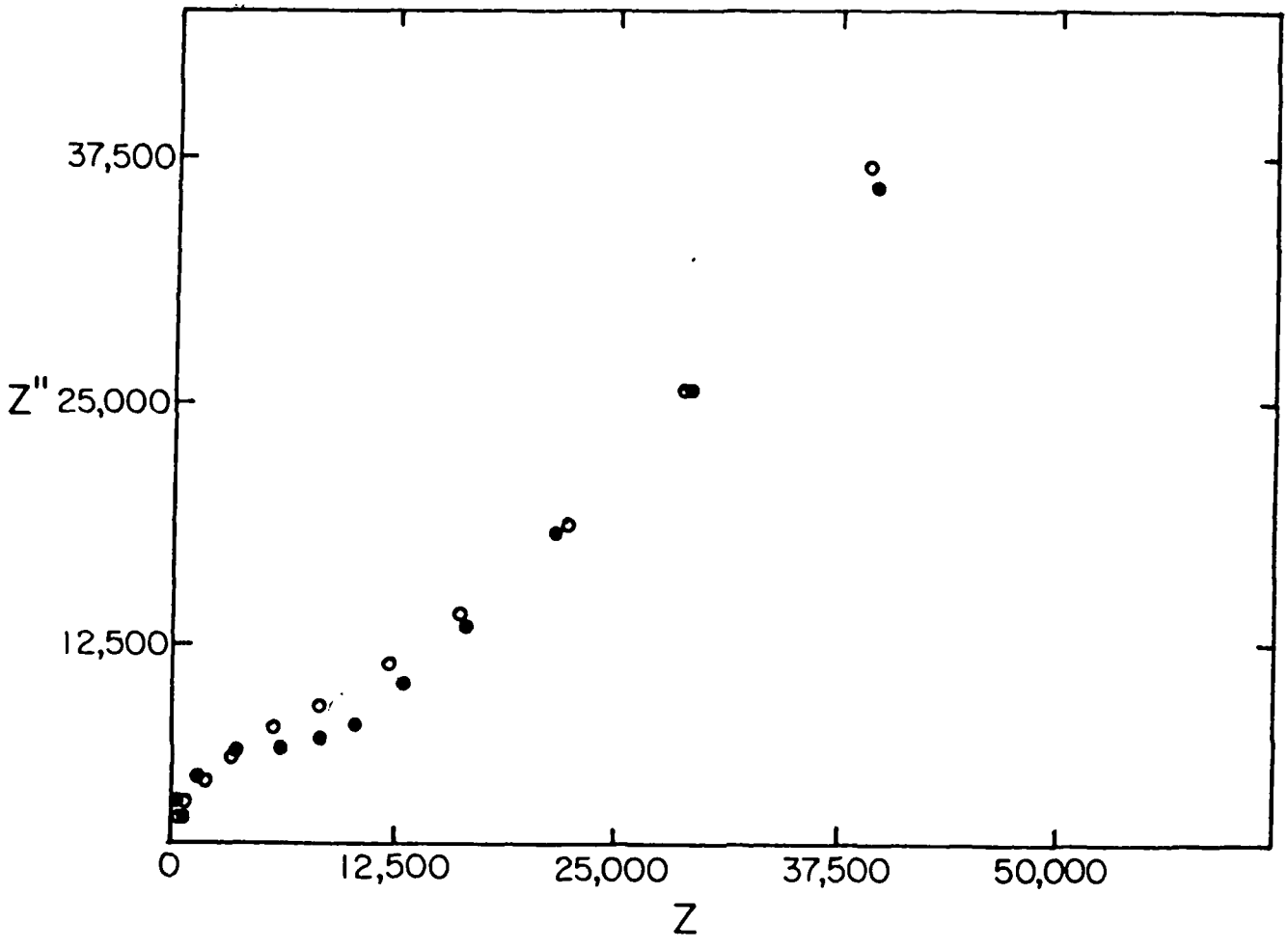

Figure 2. Nyquist plot of impedance data for single crystal nickel in phosphate solution. E = 0.1V(SCE), pH = 10

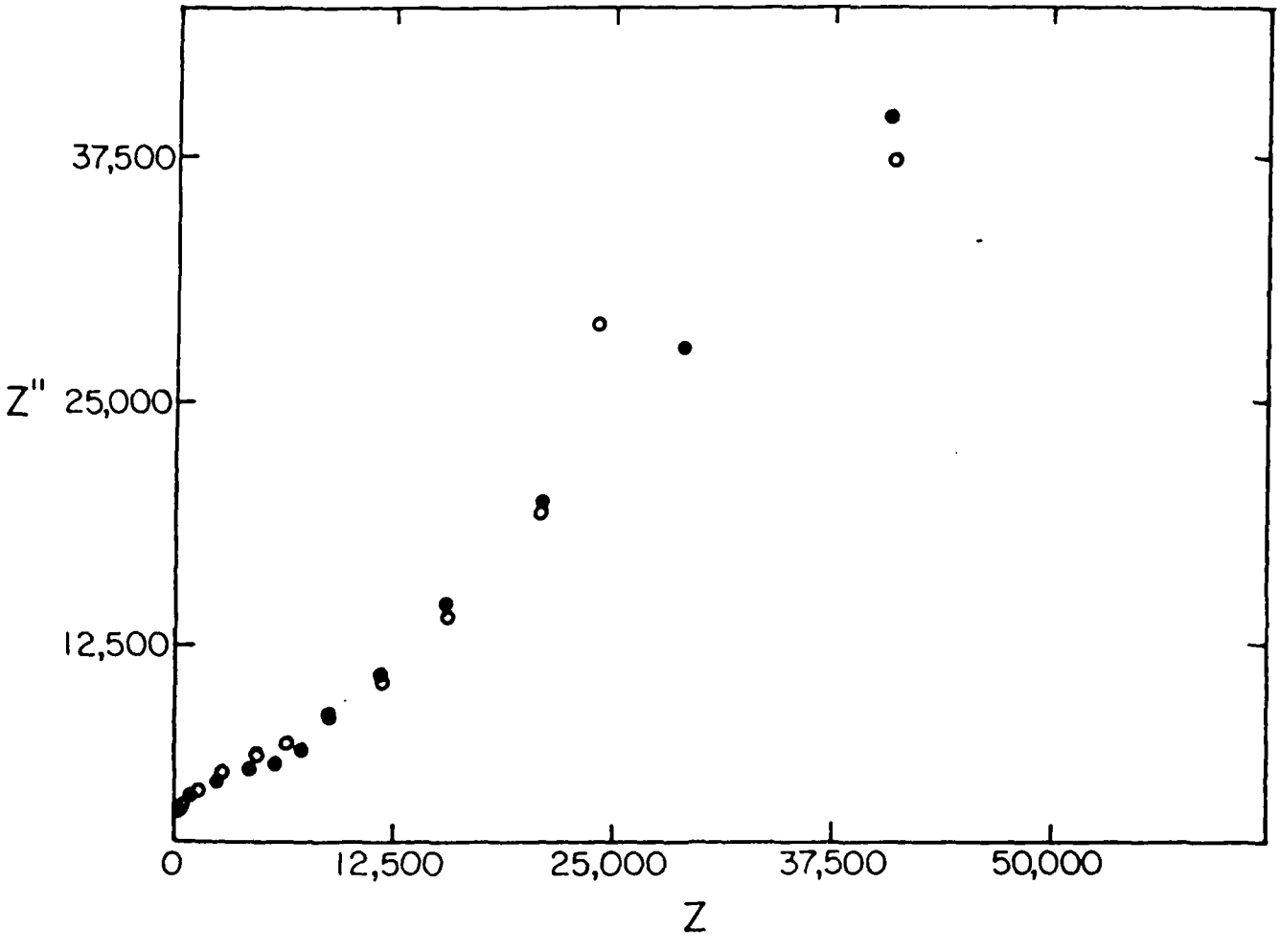

Figure 1. Nyquist plot of impedance data for single crystal nickel in phosphate solution. E = 0.3V(SCE), pH = 9

Table 1

Parameters Derived From Impedance Data
For β-$Ni(OH)_2$ Films On Single Crystal Nickel

pH	E/V	C_p/μF cm^{-2}	R_p/Ω cm^2	σ/Ω $cm^2 s^{-1/2}$
7	0.1	16.8	9573	2859±143
	0.3	19.5	10956	3486±174
8	0.1	17.9	6979	3493±175
	0.3	24.3	3640	5605±280
9	0.1	16.4	2946	2827±141
	0.3	24.6	4593	2912±146
10	0.1	18.1	6948	3859±193
	0.3	27.3	2343	5783±289
11	0.1	19.9	5585	3786±189
	0.2	24.7	4831	3915±196
	0.3	33.2	4294	3956±198
	0.4	40.6	2833	4116±206
12	0.1	20.7	2715	3154±158
	0.3	36.1	2089	3089±154

Values of the various circuit elements are given in Table 1. The Warburg coefficient is independent of potential within experimental error for pH values of 9, 11, and 12. However it does exhibit a steady increase with potential at each pH in the range studied (at pH values of 7, 8, and 10, this increase is greater than the experimental error). In contrast, except for pH values of 7 and 10, R_t decreases with increasing potential.

The capacitance is also potential dependent which is consistent with data reported by Madou and McKubre (5) for $Ni(OH)_2$ films in KOH. These workers attributed the measured capacitance to the presence of a space charge layer in the film, although the values appear to be too high to be completely attributed to this source. Instead, the values listed in Table 1 are also characteristic of the electrical double layer suggesting that the capacitance of $Ni(OH)_2$ films in phosphate media is due to space charge in the solution (double layer).

The values derived for the various circuit elements were used to calculate the total impedance of the equivalent circuit used in the analysis. Typical Nyquist plots of calculated and experimental data are shown in Figures 1 to 4. The two sets of data are in generally good agreement, particularly in the high and low frequency regions. At intermediate frequencies, there was, in some cases, a small difference between the two sets of plotted data. This difference might indicate the need for an additional component in the equivalent circuit, but more likely it reflects the difficulty of representing a region of joint activation/diffusion control in film growth by "ideal" circuit elements. Nevertheless, the equivalent circuit used appears to adequately represent the impedance associated with film formation on nickel in phosphate solutions.

Discussion

Previous studies by Macdonald and co-workers (6,3) have shown that, for the passive film on nickel in a Na_2HPO_4 solution (pH=9.1), the electric field strength, the charge transfer coefficient and the dc steady state current, I_{dc} are independent of potential. Under these conditions, it is predicted from the point defect model proposed by Chao *et al*. (6,3) that σ should also be independent of potential. Over the pH range (7 to 12) used in the present

SECTION 2

THE ANALYSIS OF AC IMPEDANCE DATA FOR NICKEL ELECTRODES

The growth of hydroxide films on single crystal nickel in phosphate solutions* (pH=7 to 12) was investigated using ac impedance and ellipsometric techniques, and details of the experimental work and results have been presented previously (4). A subsequent analysis of the ac impedance data has been carried out and the results are as follows.

Analysis

The impedance data were analyzed in terms of an equivalent circuit model in which the electrochemical interface can be represented by a capacitance, C_p, in parallel with a series combination of a charge transfer resistance, R_t, and a Warburg (diffusion) impedance, Z_W. The latter is given (1) by

$$Z_W = (1-j)\sigma\omega^{-(1/2)} \qquad (1)$$

where $j = -1$, $\omega = 2\pi f$, f is the frequency of the ac signal and σ is the Warburg coefficient. The values of the circuit elements were determined by deconvolution of the experimental data in a series of steps. Firstly, the contributions of the uncompensated solution resistance and C_p were removed. The solution resistance was determined from the high frequency intercept of the impedance data plotted in the complex plane, while C_p was obtained from a Bode plot (log |Z| versus log , where Z is the impedance). The real component of the reduced impedance data was then plotted against $\omega^{-(1/2)}$, and a linear regression performed to yield values of R_t and from the intercept and slope, respectively.

---

* These solutions contained varying amounts of $NaH_2PO_4 \cdot H_2O$, Na_2HPO_4, and $Na_3PO_4 \cdot 12H_2O$ adjusted to give a total phosphate concentration of 0.1 mol ℓ^{-1} at the desired pH.

SECTION 1

INTRODUCTION

Reactive metals such as aluminum, chromium, titanium, and zirconium, all of which play an important role in our metals-based civilization, can be used in practice only because of the existence of a thin oxide film at the metal surface. This "passive" film serves to isolate the underlying metal from the environment, and hence is responsible for the kinetic stability of metals when exposed to oxidizing atmospheres. However, passive films generally are not perfect and may breakdown, resulting in localized corrosion, (pitting, etc.). Breakdown is normally induced by some aggressive species (e.g. Cl^-) in the solution. Even if breakdown does not occur, the passive film will continue to grow and itself may slowly dissolve into the environment, resulting in a steady state thickness on the metal surface.

The mechanism(s) of growth of passive films on metal surfaces have been under extensive investigation since the middle of the nineteenth century. This work has sought to provide an explanation of experimental data regarding the kinetics of film growth and the conditions under which breakdown occurs. In general, these efforts have been unsuccessful, either because the various models proposed are unrealistically simple or because insufficient data have been available to distinguish between them.

In this final report, we present experimental data which have been obtained and describe the various theoretical developments which have been achieved throughout the program. The experimental studies include impedance analysis of passive films formed on single crystal nickel in phosphate solutions, as well as our recent work on passivity breakdown of single crystal nickel in buffered sodium chloride solutions. The theoretical studies involve the further development of the point defect model which was originally described by Chao, Lin, and Macdonald (1-3). The theoretical work is far from complete but we believe it will form a new basis for the design of future experiments to test various theortical descriptions of passive films which are currently being developed.

LIST OF TABLES

Table No.		Page
1	Parameters derived from impedance data for β-$Ni(OH)_2$ films on single crystal nickel.	4
2	The critical pitting potentials (V_c) of pure nickel (100) in borate buffer solution at different chloride concentrations ($[Cl^-]$).	22
3	The induction time (t) of pitting corrosion of single crystal nickel (100) in borate buffer solution ($[Cl^-]$ = 0.2 M) at different breakdown overpotential (ΔV).	27
4	Experimental and theoretical values of growth of passive film solution.	44
5	Experimental and theoretical values for growth of nickel film in phosphate solutions.	48

Figure No.		Page
36	Influence of K_n on the pitting potential as a funciton of % molybdenum.	92
37	Influence of the concentration of cations vacancies on pitting potential and incubation times as a function of molybdenum content. $\Delta V=V_c(X_{Mo}) - V_c(X_{Mo}=0)$.	93
38	Influence of complex stoichiometry (q) on the pitting potential and incubation time as function of molybdenum content. $\Delta V=V_c(X_{Mo})-V_c(X_{Mo}=0)$.	95

Figure No.		Page
27	Calculated electric field strength versus film thickness. Note that in this case the anion and ionized-anion vacancy concentration at the film/solution interface are varied. In all cases, the deviation from neutrality is negligibly small.	74
28	Calculated field strength versus thickness. Note that in this case, the concentration of positive holes Δp is varied.	75
29	Calculated electric field strength versus film thickness. In this case the concentration of electrons Δn is varied.	76
30	Calculated electric field strength versus film thickness. Note that in this case the anion and ionized-anion vacancy concentration at the film/solution interface are varied and the concentration of cation vacancy at interfaces is null. In all cases the deviation from electro-neutrality is small.	77
31	Calculated electric field strength versus film thickness. Note that in this case the anion and ionized-anion vacancy concentration at the metal/film interface is varied and the concentration of cation vacancy at interfaces is null. In all cases the deviation from electro-neutrality is small.	78
32	Calculated electric field strength versus film thickness. Note that in this case the cation and ionized-cation vacancies concentrations at the metal/film interface are varied; and the concentration of ion vacancy is null. In all cases the deviation from electro-neutrality is negligibly small.	79
33	Calculated electric field strrength versus film thickness. Note that in this case the cation and ionized-cation vacancies concentrations at the film/solution interfaces are varied; and the concentration of ion vacancy is null. In all cases the deviation from the electro-neutrality is negligibly small.	80
34	Pitting potentials versus % molybdenum in 18%-Cr ferritic stainless steel. (● experimental work in 1 M NaCl solution at 25°C (24). Theoretical results q=1; $n_v = 4x10^{20}cm^{-3}$, $K_n=10^{-4}cm^3$ (○); $n_v=4x10^{19}cm^{-3}$, $K_n=10^{-17}cm^3$ (□)0.	90
35	Effect of Molybdenum on induction time for pit-initiation according to the solute vacancy interaction model (SVIM). q=1, $n_v=4x10^{20}cm^{-3}$, $K_n=10^{-4}cm^3$).	91

SECTION 3

FILM BREAKDOWN STUDIES

General Objective

Pitting corrosion at passivated metals is a direct result of the breakdown of passive films on the surface. For several decades, the subject of pitting corrosion has been studied extensively, yet none of the theories proposed have been able to account for all of the experimental results. The recently developed point defect model (1) provides a quantitative explanation of passivity breakdown in terms of electrochemical phenomena. However, this model lacks experimental support, since most of the existing data for pitting corrosion were not obtained from carefully controlled experiments. The purpose of this study, therefore, was to test the point defect model by collecting passivity breakdown data under well-defined experimental conditions.

Previous Work

During the preliminary portion of this study (13,14), an experimental apparatus was assembled, a combined mechanical/electrolytic polishing procedure was developed, and a Teflon shield was designed in order to reduce crevice corrosion. Several film breakdown potentials (V_b) were measured in borate buffer solution containing chloride, but no analysis of the data was carried out (4). During the second year of study, small changes were made to the experimental system and included using a PAR 173 potentiostat/galvanostat with a PAR 179 digital coulometer module instead of a Wenking 66TS10 potentiostat and a PAR 379 coulometer. The present most sophisticated experimental system is shown schematically in Figure 5. The polishing of the single crystal nickel electrode follows the procedure developed in the first year, except that a final 0.05 μm alumina polishing was performed in order to remove any film formed during the preceding electro-polishing step. The same Teflon shield was utilized to reduce crevice corroson but, in order to ensure

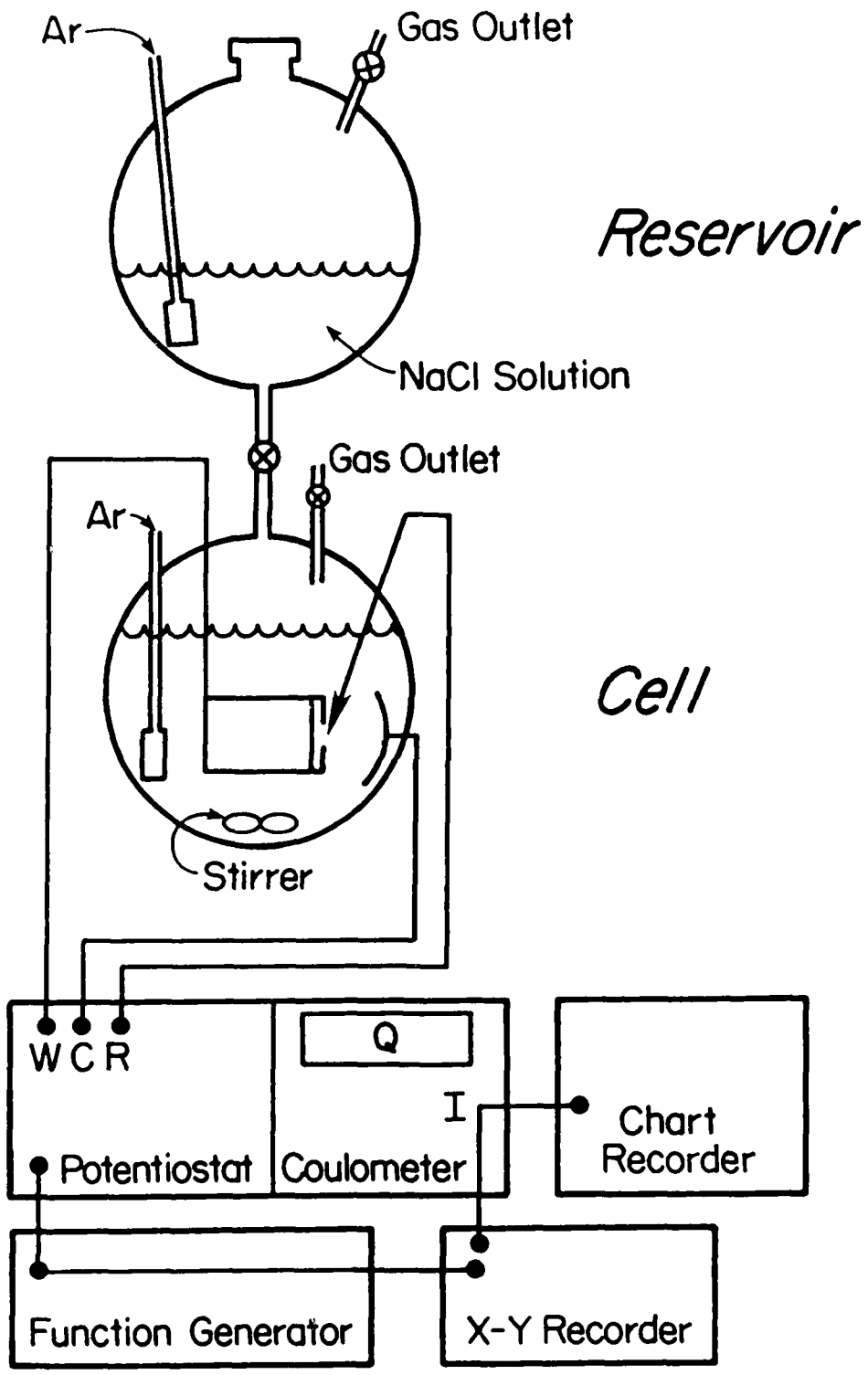

Figure 5. Experimental apparatus for passivity breakdown studies on nickel in borate buffer/NaCl solutions.

a constant exposed surface area (Figure 6), the use of microstop was discontinued.

A major change made in the experimental procedure was the growth of the passive film in the chloride-free solution, which greatly increased the reproducibility of the data, and resulted in better-defined breakdown potentials. The sodium chloride solution was added after a β-$Ni(OH)_2$ film had been grown to a constant thickness (charge $Q=5.000 \times 10^{-3}$ coulomb) on the single crystal nickel (100) in the chloride-free borate buffer solution at 100 mV_{SCE}. The time required to add and mix the sodium chloride solution with the borate buffer solution was short, such that the change of film thickness during this period was negligible (less than 2%). Potential sweep (film breakdown potential measurements) or the potential step (induction time measurements) type of measurements were performed immediately after the mixing to determine the breakdown potential (V_b) or induction time (t), respectively. Figures 7(a) and 8(a) show the potential-time profiles for these two experiments.

Results and Discussion

i) Film Breakdown Potentials (V_b)

From potential sweep experiments, the film breakdown potential (V_b) was measured at the point where the current increases sharply on the anodic polarization curve as shown in Figure 7(b). In the earlier work, when the passive film was grown in the chloride-containing solution, the film breakdown potential was difficult both to determine and to reproduce satisfactorily (4). In the more recent work, however, the film was grown in the chloride-free solution and the breakdown potential was better defined and was also reproducible (Figure 9). This difference in the behavior of V_b indicates that chloride ions modify the passive film during the growth stage, and consequently influence the susceptibility of the film to breakdown. For example, MacDougall et al. (15) claim that chloride ions penetrate the passive film on nickel, but this conclusion has not been established unequivocally because of the difficulty of depth-profiling thin films using sputtering/Auger Electron Spectroscopy and Secondary Ion Mass spectrometry (SIMS).

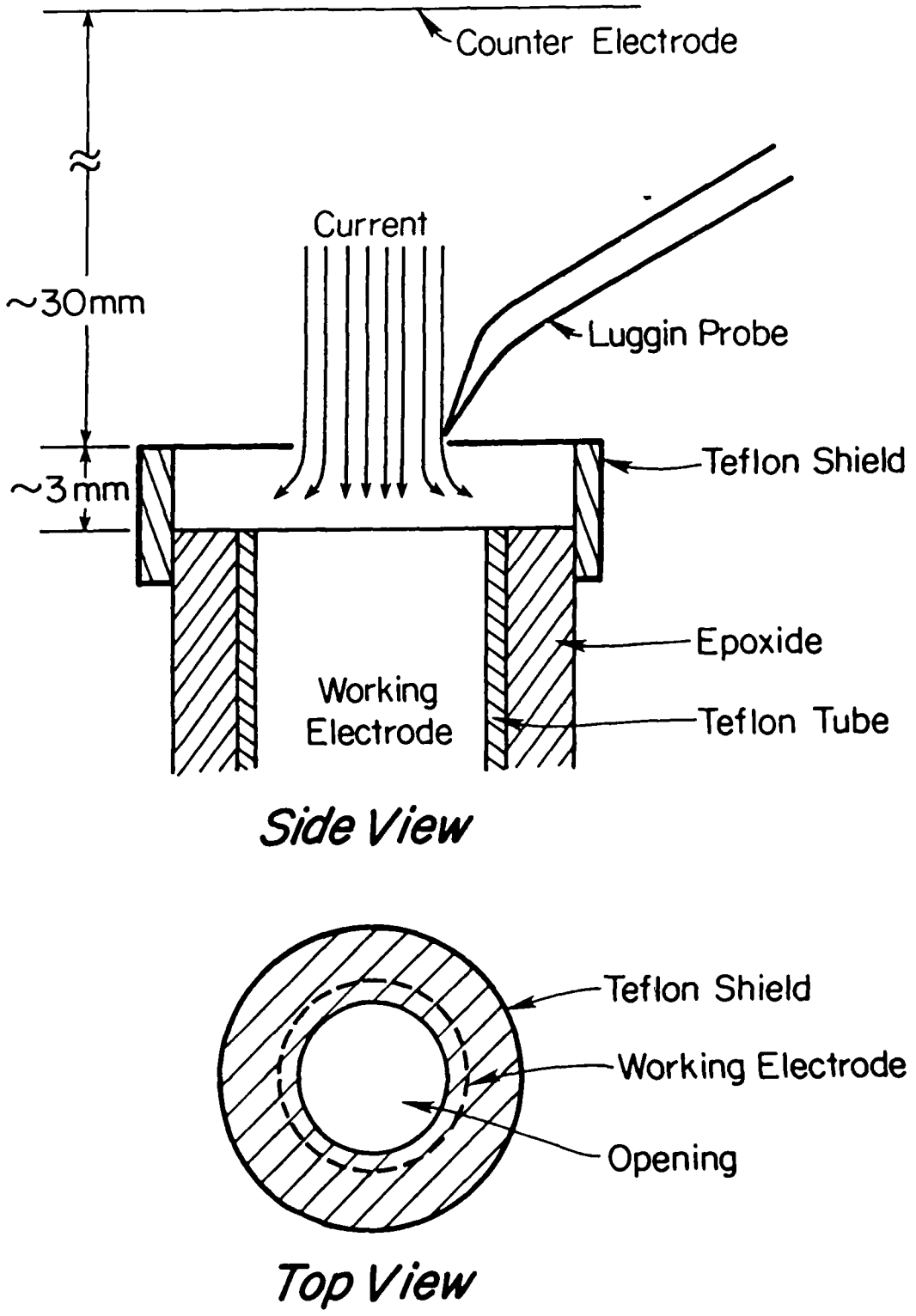

Figure 6. Shield design for reducing crevice corrosion.

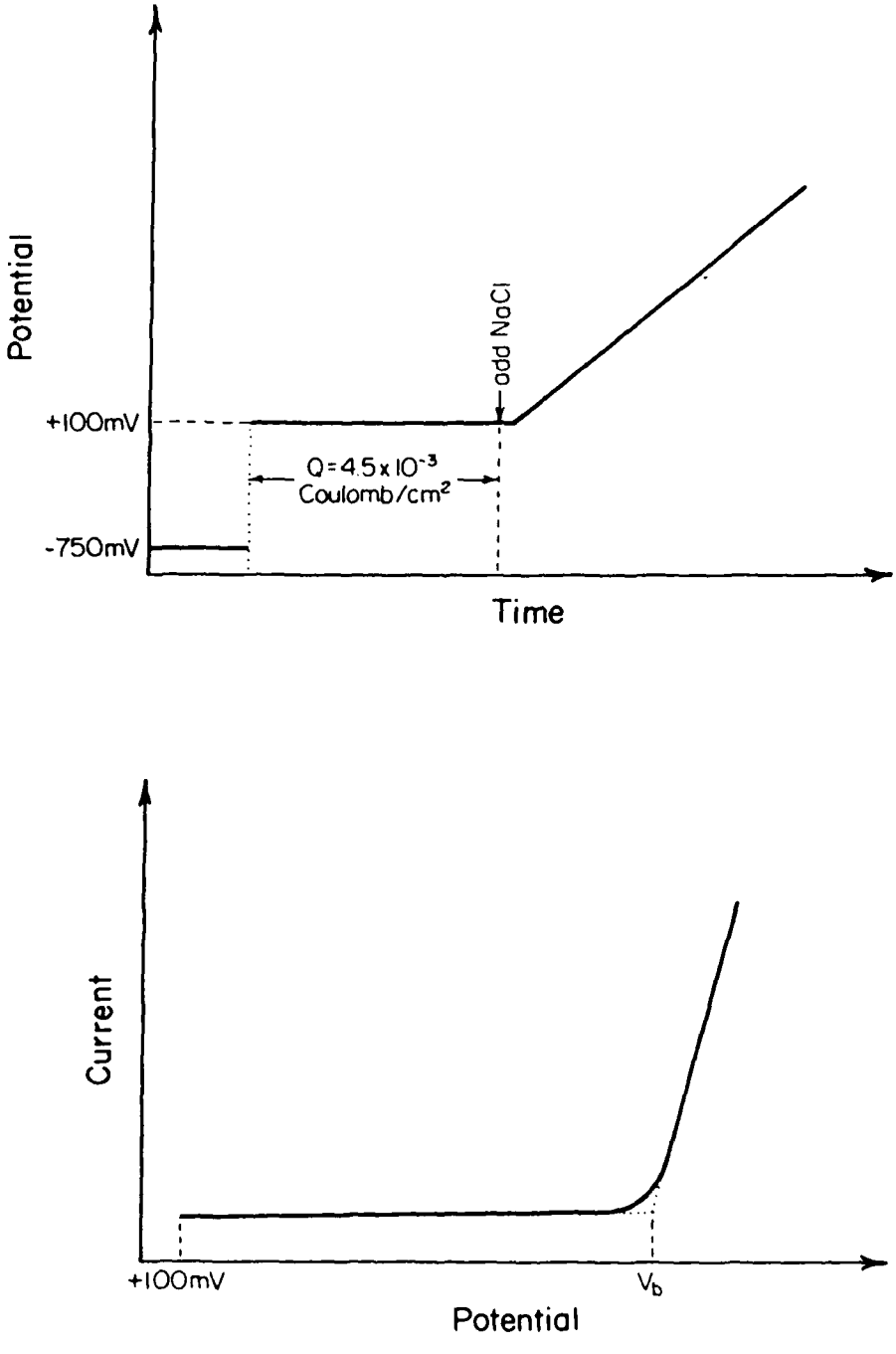

Figure 7. (a) Potential-time profile used in film breakdown studies, (b) Schematic current-potential curve illustrating film breakdown.

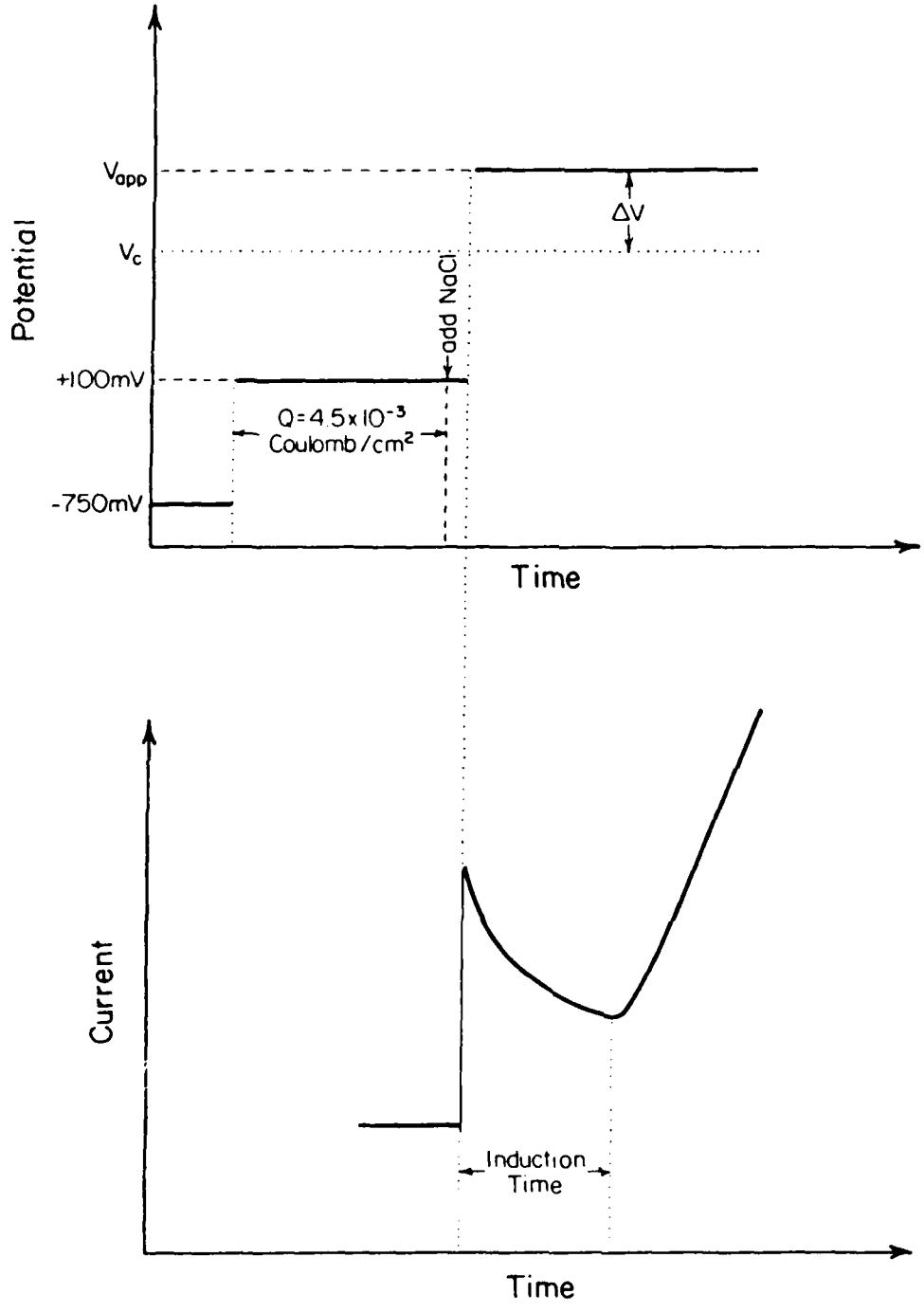

Figure 8. (a) Potential-time profile used to determine induction time for passivity breakdown, (b) Schematic current-time curve illustrating passivity breakdown.

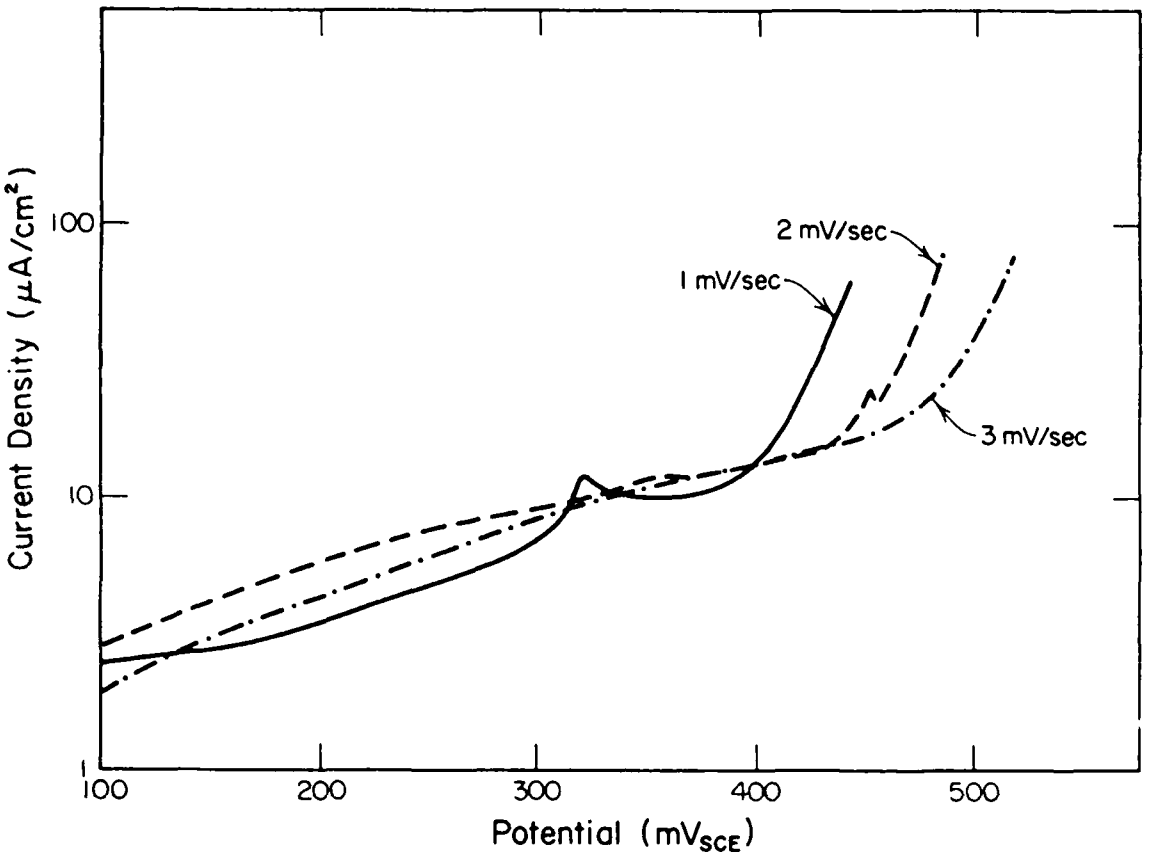

Figure 10. Current-potential curves for Ni(100) in buffered borate solution with 0.2N chloride at different sweep rates.

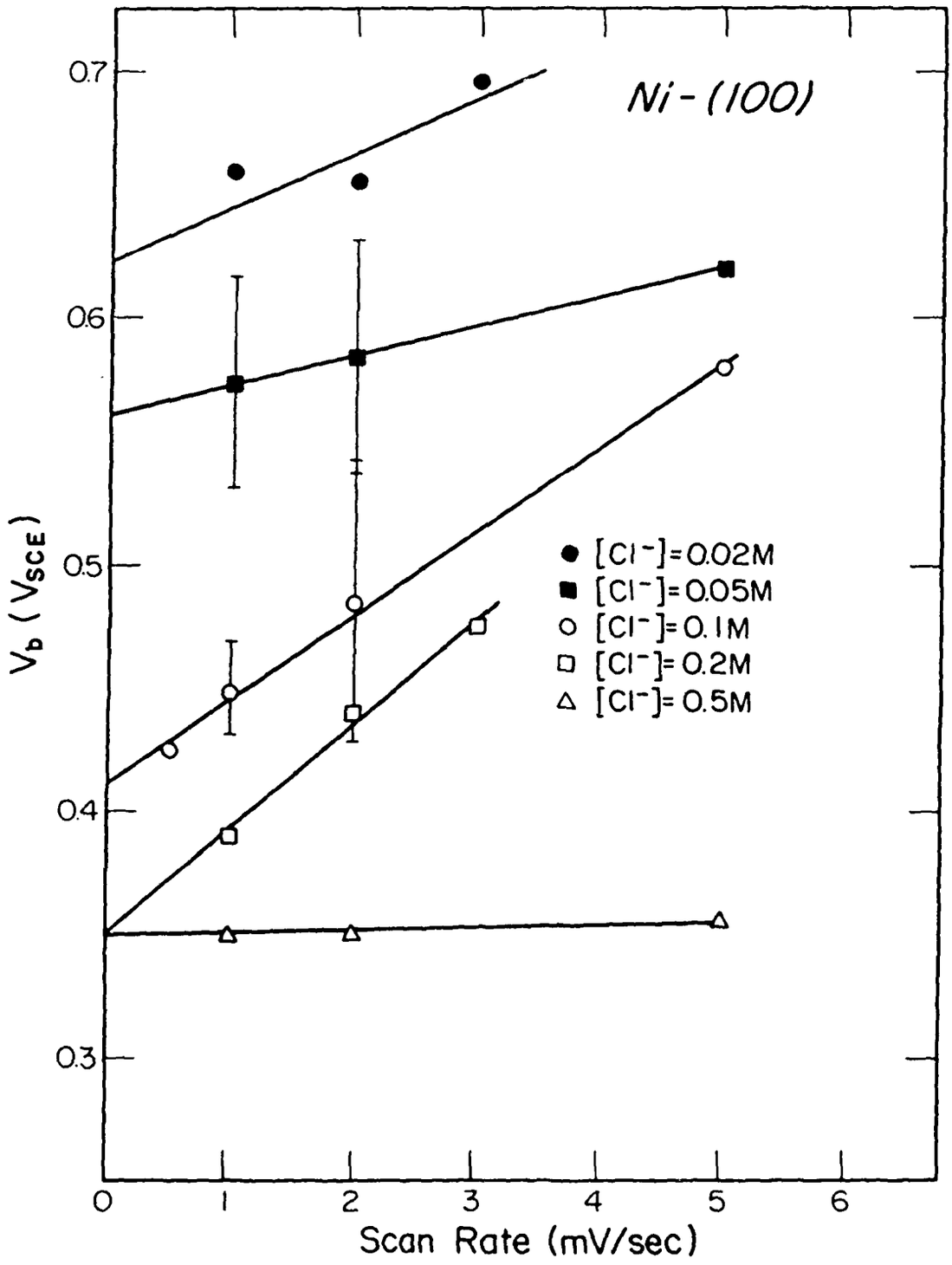

Figure 11. The effect of sweep rate on the film breakdown potential of Ni(100) in borate buffer solution as a function of chloride concentration.

Table 2

Critical Pitting Potentials (V_c) for Nickel (100) in Borate Buffer Solution at Different Chloride Concentrations ($[Cl^-]$).

	$[Cl^-]$ (M)				
	0.02	0.05	0.1	0.2	0.5
V_c (V_{SCE})	0.620	0.560	0.412	0.350	0.350

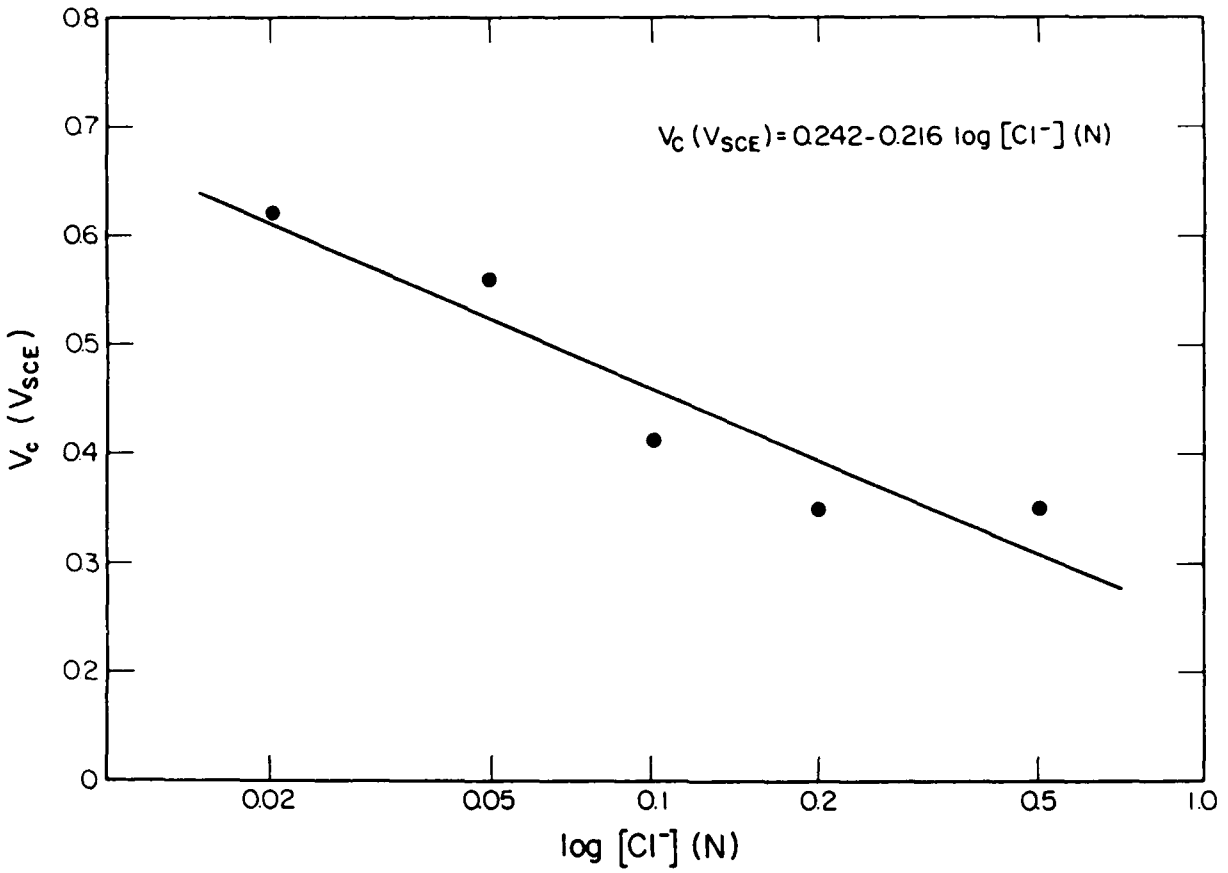

Figure 12a. Relationship between the critical pitting potential and chloride concentration fro Ni(100) in borate solution.

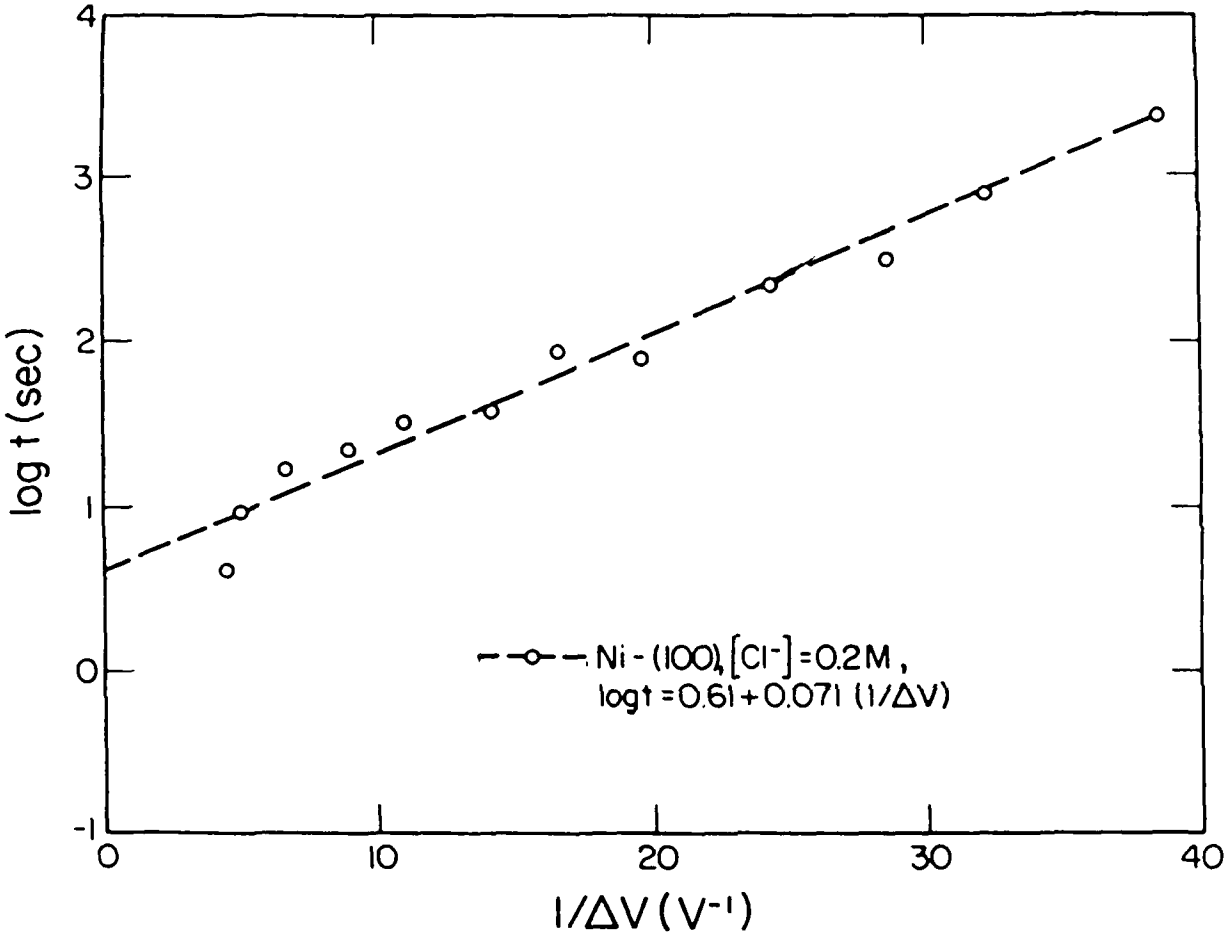

Figure 12b. Plot of the logarithm of induction time (log t) versus the inverse of overpotential (1/ΔV).

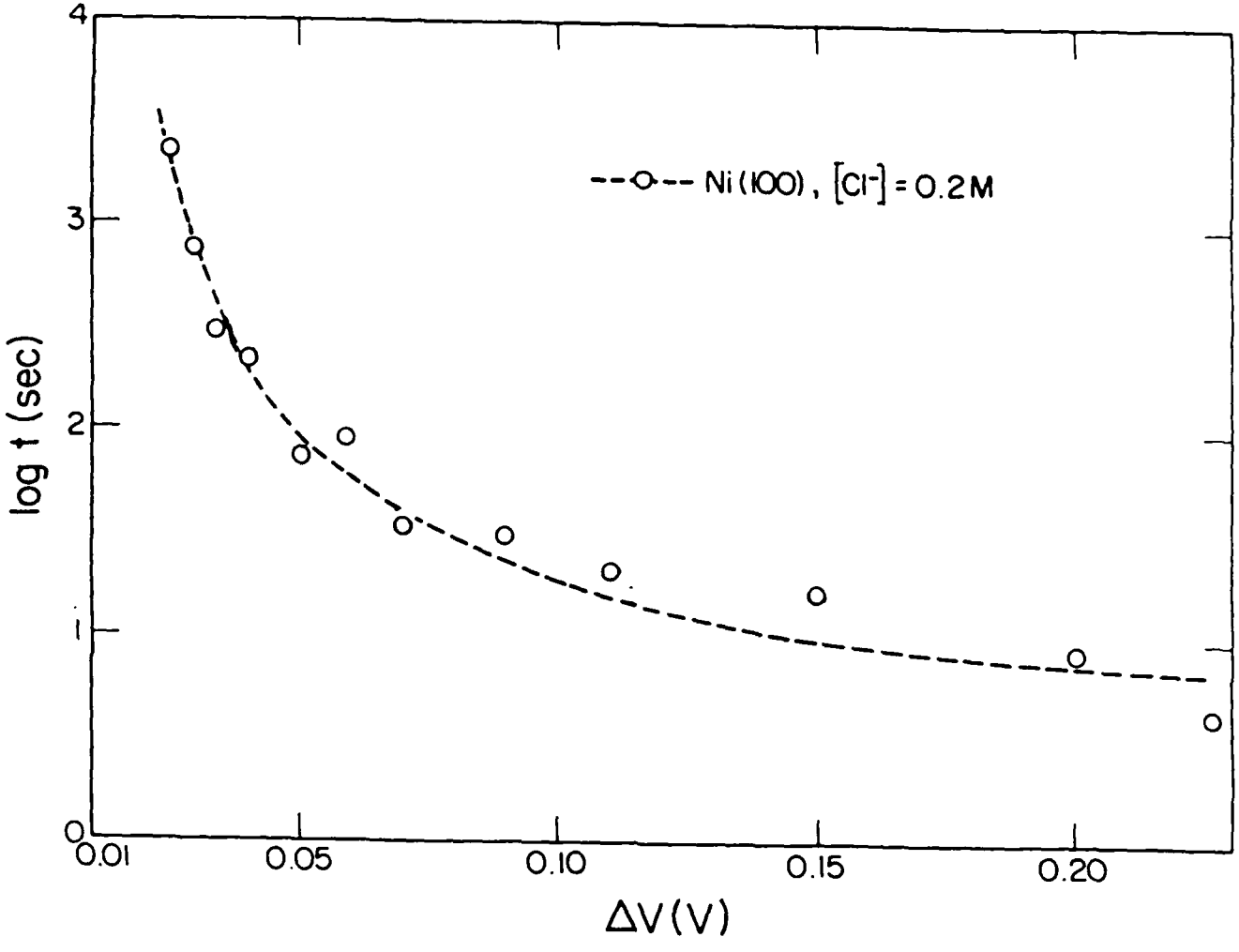

Figure 12c. Plot of the logarithm of induction time (log t) versus overpotential (ΔV) according to the point defect model.

$$B = \frac{2.303RT}{\alpha F}$$

where α is the fraction of the applied potential contributing to the potential drop at the film/solution interface, and F, R, and T have their usual meaning. The intercept A cannot be analyzed because no data are available for the parameters, u, J_m and J°. Furthermore, the available data for B do not permit an accurate estimate of α at this time although the data given in Figure 12a indicate that the value is of the order of 0.27. This value is much lower than that (0.878) quoted by Chao et al (18) for polycrystalline nickel in phosphate solution (pH 4.5). It is important to note that both the solution, in particular the pH, and the crystalline form of the nickel differ in the two studies, and either of these factors could well account for the above difference to a large extent.

iii) Induction Time (t).

The induction time (t) of pitting corrosion at a certain breakdown overpotential ($\Delta V = V_{app} - V_c$) can be determined from the current-time curve in the potential step experiment (Figure 10(b)). For single crystal nickel (100) surface the induction time was measured at twelve different overpotentials in the borate buffer solution containing 0.2 mole/liter sodium chloride while other parameters such as film thickness ($Q = 5.0 \times 10^{-3}$ coulomb), film formation potential (+100 mV), temperature (25°C), etc. were kept constant. The induction time increased very rapidly with decreasing overpotential (Table 3). The relationship between the induction time and overpotential can be presented in two ways:

a. log t vs $1/\Delta V$

When the logarithm of the induction time plotted against the inverse of the overpotential (Figure 12b), a linear relationship was found with very good correlation coefficient (0.98):

$$\log t = 0.61 + 0.071\ (1/\Delta V) \qquad (4)$$

The intercept at $1/\Delta V = 0$ (or $\Delta V \rightarrow \infty$) was 4 seconds.

Table 3

Induction Times (t) Of Nickel Specimens In ($[Cl^-]$=0.2M) At Different Overpotentials (ΔV).

Ni-(100)	
ΔV (V)	t (sec)
0.026	2300
0.031	774
0.035	305
0.041	229
0.051	78
0.06	94
0.071	38
0.091	32
0.111	22
0.151	17
0.201	9
0.226	4

Results

The model developed in the previous sections will be used to calculate film properties which can be compared with available experimental data. The experimental data of particular interest pertains to the growth of passive films on iron in borate solutions (1), and on nickel in phosphate solutions (6). To obtain film properties from the theoretical first-order point defect model, it is necessary to input numerical data for a number of parameters. Values for some of these parameters are well-known. However, values for others where chosen by adjusting various parameters so that the calculated thickness agreed with experiment at one point; normally that at -0.4 V after one hour of polarization for which the film thickness $L = L_o$. Details of these calculations for passive films formed on iron and nickel are presented in the following sections.

I. Iron (Fe-Fe_2O_3)

The parameters that are required for applying the model to the formation of oxide films on iron were chosen as follows:

i) Experimental Data (1)

$\alpha = 0.728$ (at 20°C)	from Eq. (10)
$\beta = 0.0144$ V	from Eq. (10)
pH = 11.5	from Eq. (10)
$D = 2 \times 10^{-20}$ cm^2/s	from Eq. (5)
$\Omega = 30$ cm^3/mol	from Eq. (4)

ii) Physical Constants

$q = 2$	from Eq. (5)
$F = 96487$ coul/mol	from Eq. (6)
$R = 8.314$ J/mol°K	from Eq. (6)
$T = 298$ °K	from Eq. (6)

$$M_n = \left.\frac{dX}{dt}\right|_{X_n}, \qquad M_n' = \left.\frac{d^2X}{dt^2}\right|_{X_n}$$

$_1 = (t_o + nh)$ and increment $h = (t_n - t_{n-1})$. The Taylor series is often used
$_1$ starting a solution to be carried on by some other method.

A more accurate method of extrapolation uses instead of a straight line, a
ırve represented by an algebraic equation of degree higher than one. This is
ıe basis for what is known as the Adams method. The curve used in this
ethod is a parabola which can be represented by an algebraic equation of
econd order as follows:

$$X_{n+1} = X_n + h\left[M_n + (1/2)\,(M_n - M_{n-1})\right]$$

, a similar process a curve of fifth degree can be used with the resulting
ıuation for extrapolation:

$$X_{n+1} = X_n + h\,M_n + (1/2)\Delta M_{n-1} + (5/12)\Delta^2 M_{n-2} + (3/8)\Delta^3 M_{n-3} + (251/720)\Delta^4 M_{n-4}$$

ere

$$\Delta M_{n-1} = M_n - M_{n-1}$$

$$\Delta^2 M_{n-2} = \Delta M_{n-1} - \Delta M_{n-2}$$

$$\Delta^3 M_{n-3} = \Delta^2 M_{n-2} - \Delta^2 M_{n-3}$$

$$\Delta^4 M_{n-4} = \Delta^3 M_{n-3} - \Delta^3 M_{n-4}$$

ese are the successive differences in the quantity M, and similar succesive
fferences for x are also defined. When the thickness of the film is
lculated from the model, it is possible to then compute the concentrations
oxygen ion vacancies at each point. These calculations are then repeated
a different number of discrete units to simulate growth of the film. The
ıber of slices is chosen arbitrarily.

$$\frac{dL}{dt} = \frac{\Omega}{N_v} \frac{Dqk}{2} \left\{ \exp\left[-(q^2k^2D/4)t \right] \cdot \exp\left[(qk/2)L \right] \cdot \right. \tag{19}$$

$$\left[C(f/s) + \frac{C(m/f)\ \exp\left[(qk/2)L_o\right] - C(f/s)}{L_o} \cdot L \right.$$

$$\left. \left. -2\ \frac{C(m/f)\ \exp\left[(qk/2)L_o\right] - C(f/s)}{L_o} \right] \right\}$$

It is not possible to obtain an analytical solution to this equation, and hence it will be necessary to use a numerical method to theoretically evaluate the kinetics of film growth. A numerical method was developed for an Apple II-e microcomputer, and this program has allowed the generation of information on the following: i) growth of the film, ii) thickness of the film as a function of applied potential, V_{ext}, and iii) concentration of ion vacancies throughout the film. In generating numerical data for L as a function of time and applied potential, the basic problem is to solve the first-order differential equation

$$\frac{dL}{dt} = f(L,t)$$

subject to the initial condition that, at $t = 0$, $L = L_o$. It is assumed also that the function $f(L,t)$ is generally continuous and single-valued, and has definite derivatives. The numerical analysis is carried out by first assigning discrete values to the properties of the film as a function of distance and time, followed by successive extrapolation to determine specific properties at each point.

Perhaps the most obvious way to extrapolate from one step to another is to develop a solution to the differential equation in terms of a Taylor series. This solution has the form:

$$X_{n+1} = X_n + M_n h + 1/2\ M_{n'} h^2 + 1/6\ M_{n''} h^3 + \ldots$$

where

$$Y = e^{px} \left[C_1'' \cos(qx) + C_2'' \sin(qx) \right] \tag{17}$$

where $p = -a/2$, $q = \sqrt{b \cdot a - (a^2/4)}$, $i = \sqrt{-1}$ and C_1'', C_2'' are integral constants. The appropriate combinations of these equations yield the particular solution which allows the computation of the concentration of vacancies as a function of time and distance. The most acceptable solution, physically, is the one where both roots m_1 and m_2 are equal. Accordingly, the general solution can be written as follows

$$C(x,t) = (A + Bx) \exp [(qk/2)x] \exp [-(q^2k^2D/4)t]$$

in which the constants A and B are obtained from the initial and boundary conditions:

$$C(0,0) = C(f/s)$$

$$C(L_o,0) = C(m/f)$$

where L_o is the initial thickness of the film. Accordingly, the solution becomes

$$C(x,t) = \exp [-(q^2k^2D/4)t] \left\{ C(f/s) + \frac{C(m/f) \exp (qk/2)L_o - C(f/s)}{L_o} \right\} X \exp [(qk/2)x] \tag{18}$$

From Equation (4) and (5), it is possible to obtain information about the growth of the film. Substituting Equations (18) and (5) into (4) we can write:

The sign of ξ^2 will be chosen to provide a realistic physical description of the growth of a passive film on a metal surface. It is evident that for any given value of x, as the film grows, the concentration of $V_{O}^{\cdot\cdot}$ at this point will decrease with time. Accordingly, the minus sign corresponds to the physically realistic situation, and Eq. (12) becomes

$$R(t) = A \exp(-\xi^2 t) \tag{14}$$

where ξ is a real number and A is an integral constant. Three particular solutions of Eq. (13) are possible, depending upon the roots of the quadratic equation in m:

$$m^2 + am + b = 0$$

where $a = -qK$ and $b = +\xi^2/D$. Let m_1 and m_2 be the roots of the equation above. Accordingly,

CASE 1.

$m_1 \neq m_2$, and m_1 and m_2 are real numbers

$$Y = C_1 \exp(m_1 x) + C_2 \exp(m_2 x) \tag{15}$$

CASE 2.

$m_1 = m_2$, and m_1 and m_2 are real numbers

$$Y = \exp(m_1 x)\,[C_1' + X \cdot C_2'] \tag{16}$$

CASE 3.

$m_1 \neq m_2$, and m_1 and m_2 are imaginary numbers

$m_1 = p + iq$

$m_2 = p - iq$

nonsteady state are presented, in which the electrical field strength is considered to be constant.

Solution of Diffusion Equations

For each species moving with the passive film, Ficks' second law can be written as

$$\frac{\partial C}{\partial t} = + D \frac{\partial C^2}{\partial x^2} - Dqk \frac{\partial C}{\partial x}$$

where D, q, K, are considered to be independent of distance and time (field strength through the film is constant). An analytical solution is developed by using the separation of variables technique. This yields the following equation:

$$C(x,t) = Y(x)\ R(t)$$

and substitution with Eq. (6) yields

$$\frac{1}{R(t)} \frac{\partial R(t)}{\partial t} = \frac{D}{Y(x)} \frac{\partial^2 Y(x)}{\partial x^2} - \frac{Dqk}{Y(x)} \frac{\partial Y(x)}{\partial x}$$

Because the two sides are separately pure functions of R(t) and Y(x) we may equate both to the same constant, ξ^2

$$\frac{1}{R(t)} \frac{\partial R(t)}{\partial t} = \pm \xi^2 \qquad (12)$$

$$\frac{D}{Y(x)} \frac{\partial^2 Y(x)}{\partial x^2} - \frac{Dqk}{Y(x)} \frac{\partial Y(x)}{\partial x} = \pm \xi^2 \qquad (13)$$

By involving the assumption of equilibrium at the two interfaces, it is possible to specify the boundary conditions as follows (1):

a) Metal/film interface.

The boundary and initial conditions for the equation (6) are

$$C(m/f) = \frac{n_v}{\Omega} \exp \frac{2F\phi_{m/f} - (2/\chi)\Delta G^{\bullet}_{21}}{RT} \tag{8}$$

b) Film/solution Interface

$$C(f/s) = \frac{n_v}{\Omega} \exp \frac{\Delta G^{\bullet}_{31} - 2F\phi_{f/s}}{RT} - 4.606\ pH \tag{9}$$

where

$$\phi_{f/s} = \alpha V_{ext} + \beta\ pH + \phi^{\circ}_{f/s} \tag{10}$$

$$\phi_{m/f} = (1-\alpha)V_{ext} - \beta\ pH - \phi^{\circ}_{f/s} + \phi_R - \phi_f \tag{11}$$

α = Constant

β = Constant

pH = pH of solution

ϕ_f = potential drop across the film

V_{ext} = Externally applied potential

ϕ_R = Reference potential

$\phi^{\circ}_{f/s}$ = Initial potential at film/solution interface

ΔG°_{31} = Gibbs energy of the reaction: $V_{O}^{\cdot\cdot} + H_2O \rightleftharpoons 2H^{+}(aq) + O_O$

In the following section, we report the results obtained from a formal solution (analytical and numerical) of the diffusion equation for the

$$\frac{dL}{dt} = \frac{\Omega}{n_v} J_{V_O^{\cdot\cdot}} \tag{4}$$

where Ω is the molar volume per cation, n_v is Avogadro's number, and $J_{V_O^{\cdot\cdot}}$ is the flux of oxygen vacancies, $V_O^{\cdot\cdot}$ towards the metal/film interface.

The flux $J_{V_O^{\cdot\cdot}}$ can be obtained from Fick's first law , as follows:

$$J_{V_O} = - D \frac{\partial C}{\partial x} + DqkC \tag{5}$$

where C is the concentration of $V_O^{\cdot\cdot}$. The concentration, C, as a function of distance and time is obtained by solving Fick's second law

$$\frac{\partial C}{\partial t} = D \frac{\partial^2 C}{\partial x^2} - Dqk \frac{\partial C}{\partial x} \tag{6}$$

where k is given by

$$k = - \frac{F}{RT} \frac{d\phi}{dx} \tag{7}$$

The others parameters are as follows:

D = Diffusivity of $V_O^{\cdot\cdot}$
q = Number of charges on species, $V_O^{\cdot\cdot}$
R = Gas constant
T = Temperature
F = Faraday constant
ϕ = Electrical potential through the film
x = Distance
t = Time

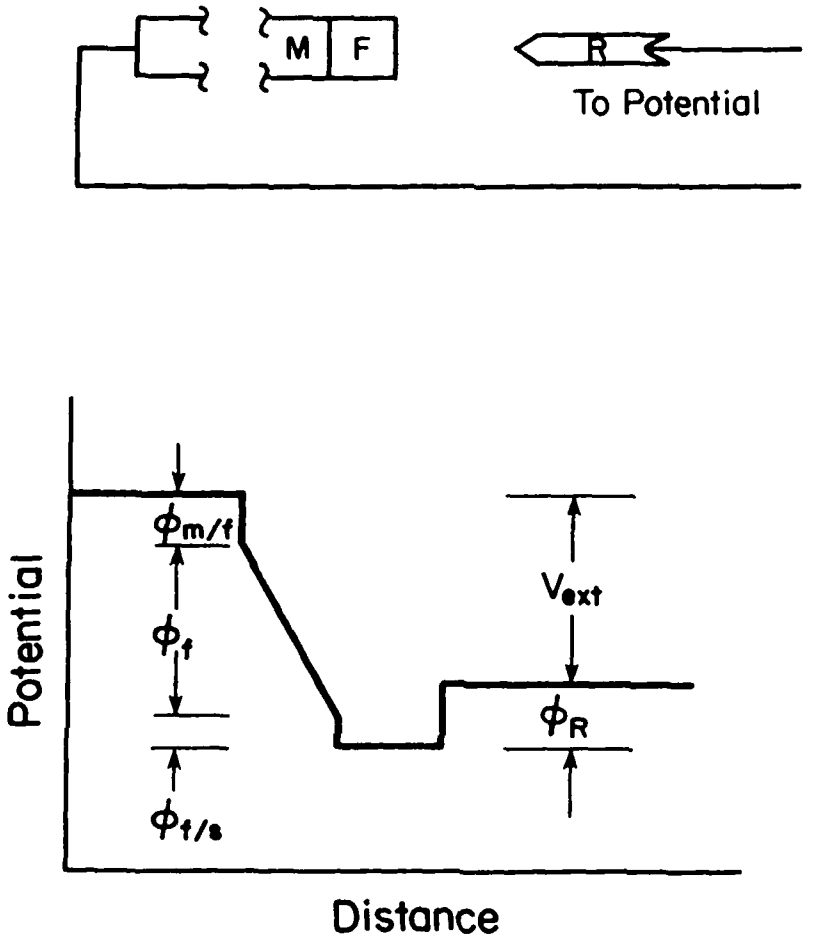

Figure 13. Schematic of the working and reference electrode in a typical electrochemical cell (upper figure) and the corresponding potential-distance relationships (lower figure).

In developing the first-order model, the previously-employed simplifying assumptions were involved as follows:

i) The film is assumed to be an oxide of composition $MO_{x/2}$

ii) The passive film contains a high concentration of point defects; the species present are V_{MX}'', $V_{O}^{\cdot\cdot}$, e', $\dot{h}$, but only $V_{O}^{\cdot\cdot}$ is responsible for the growth of the film (1).

iii) The electric field strength which exists within the film is assumed to be constant and buffered by mobile charge carriers.

iv) Interactions between point defects are considered to be negligible.

v) Equilibrium exists at the metal film and film/solution interfaces with regard to the concentrations of the point defects.

However, in the first order model developed here it is <u>not</u> assumed that the film is in a quasi-steady state, as was done in the original treatment (1). Consequently, the movement of point defects is described exactly by Ficks' second law (Nernst-Planck equation) rather than approximately by the Ficks first law expression.

Figure 13 shows schematically the relationship between the working electrode and the reference electrode in an electrochemical cell, and the corresponding potential/position relationships. According to assumption (ii) above, growth proceeds by the movement of oxygen ion vacancies from the metal/film interface to the film/solution interface or of oxide ions in the reverse direction. Accordingly, film growth occurs exclusively at the metal/film interface, with this interface advancing into the metal phase. This interface is considered to be planar and perpendicular to the direction of film growth. The mathematical problem presented here is clearly a linear one, since growth takes place in one direction only. Since we have assumed that movement of oxide vacancies only is responsible for growth of the film, the rate of film thickening (dL/dt) may be written as

metal surfaces. The theoretical equations were simplified involving certain assumptions (1), as a first step in the development of the model. The theoretical results obtained were then compared with experimental data, and the agreement was sufficiently good to warrant further development. In formulating this model, the following processes are considered to occur at the two interfaces during growth of the film.

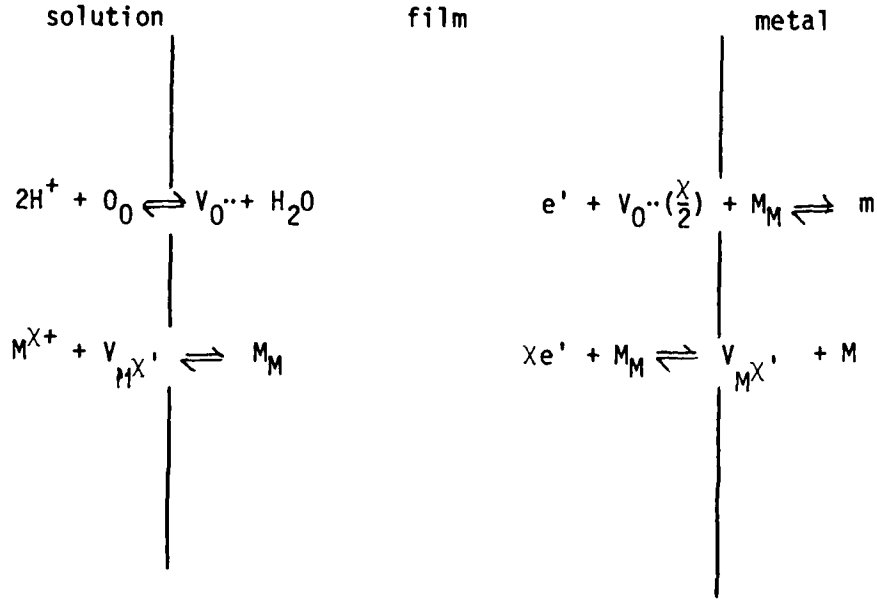

Any general model is characterized by the following features:

i) The species present are $V_{M^{X'}}$ (metal vacancies); $V_O^{\cdot\cdot}$(oxygen vacancies; e' (electrons); $\dot{h}$ (holes).

ii) The various species interact with one another.

iii) Movement of these species within the passive film is described by the Nernst-Planck equation.

iv) The interfaces exist under non-equilibrium conditions.

v) The field strength within the film may be a function of distance and time.

SECTION 4

THEORETICAL DEVELOPMENT OF POINT DEFECT MODEL

In parallel with the experimental studies reported in the previous sections, the development has continued of a point defect model for the growth and breakdown of passive films on metal surfaces. These developments stem from the initial work of Chao and co-workers (1-3), and involve principally the relaxation of certain simplifying assumptions in the original model and an extension of the theories to take into account the semi-conductor properties of passive films. This new model is far from complete; however, the basic concepts have been sufficiently well developed as to be presented in detail in this final report.

The theoretical modeling work on film growth has been carried out at three levels of sophistication. At the first level (Subtask 4.1) only one mobile species and a constant electric field strength is considered, whereas in Subtask 4.2 six charged species are considered with the film in a quasi steady-state, and accordingly, film growth is not included directly in the mathematical description. This model was developed to explore the dependence of the electrical and electronic properties of passive films on the concentrations of charge carriers. Finally (Subtask 4.3) the general point defect model is extended to consider the effect of minor alloying elements on passivity breakdown. This latter "solute-vacancy interaction model" represents a major departure from traditional theories for the role(s) played by minor alloying elements in the breakdown of passivity at metal surfaces.

4.1 FIRST ORDER POINT DEFECT MODEL

Introduction

Assumption

A model based on the movement of point defects in an electrostatic field has been proposed (1-3) to interpret the growth behavior of passive films on

1) Comparing the passivity breakdown behaviors (V_b) of the films grown in chloride-free and chloride-containing solutions suggests that chloride ions modify the properties of the passive film such that sharp breakdown is not observed.

2) The film breakdown potential is found to increase linearly with the sweep rate for five different chloride concentrations, although the slope varies with the chloride concentration.

3) The critical pitting potential is proportional to the logarithm of the chloride concentration as

$$V_c(V_{SCE}) = 0.24 - 0.22 \log[Cl^-]$$

According to the point defect model, the constant α for single crystal nickel (100) in borate buffer solution is calculated from equation (2) as 0.27.

4) Induction time is obtained for chloride concentration of 0.2 mole/liter at twelve different overpotentials. The relation between the induction time and overpotential qualitatively agrees with the point defect model. Quantitative agreement, e.g. the value of constant α, cannot be determined because of the unknown constant ξ' in the equation (5).

b. log t vs ΔV

The point defect model derived the relationship between the induction time and the overpotential as

$$t = \xi' \left[\exp\left(\frac{\chi F \alpha \Delta V}{2RT}\right) - 1 \right]^{-1} + \tau \qquad (5)$$

where τ was the contribution of transient period, χ was the number of charge on nickel cation, and

$$\xi' = \xi / J^{\circ}\, u^{-\chi/2}\, ([Cl^-])^{\chi/2} \exp \frac{\chi F \alpha \Delta V_c}{2RT} \qquad (6)$$

where J°, u, and ξ were constants.

Figure 12c showed the plot of log t versus ΔV. At large ΔV the induction time approached the limiting value of τ which was estimated at 4 seconds in this case. Substituting $\chi=2$, $\tau=4$, and constants R,T, and F, equation (5) became

$$t - 4 = \xi' \, [\exp(39 \times \Delta V \times \alpha) - 1]^{-1} \qquad (7)$$

By adjusting the values of α and ξ', curves like the one on Figure 12c could be drawn which had fairly good agreement with the experimental data. However, the value of α could not be determined unambiguously because the constant ξ was unknown.

Summary

During the second year of this research, the passivity breakdown of single crystal nickel (100) has been studied under carefully controlled experimental conditions. The results may be summarized as follows:

iii) Reasonable Estimates

$C(L_o,0)(m/f) = 1.42 \times 10^{24}\ cm^{-3}$ from Eq. (8)

$C(0,0)(f/s) = 10^{12}\ cm^{-3}$ from Eq. (9)

$\Delta G_2^\circ = -60,000$ J/coul from Eq. (8)

iv) Values chosen such that agreement exists between the experimental and theoretical initial thickness as a function of applied potential.

$L_o = 20\ \mathring{A}$ from Eq. (11)

$\phi_{f/s}^\circ = 0.38$ V from Eq. (11)

$\phi_R = 0.27$ V from Eq. (11)

$\phi_f = 0.2$ V from Eq. (11)

The parameters that were adjusted to obtain agreement between theory and experiment for the initial thickness of the film given by Chao et al. (1), are as follows: Thickness at the initial potential (-0.4 V) after one hour of polarization, L_o, initial potential at the film/solution interface, $\phi_{f/s}^\circ$; initial concentration of ionized vacancies at metal/film interface, $C(L_o,0)(m/f)$; reference potential, ϕ_R; and the potential drop through the film, ϕ_f. Accordingly, the first point calculated theoretically (thickness versus applied potential) corresponds to the initial point in the plot obtained from the experimental data quoted by Chao et al (1). The subsequent values of thickness, L, for a polarization time of one hour as a function of applied potential, V_{ext}, calculated from the model are compared with experimental data in Table 4 and in Figure 14. It is apparent that the theoretical points are close to the experimental ones, and in both cases the dependency of film thickness on potential is linear.

Figure 15 shows the growth of the film as a function of time. The film grows at the metal/film interface upon stepping the potential from -0.4 V to 0.785 V with an initial thickness of $L_o = 20\ \mathring{A}$. After one hour of growth at a potential of 0.785 V, the thickness is close to 48 $\mathring{A}$. The film starts to grow slowly, then more rapidly, and finally reaches a plateau at much longer times (not shown). This behavior is in agreement with experimental observations (2).

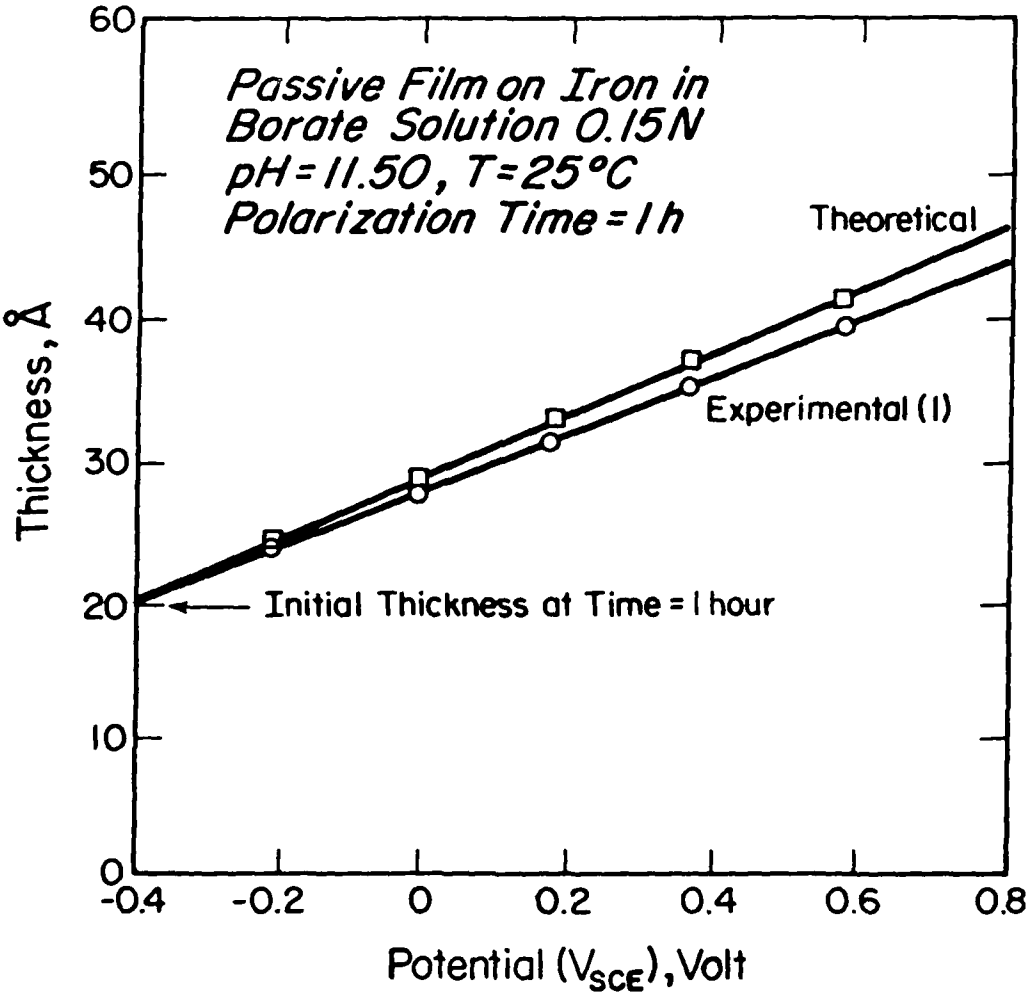

Figure 14. Film thickness as a function of external potential for the passive film on iron in borate buffer solution. Film thickness calculated after one hour of polarization.

The concentration of oxygen ion vacancies at the metal/film interface during the growth of Fe_2O_3 on iron under the same conditions shown in Figure 15 is shown as a function of film thickness in Figure 16. The increase in the interfacial oxygen ion concentration is a direct consequence of Equation (8) because of the decrease in $\phi_{m/f}$ as the film thickens. Note that in this first-order model, it is assumed that equilibrium exists at both interfaces with respect to the point defects.

Table 4

Experimental and Theoretical Values for the Thickness of the Passive Film On Iron in Borate Buffer Solution After 1 hr of Polarization
(See Reference (1) for a discussion of the Experimental Data.)

Experimental		Theoretical	
Potential (V)	Thickness (Å)	Potential (V)	Thickness (Å)
-0.4*	20*	-0.4050*	20.10*
-0.2	24	-0.2300	24.11
0.0	28	-0.0150	29.11
+0.2	32	+0.1960	34.04
+0.4	36	+0.4110	39.07
+0.6	40	+0.6515	44.70
+0.8	44	+0.7846	47.84

* Values adjusted (-0.4050, 20.1) to experimental first point (-0.4, 20)

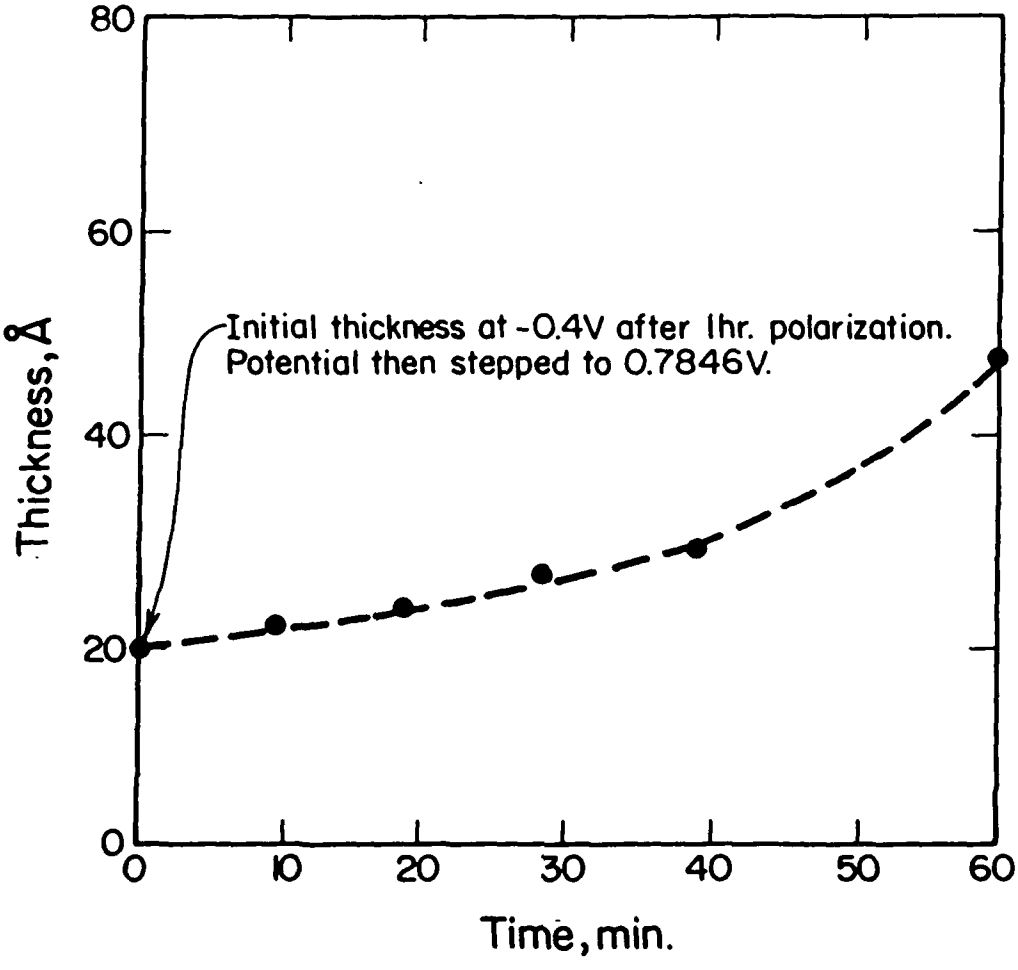

Figure 15. Theoretical growth of the passive film (Fe_2O_3) as a function of time, for iron in borate buffer solution. Condition as in Figure 14.

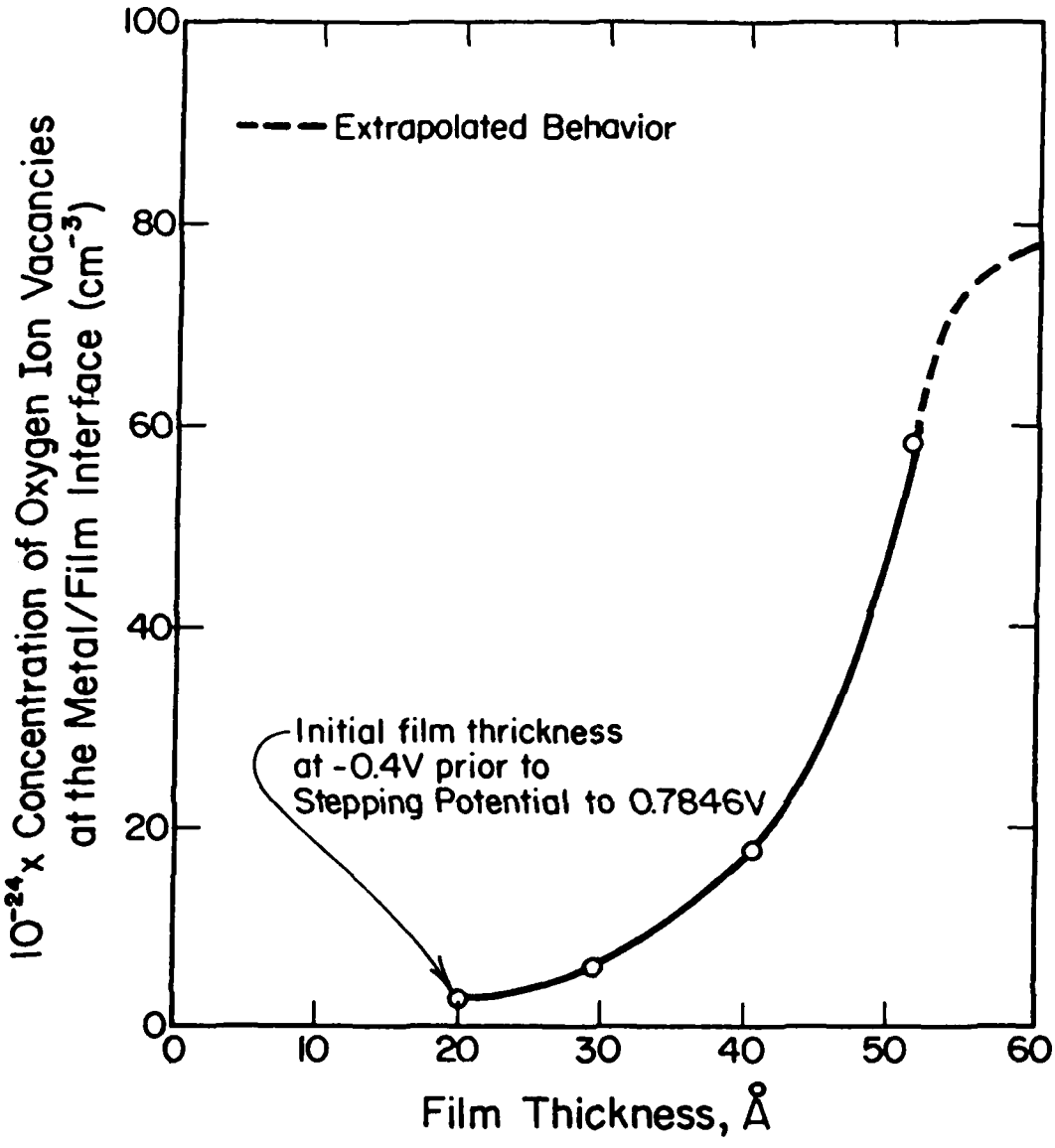

Figure 16. Concentration of oxygen ion vacancies at the metal/film interface as a function of film thickness according to the first order point defect model. The calculations are for an Fe_2O_3 film on iron in borate buffer solution under the conditions stated in Figure 14.

2. Nickel ($Ni-Ni(OH)_2$)

Experimental and theoretical data have been discussed by Macdonald et al. (6) for the growth of passive films on nickel over a wide range of pH (1.5-12.6) in phosphate solution. The results show that the solution pH has a strong influence on the formation and growth of passive films. However, it was reported that in basic solutions (pH: 9.1-12.6), and in moderately acidic solutions (pH = 4.5), the passive films possess the same optical constants, but exhibit different growth behaviors. The experimental film thickness values were plotted against time in accordance with the logarithmic, the inverse logarithmic, and parabolic laws, for different values of applied potential(6). It was apparent that different growth laws apply during the various stages of growth.

Using the rate law developed from the point defect model, and by comparing the experimental data presented in reference (6) with this rate law, it is possible to fit the parameters used in the theoretical model in order to obtain an estimate of the film thickness at the initial time (1 minute of polarization). Table 5 summarizes values for film thickness at different times, as computed from the experimental data reported by Macdonald et al (6), as well as theoretical values obtained from the first order point defect model. The values presented in Table 5 correspond to passivation of nickel in a 0.05M NaH_2PO_4 (pH = 4.5) solution at 25°C and at an applied voltage of 1.24 V (vs SCE).

In order to adjust the initial thickness (i.e., that at 1 min.) calculated from the model, so that it coincides with the experimental data, the values chosen for the parameters are as follows:

Electric field strength (ε) = 1.4×10^{6} V/cm

Initial thickness (L_o) = 16×10^{-8} cm

Coefficient of diffusion (D) = 1.3×10^{-17} cm^2/s

Concentration of oxygen ion vacancies:

(i) At film/solution interface, $C(f/s) = 10^{12}$ cm^{-3}

(ii) At metal/film interface, $C(m/f) = 0.74 \times 10^{22}$ cm^{-3}

Table 5

Experimental and Theortical Values for Growth of Nickel Oxide Film on Nickel Phosphate Solution (V = 1.24 V vs SCE, pH = 4.85, T = 25°C)

From Reference (6)		From first order Point Defect Model	
Thickness (Å)	t(min)	Thickness (Å)	t(min)
16.3	1	16.3	1
18.5	3	16.9	3
25.0	10	19.2	10
27.5	15	20.8	15
29.5	20	22.6	20
33.0	30	29.1	30

All of these values are considered to be physically reasonable. Also, the electrical field strength is of the order of that required for electron/hole pair generation and subsequent field buffering, as assumed in the point defect model, and the initial thickness reasonably approximates that for an air-formed film. The concentration of oxygen ion vacancies at the film/solution interface is very low, as expected, because of their reaction with water molecules. The concentration of oxygen ion vacancies at the metal/film interface corresponds to about 25% of the oxygen ion sites being vacant; a requirement that also seems to be eminently reasonable. Figure 17 shows experimental and theoretical plots for the growth of the passive film as a function of time. Although significant differences exist between both data sets, the form of the change in film thickness with time is the same in both cases. It is assumed that better agreement could have been obtained by

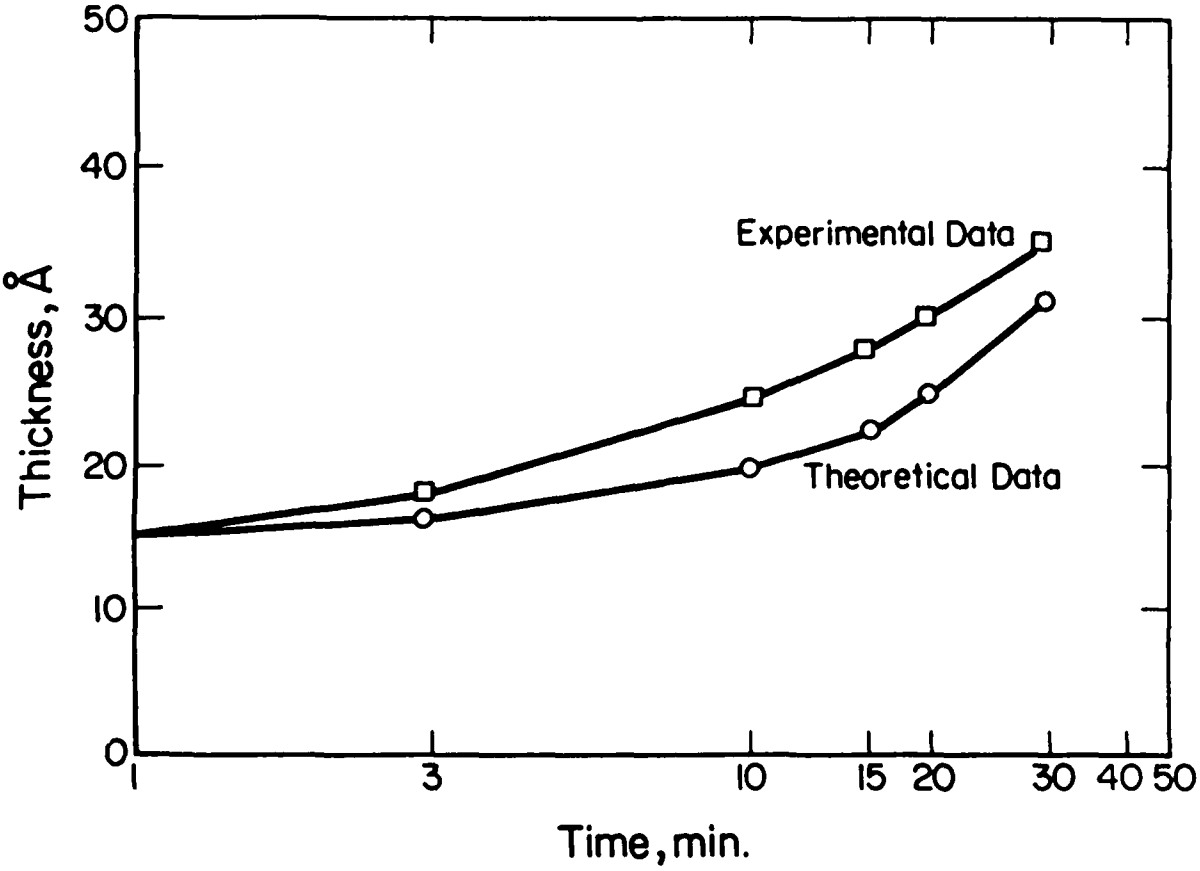

Figure 17. Theoretical and experimental data for the growth of the passive film on nickel in 0.1 N $Na_2H_2PO_4$ (pH = 4.85) solution at 25°C and at an applied voltage of 1.24 (V vs SCE).

further refinement of some of the parameters in the model, but this would have proven little of physical significance.

Because some of the parameters used in calculating the film thickness from the first order point defect model are not well-known, it is necessary to carry out a sensitivity study of the model in order to determine how the calculated film thickness responds to each of the parameters of interest. This is done by varying each of the parameters in turn over a wide range.

Sensitivity Study

The sensitivity study was carried out using the mathematical model described in the previous section. The values of some of the parameters used for calculating the properties of the passive film formed on iron in borate solution were varied systematically, and the rate of growth of the film and changes in the concentration of oxygen ion vacancies were observed. The parameters chosen for variation in this analysis were the oxygen ion vacancy concentration at the metal film interface, and the vacancy diffusivity. These parameters were varied over the ranges of 1×10^{22} cm^{-3} to 5×10^{23} cm^{-3} and 1.3×10^{-24} cm^2/s to 1.3×10^{-16} cm^2/s, respectively. The values for the other parameters remained the same as those in the previous section for $Ni(OH)_2$ films on nickel.

Figure 18 shows the sensitivity of the rate of growth of the film to variations in the diffusion coefficient. Clearly, the diffusion coefficient can have a strong effect on the growth kinetics of the passive film on nickel, at least in the case considered. Also, as shown in Figure 19, a range exists in the value of the diffusion coefficient over which this parameter has a profound effect on the kinetics of film growth. This range appears to include the likely values for the diffusivity of oxygen ion vacancies, although some data indicate that D is of the order of 10^{-21} cm^2/s (1).

A better understanding of the behavior observed in Figure 19 is obtained if the structure of Equation (19) is studied, which relates the growth of the film to the diffusion coefficient. Equation (19) can be written as follows

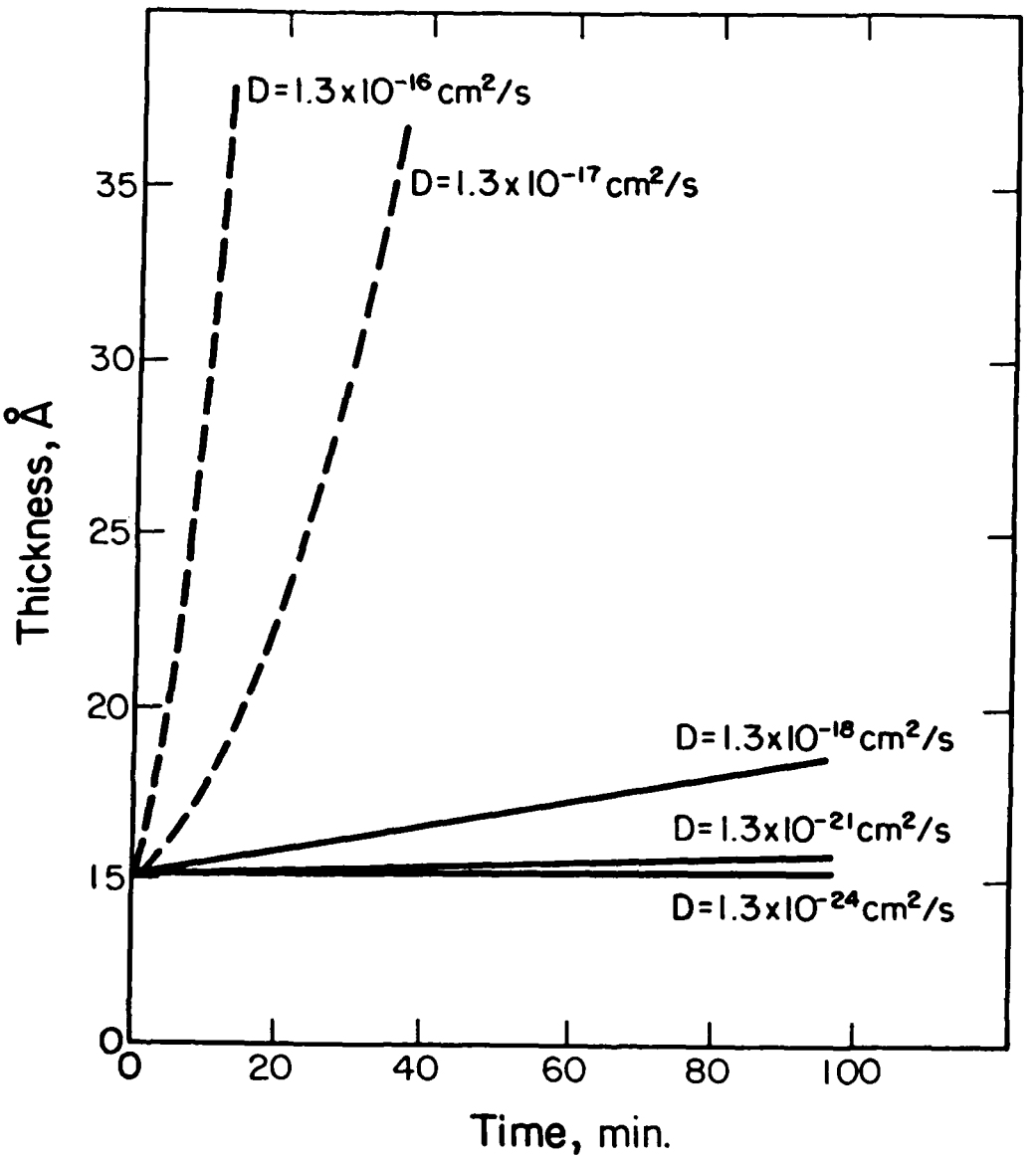

Figure 18. Variation of film thickness and oxygen ion vacancy concentration as a function of time, for different values of the vacancy diffusion coefficient.

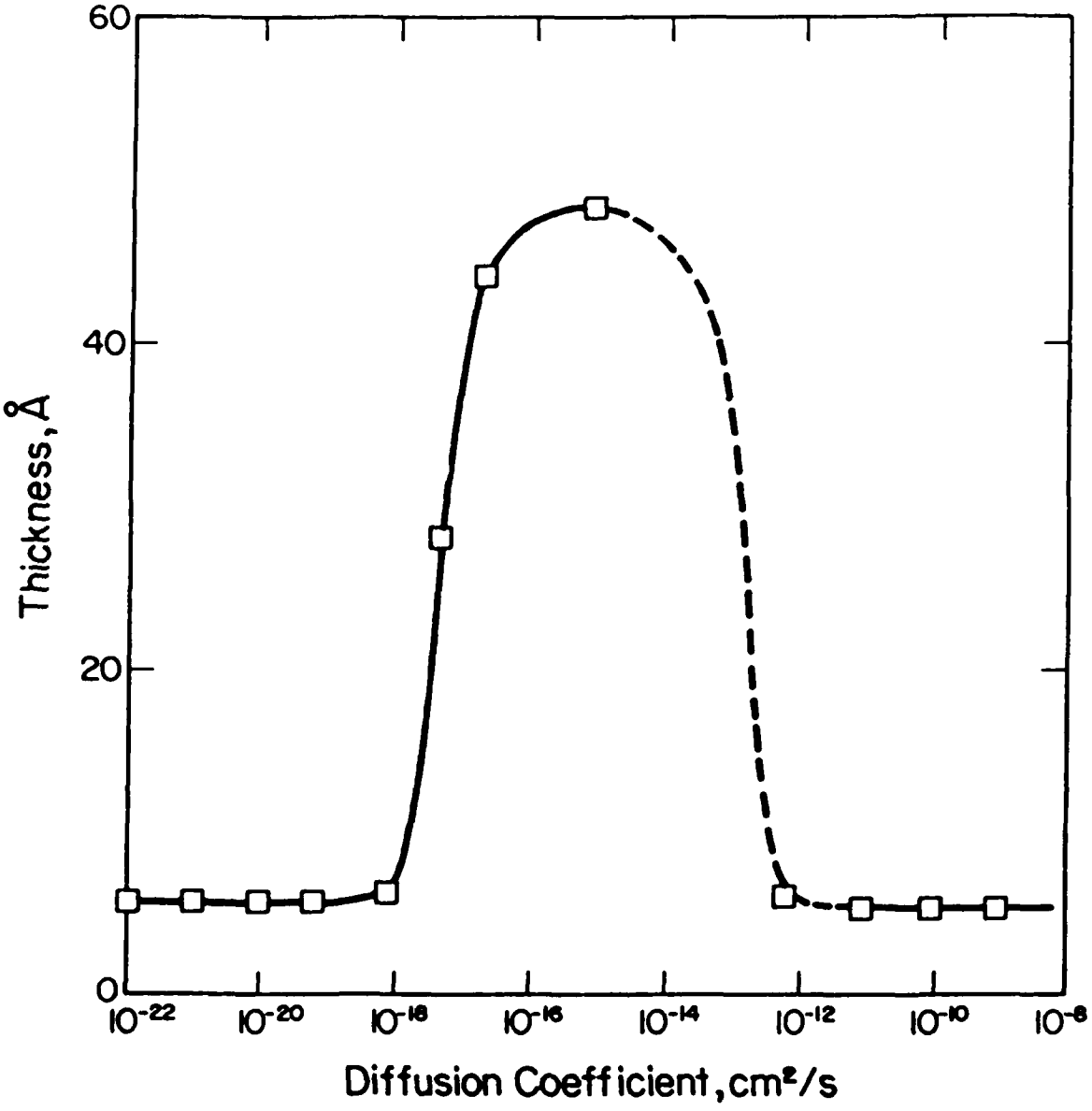

Figure 19. Calculated thickness of the passive film on nickel as a function of the diffusion coefficient. Polarization time = 30 min, other parameters as indicated in the text.

$$\frac{dL}{dt} = AD(B + CL)\exp(-\alpha Dt)\exp(\beta L)$$

where, for the present purposes, A, B, C, α, and β will be considered to be constants. Equation (19) predicts the following behaviors:

i) If $D \rightarrow 0 \longrightarrow dL/dt \rightarrow 0$ (i.e., the film doesn't grow, if L remains finite)

ii) If $D \rightarrow \infty \rightarrow dL/dt \rightarrow 0$ (again, the film doesn't grow, if L remains finite)

iii) There exists a value for D such that dL/dt goes to a maximum. This value is identified in Figure 19.

We have yet to fully appreciate the physical implications (if any) of (ii) and (iii) above, but that indicated by (i) is quite obvious. It may well be that (ii) is a mathematical artifact; a possibility that should be considered in future work. Figure 20 shows the thickness as a function of time for different values of initial concentrations of oxygen vacancies at the metal/film interfaces. Although this parameter is strictly not an independent variable since it depends upon the applied voltage (see Equations (8) and (11)) it is apparent from the data in Figure 20 that the rate of film growth is extraordinarily sensitive to variations in the concentration of oxygen ion vacancies at the metal/film interface.

Kinetics of Film Growth

Over the past several decades, a great deal of effort has been invested to explain the kinetics in the growth of anodic passive films. A number of empirical-theoretical rate laws have been proposed; the best known being the "logarithim law" and the "inverse logarithim law". In this section, a comparison is presented of the two rate laws in terms of the mathematical and physical structure of the first order point defect model presented earlier in this report.

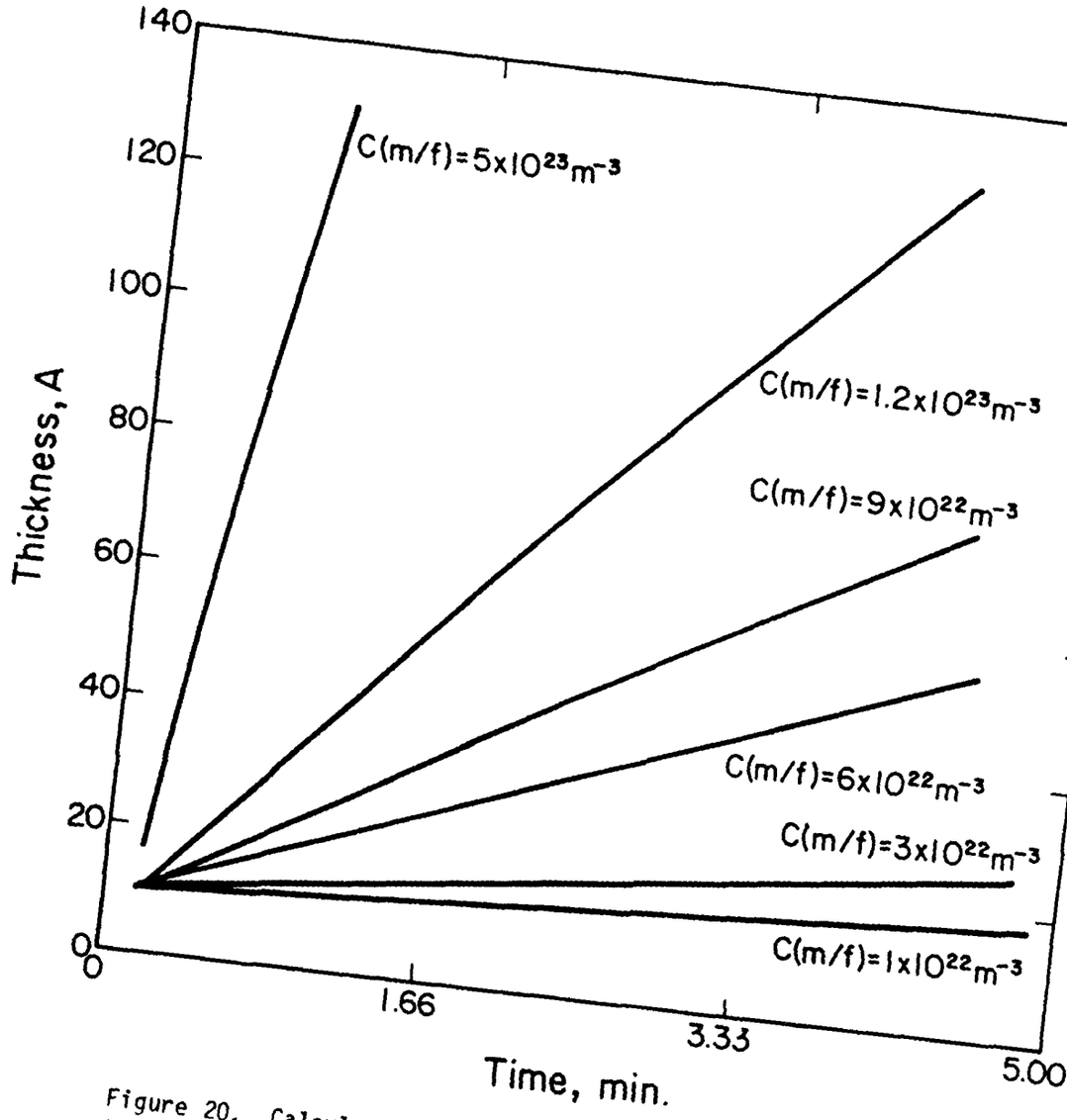

Figure 20. Calculated film thickness for $Ni(OH)_2$ on nickel as a function of time, for different values of concentration of oxygen ion vacancies at the metal/film interface. Other parameters as indicated in the text.

general analysis of Equation (18) allows the prediction of the form of ate of growth of the film as a function of time. From previous analysis, ion (18) can be written as follows:

$$C(x,t) = (A + Bx)\exp(-\beta t)\exp(\alpha x) \tag{21}$$

e A, B, β, and α are considered to be constants for the present purpose. rdingly, the growth of the film is expressed as

$$dL/dt = (A + BL)\exp(-\alpha' t)\exp(\beta L) \tag{22}$$

$$A = \frac{\Omega}{n_v}\left[\frac{Dqk}{2}\, C(f/s) - D\,\frac{C(f/m)\exp(-qkL_o/2) - C(f/s)}{L_o}\right]$$

$$B = \frac{\Omega}{n_v}\left[\frac{Dqk}{2}\left(\frac{C(f/m)\exp[(-qk/2)L_o] - C(f/s)}{L_o}\right)\right]$$

$$\beta = \frac{qk}{2}$$

$$\alpha' = \frac{q^2k^2D}{4}$$

orm of the equation shows that

i) for $t \rightarrow +\infty$, $dL/dt \rightarrow +0$

i) $t \rightarrow +0$, $dL/dt \rightarrow$ constant

i) $d^2L/dt^2 = 0$, inflexion point

eneral shape of the curve $L = f(t)$ can be presented by the plot shown in e 21. The form of the rate equation shown in this figure will now be

0) = 10^{14} m^{-3}

L) = 10^{14} m^{-3}

L) = 1014 m^{-3}

L) = 10^{24} m^{-3}

L) = 10^{24} m^{-3}

nally, it is necessary to specify tolerances for $\emptyset$, the potential, and
or ε, the field strength.

rameter	Tolerance**	Initial Value
$\emptyset_f$*	2×10^{-7}%	5×10^{-2} V
ε	10^{-5}%	10^{8} V/m

ltage drop across the film.
of initial values

ts

he algorithim used in these calculations was developed for and executed
Apple IIe≠ microcomputer. The algorithim was executed for both sets of
ary conditions discussed above, and the resultant electric field strength
oltage, $\Delta\emptyset$ (where $\Delta\emptyset = [\varepsilon^j(x) - \varepsilon^o]\Delta x$) are plotted in Figures 24 and 25,
ctively. This latter quantity is a measure of the deviation of the
tial from the constant field approximation, and hence is a direct
ator of the importance of space charge. From Figures 24 and 25 it is
ent that space charge is far less important when the electrical
ality constraint is invoked than when it isn't. This same behavior was
by many sets of data, the results of which are not displayed here (see
section).

---

demark of Apple Computer, Inc., Cupertino, California

$$-2\,C_D(0) - C_{D+}(0) + 2\,C_A(L) + C_{A-}(L) - \Delta n + \Delta p \tilde{\gtrless} 0$$

ere L represents the metal/film interface and 0 the film/solution interface.

As far as the boundary conditions are concerned, the concentrations of ch of the species at the two interfaces must be specified. Accordingly, the undary conditions are simply stated as follows:

Δn: density of electrons across the film = 10^{24} m^{-3}

Δp: density of holes across the film = 10^{24} m^{-3}

$C_{D+}(0)$: density of C_D+ at f/s interface = 10^{24} m^{-3}

$C_D(0)$: density of C_D at f/s interface = 10^{24} m^{-3}

$C_{A-}(0)$: density of C_A- at f/s interface = 10^{14} m^{-3}

$C_A(0)$: density of C_A at f/s interface = 10^{14} m^{-3}

$C_{D+}(L)$: density of C_D+ at m/f interface = 10^{14} m^{-3}

$C_D(L)$: density of C_D at m/f interface = 10^{14} m^{-3}

$C_{A-}(L)$: density of C_A- at m/f interface = 10^{24} m^{-3}

$C_A(L)$: density of C_A at m/f interface = 10^{24} m^{-3}

ese values have been chosen such that electrical neutrality is obeyed.

A second set of boundary conditions was chosen without regard for ctrical neutrality. This was done to explore the commonly-involved uation in calculations of this type of not requiring the film as a whole to electrically neutral. The boundary conditions chosen in this case are as lows:

$\Delta n = 10^{24}\ m^{-3}$

$\Delta p = 10^{25}\ m^{-3}$

$_{D+}(0) = 10^{24}\ m^{-3}$

$C_D(0) = 10^{24}\ m^{-3}$

$_{A-}(0) = 10^{24}\ m^{-3}$

$_1$: number of charges for specie C_{D+} = 1
$_2$: number of charges for specie C_D = 2
$_3$: number of charges for specie C_{A^-} = -1
$_4$: number of charges for specie C_A = -2
$_o$: initial thickness = 1Å
$_F$: Final thickness = 5Å
): Potential at film/solution interface = 0.01 V
.): Potential at metal/film interface = 0.05 V

that the thickness of the film has been set at 5A, which represents the nsion expected for the very thin films which form on metals and alloys as nickel*, iron and stainless steels under some conditions.

In addition to the normal boundary conditions, the film must be trically neutral, i.e.,

$$\int_0^L q_D \left(\frac{\partial C_D}{\partial x}\right)dx + \int_0^L q_{D+} \left(\frac{\partial C_{D^+}}{\partial x}\right)dx + \int_0^L q_A \left(\frac{\partial C_A}{\partial x}\right)dx$$

$$\int_0^L q_{A^-}\left(\frac{\partial C_{A^-}}{\partial x}\right)dx + \int_0^L e\left(\frac{\partial p}{\partial \phi}\right)\epsilon(x)\ dx - \int_0^L e\left(\frac{\partial n}{\partial \phi}\right)\epsilon(x)\ dx = 0 \qquad (35)$$

use only the steady state condition is considered, the concentrations are functions of x, so that the partial differentials become normal erentials and it is possible to write Equation (35) as:

$$q_D[C_D(L) - C_D(0)] + q_{D+}[C_{D+}(L) - C_{D+}(0)] + q_A[C_A(L) - C_A(0)]$$

$$+ q_{A^-}[C_{A^-}(0) - C_{A^-}(0)] - en_o + ep_o \tilde{\sim} 0$$

ese values were deduced from the experimental data obtained for ssive films on Ni (18), $\Delta\phi/\Delta x = 10^6$ V/cm.

$$\frac{\partial^2 \emptyset}{\partial x^2} = -\frac{1}{\delta \xi} \Big\{ ep_o \exp(-\beta\emptyset) - en_o \exp(\beta\emptyset) + A_1 \exp\left[-q_1 k\left(\frac{\partial \emptyset}{\partial x}\right) X\right]$$

$$+ A_2 \exp\left[-q_2 k\left(\frac{\partial \emptyset}{\partial x}\right) x\right]$$

$$+ A_3 \exp\left[-q_3 k\left(\frac{\partial \emptyset}{\partial x}\right) x\right] + A_4 \exp\left[-q_4 k\left(\frac{\partial \emptyset}{\partial x}\right) x\right]$$

$$+ q_1 B_1 + q_2 B_2 + q_3 B_3 + Q_4 B_4 \Big\} \qquad (33)$$

Equation (28) can be expressed in general form as

$$\frac{\partial^2 \emptyset}{\partial x^2} = f\left(\frac{\partial \emptyset}{\partial x}, \emptyset, x\right) \qquad (34)$$

It is possible to construct an algorithim to solve for $\emptyset$, in which the initial filed strength (ε°) is considered to be constant. The value obtained is then used in Equation (33) to determine a new value for ε (i.e. $\varepsilon(x)$), and so forth for j iterations. The ε^j and $\varepsilon^{(j-1)}$ values are compared and if the difference is less than a preselected tolerance, the value $\varepsilon^j(x)$ is taken as representing the electric field strength within the film at point x.

In order to employ the algorithim outlined above, we must choose values for the various constants used in the equations and specified in the boundary conditions. Also the tolerance that will be used in the numerical model must be specified.

The constants of interest are as follows:

F: Faraday constant = 96487 coul/mol
R: general constant of gases = 8.314 Joule/mol°k
T: temperature = 298°K
δ: dielectric constant for oxide iron film = 3.9
ξ: dielectric constant of vacuum = 8.85419 X 10^{-12} joule/mol
e: electron charge = 1.6 X 10^{-19} coulombs
K: Boltzman constant = 1.38 x 10^{-23} Joule/°kmol

$$\nabla^2\phi = (1/\xi\cdot\delta)\,[q_{D+}\cdot C_{D+}(x) + q_D\cdot C_D(x) + q_A\cdot C_A(x) + q_{A^-}\cdot C_{A^-}(x)$$

$$- e.n + e.p] \qquad (27)$$

here ξ is the dielectric constant of the film. At steady-state, Fick's econd law for the diffusion and electromigration of charged species can be ritten as follows

$$0 = D_i \frac{\partial^2 C_i}{\partial x^2} - D_i q_i k \frac{\partial C_i}{\partial x} \qquad (28\text{-}31)$$

here i = 1,2,3,4 (i.e. for species C_D, C_{D^+}, C_A, C_{A^-}). Accordingly, the athematical problem of solving for the seven unkowns (C_1, C_2, C_3, C_4, n, , ε) requires seven independent equations given by Equations (24-31). It is mportant to note that Equations (27-31) involve coupled non-linear second rder differential equations. These must be solved numerically.

As a first step, consider that $\varepsilon = -d\phi/dx$ = constant. Therefore, from quations (28-31) it is possible to obtain a solution for the concentration of ach species of the form

$$C_i = A_i \exp(q_i k\, \varepsilon x) + B_i \qquad (32)$$

here A_i and B_i are integral constants and are functions of the boundary onditions for each species considered.

Substitution of Equation (32) into Equation (27) permits the derivation of non-linear second order differential equation which may be solved umerically for the potential ϕ

The species considered are

concentration	species	charge
C_D	donors ($V_{M}^{\chi\cdot}$)	- e
C_D^+	ionized donors ($V_{M(\chi-1)}'$)	$-(\chi-1)e$
C_A	acceptors ($V_O^{\cdot\cdot}$)	+2e
C_A^-	ionized acceptors ($V_O^{\cdot\cdot}$)	+e
n	electron (e)	-e
p	holes (h)	+e

Numerical Analysis

Consider that 6 species are involved in various reactions that take place at the film/solution and metal/film interfaces. The species correspond to C_A(acceptors), C_A-(ionized acceptors), C_D(donors), C_D+(ionized donors), electron, and holes. It is supposed that the concentrations of the ionized and unionized vacancies (C_A, C_A^-, C_D, C_D+) follow Fick's second law of diffusion, and that electron and holes exist under equilibrium conditions. Hence, their concentrations are given to first approximation by the Boltzman expressions (28)

$$n = n_o \exp(+\beta\phi) \tag{24}$$

$$P = P_o \exp(-\beta\phi) \tag{25}$$

where n is the concentration of electrons through the film, P is the concentration of holes through the film; n_o, P_o, and β are constants; and ϕ is the potential at any given point in the film. The electrical potential in the oxide is governed by the density of free charge (i.e. the "space charge") according to Poisson's equation:

$$\nabla^2 \phi = -\frac{\rho}{\xi\delta} \tag{26}$$

or

The species considered are donors ($V_{M^{\chi\cdot}}$), ionized donors ($V_{M^{(\chi-1)\cdot}}$), acceptors ($V_{O}^{\cdot\cdot}$), ionized acceptors ($V_{O}^{\cdot\cdot}$), electrons (e') and holes (h). These calculations permit the estimation of the field strength through the film, and to determine how the field strength is affected by changing the concentrations of various species, i.e. by varying the boundary conditions. Also, the results allow the determination of the conditions under which space charge within the film is important, and hence to specify the conditions under which the constant field strength hypothesis might be valid. It should be mentioned that the results obtained in this sub-task will be applicable only to steady-state films, and cannot be used to examine the effect of space charge on growing oxide films.

Since electrons and holes are obviously present in anodic films, and are intimately associated with the presence of donor and acceptor impurities, it is fitting to enquire into the roles that all of these species may play in determining the electronic and defect structure. The model adopted for this purpose can be represented as follows:

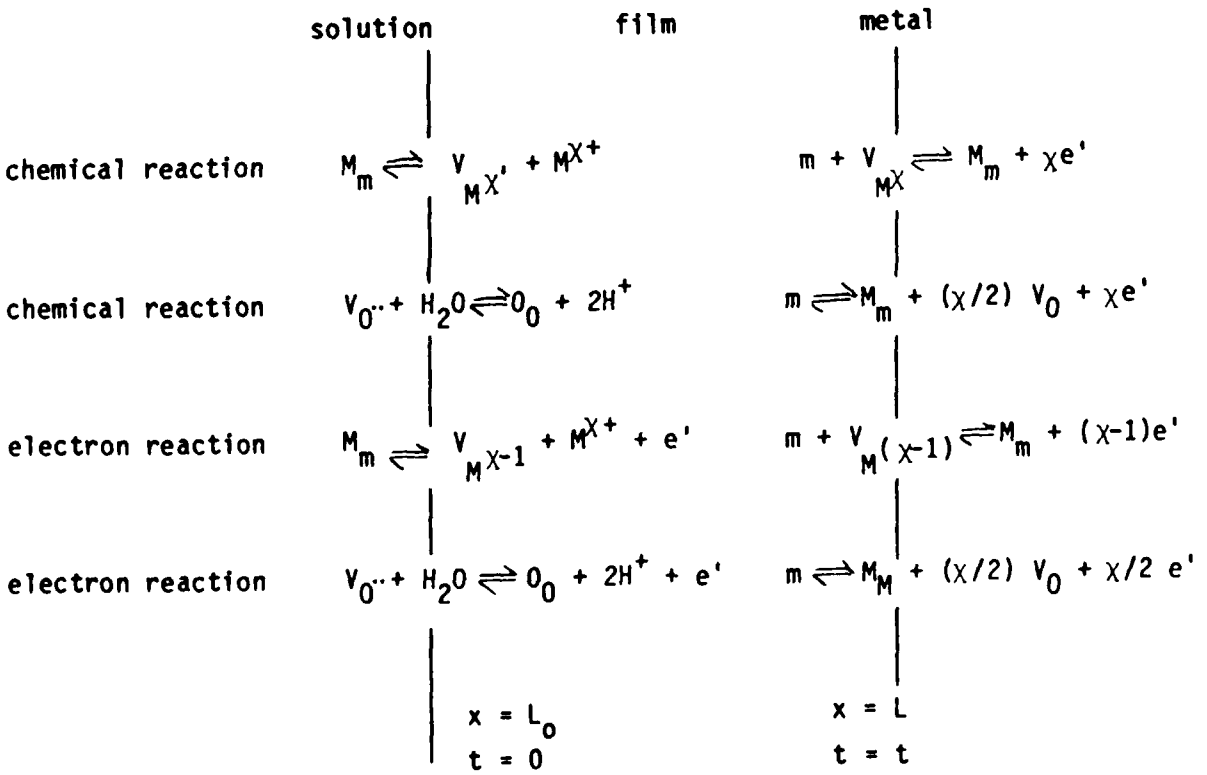

in the model, including anion vacancies ($V_{O}^{\cdot\cdot}$), cation vacancies ($V_{M}^{\chi'}$), electron (e') and holes ($\dot{h}$). Additionally, it is proposed that the oxide possesses the normal electronic band structure which characterizes classical semiconducting materials, but that the anion vacancies and cation vacancies act as electron acceptors and donors, respectively. Thus, in terms of energy, these species are assumed to occupy positions within the band gap, and because the concentrations of the vacancies are very high (10^{20} cm^{-3} vs. 10^{16} cm^{-3} for dopants in a classical semiconductor) the electonic properties of the film are expected to be dominated by the defect structure. The picture is further complicated by the fact that the vacancies are not uniformily distributed across tne film. Thus, in our view, a passive film is best described as a highly-doped n-type/p-type semiconductor with the material close to the metal/film interface being, on balance, p-type in character whereas that at the film/solution interface is thought to be n-type in character. Clearly, the model that emerges from these considerations is a complex one, but nevertheless is one which can be developed mathematically using techniques which have been employed in semi-conductor physics.

4.2 ROLE OF SPACE CHARGE IN PASSIVE FILMS

Introduction

Space charge in metal oxide films has long been recognized by some authors (24,25), but not others (26,27). This controversy has yet to be resolved, principally because of the lack of a direct experimental method for determining the distribution of charge in very thin films.

In this section, the distribution of charge within an anodic oxide film using the point defect model under steady-state conditions is calculated. These calculations differ from those previously reported, in that a much larger number of charged species are considered. A model involving six species under steady-state conditions in which the electric field strength is considered to be a function of distance is presented. The distribution of each species, and hence the space charge, is obtained by solving Fick's second law equation for each species coupled to the Poisson - Boltzmann equation.

(iii) The model also explains why, in some cases, the semi empirical logarithmic and/or inverse logarithmic laws can be fitted satisfactorily to the same experimental data.

From the sensitivity study, the model predicts that the kinetics of growth of the anodic film on nickel is a strong function of the diffusion coefficient of the oxygen ion vacancy. It is well known that, in ionic crystals with impurities, the diffusion coefficient of defects (including vacancies) is a function of both temperature and concentration (20,21). Since the concentration of vacancies changes throughout the film and is a sensitive function of the intitial boundary condition, it is likely that kinetics of the film growth will also depend upon those same factors which determine the vacancy concentration profiles. This may explain, at least in part, why poor reproducibility is often observed in anodic film growth studies. That is, experimentally it is extremely difficult to generate films that have reproducible concentration profiles and hence vacancy diffusion characteristics. Very few experimental data exist (22,23) which allow the establishment of a relationship between the diffusion coefficient and vacancy concentration, and hence between diffusivity and growth of the film. It is believed that these relationships will have to be developed if more accurate descriptions of passive films are to be devised. One experimental technique which shows considerable promise for studying the motion of defects in passive films is the AC impedance method described earlier in this report and discussed at length by Chao, Lin and Macdonald (1).

Finally, it is important to recognize the limitations of the first order point defect model developed in this section. Because only a single mobile species is considered, it is not possible to account for space charge effects in a realistic manner. Also, the model does not consider the electronic structure of the film, so that the semi-conducting properties of many passive films cannot be accounted for. In order to include phenomena such as variable field strength, space charge, dissolution of the film, and optical, electrical, and thermal excitation of electrons, it is necessary to develop a more advanced model which combines the physical and electronic properties of the film. In doing so, all charged species must be included

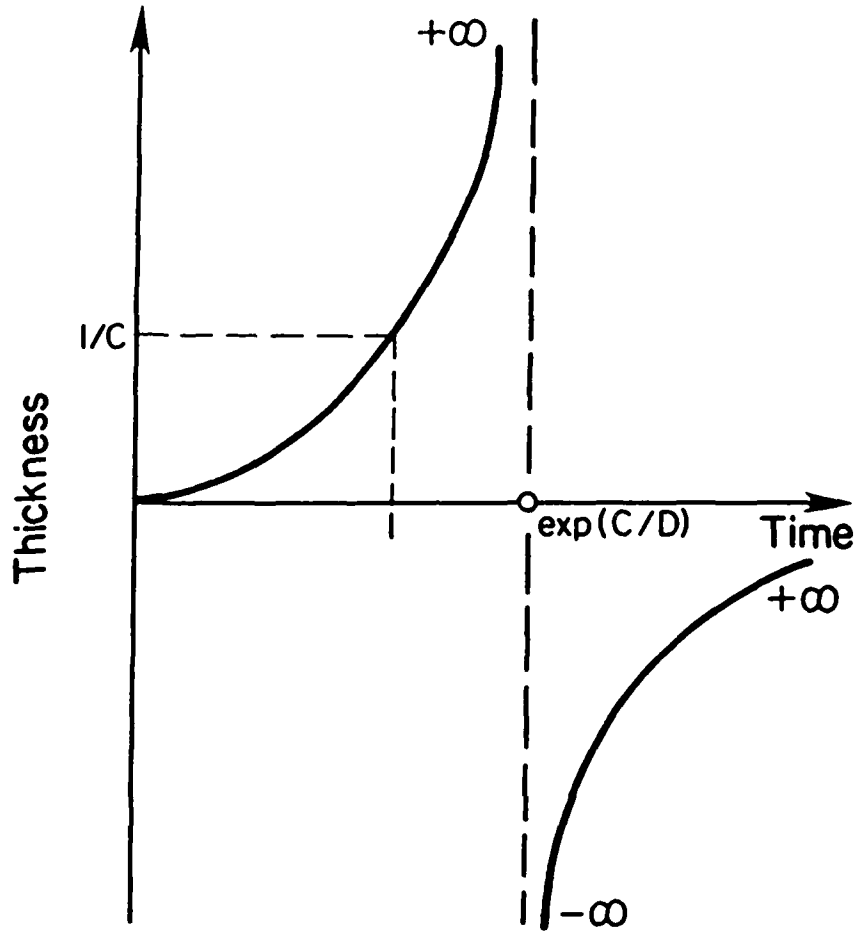

Figure 23. Schematic of film thickness versus time, as predicted by the inverse logarithmic growth law.

(i) $t \rightarrow +0$	$\ln t \rightarrow -\infty$	$L \rightarrow +0$
(ii) $t \rightarrow < \exp(C/D)$	$\ln t \rightarrow < \infty$	$L \rightarrow +\infty$
(iii) $t \rightarrow > \exp(C/D)$	$\ln t \rightarrow > \infty$	$L \rightarrow -\infty$
(iv) $t \rightarrow 1$	$\ln t \rightarrow +0$	$L \rightarrow 1/C$
(v) $t \rightarrow +\infty$	$\ln t \rightarrow +\infty$	$L \rightarrow -0$

These conditions are described by the general function plotted in Figure 23. Note that this function is discontinuous at $t=\exp(C/D)$. It is suggested that the only domain of physical significance is that for $t<\exp(C/D)$; in which case the growth law strongly resembles that predicted for short times ($t<t'$) by Equation (22) (see Figure 21).

Discussion

The results obtained from the first order point defect model developed in this work are sufficiently encouraging to warrant that the model be further explored (see later). Specifically, the simple first order variant has displayed the following features:

(i) The calculated film thickness as a function of V_{ext} follows a relationship which is in good agreement with that obtained from experimental data for iron in borate solution.

(ii) The rate of growth of the passive film on nickel in phosphate solution, as predicted by the first order point defect model, is in good agreement with experimental data (6). Also, while three different laws (logarithmic law, inverse logarithmic law, and the parabolic law) are necessary to explain the growth characteristics of the passive film on nickel in phosphate solution (6), the first order point model is able to account for the growth behavior using a single growth law over the entire range of conditions.

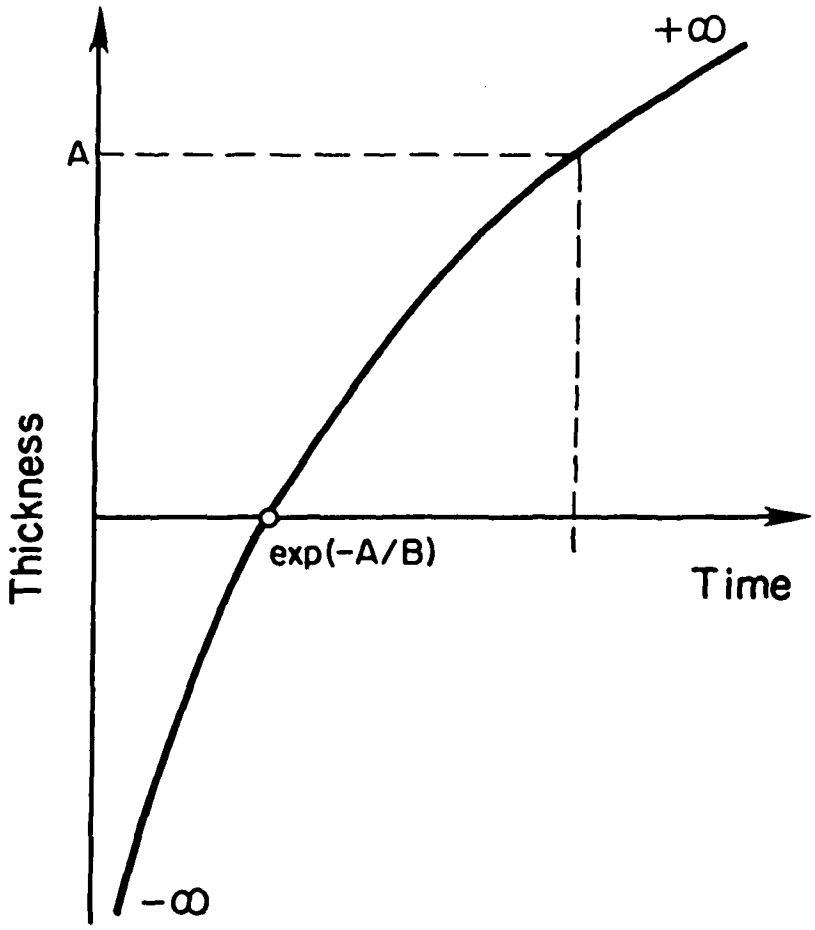

Figure 22. Schematic of film thickness versus time, as predicted by the logarithmic growth law.

compared with those inherent in the empirical/semi-theoretical logarithmic and inverse logarithmic correlations. The purpose of this comparison is to assess how the various integral rate equations differ from one another, and to determine a priori whether or not any one provides a more acceptable correlation between film thickness and time on purely mathematical grounds.

Logarithmic Law

This semi-empirical law may be expressed as follows:

$$L = A + B \cdot \ln t \tag{23}$$

where A and B are constants. A general analysis of this equation reveals the following properties:

(i) $t \longrightarrow +0$ $\quad \ln t \longrightarrow -\infty$ $\quad L \longrightarrow -\infty$

(ii) $t \longrightarrow +\infty$ $\quad \ln t \longrightarrow +\infty$ $\quad L \longrightarrow +\infty$

(iii) $t \longrightarrow 1$ $\quad \ln t \longrightarrow +0$ $\quad L \longrightarrow A$

(iv) $t = \exp(-A/B)$ $\quad L = 0$

The general form of the logarithmic law is therefore represented by the graph shown in Figure 22. The most notable feature of this plot is that it resembles that predicted by Equation (22) at times greater than that at the inflection.

Inverse Logarithmic Law

The inverse logarithmic law is usually expressed as follows:

$$1/L = C - D\ln t$$

where C and D are constants. A general analysis of the inverse logarithmic equation yields the following characteristics:

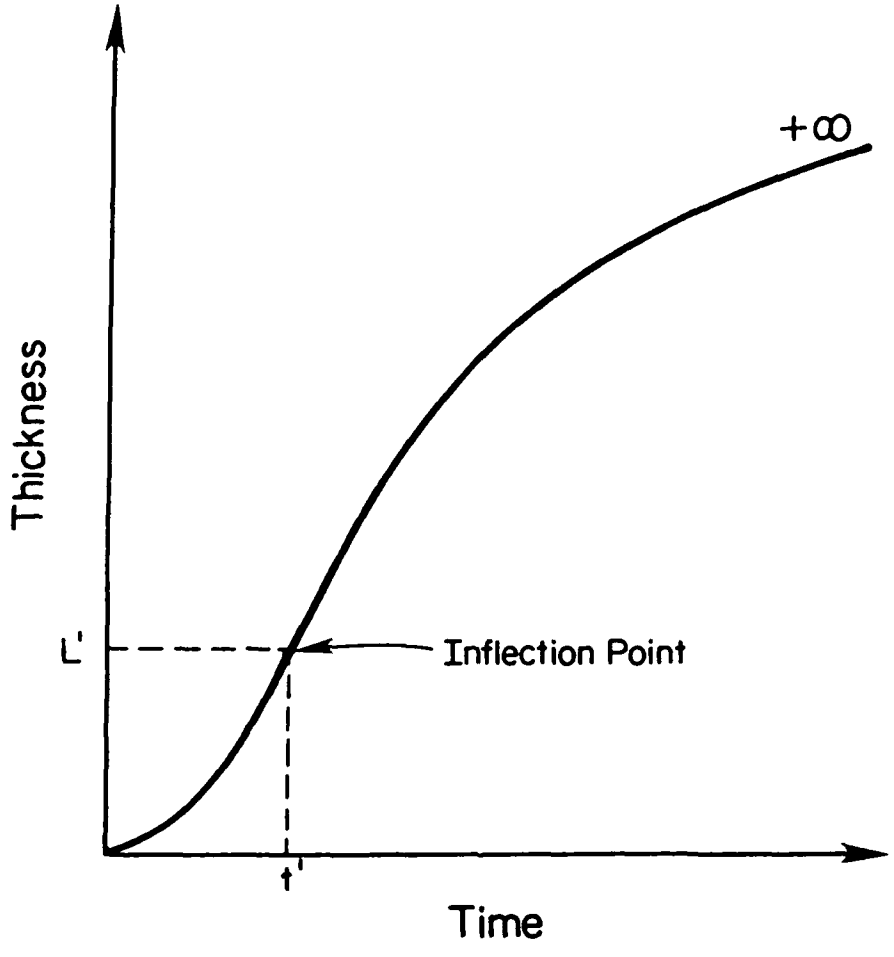

Figure 21. Schematic film thickness versus time, as predicted by the first order point defect model [Equation (22)].

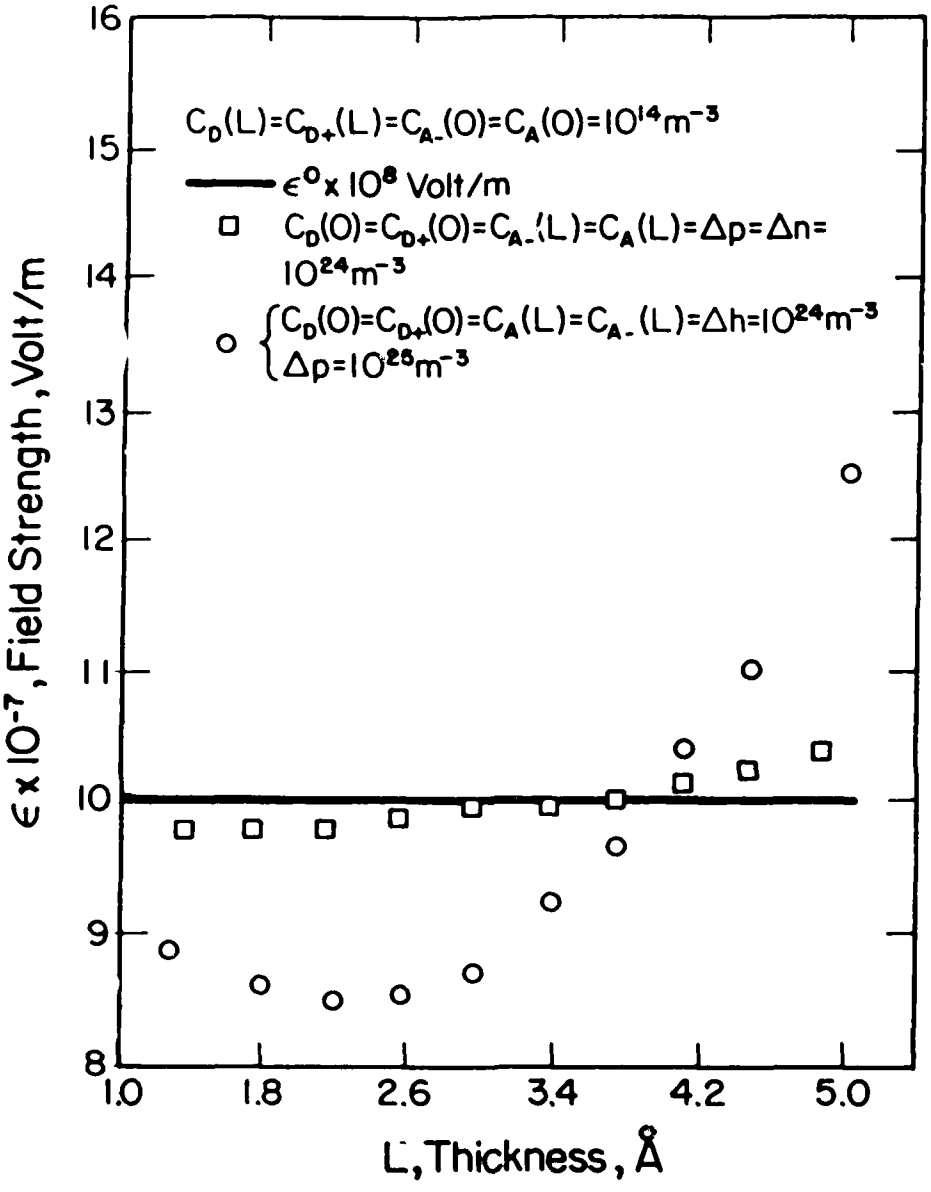

Figure 24. Calculated electric field strength vs film thickness. Note that the points designated □ obey the electro-neutrality condition.

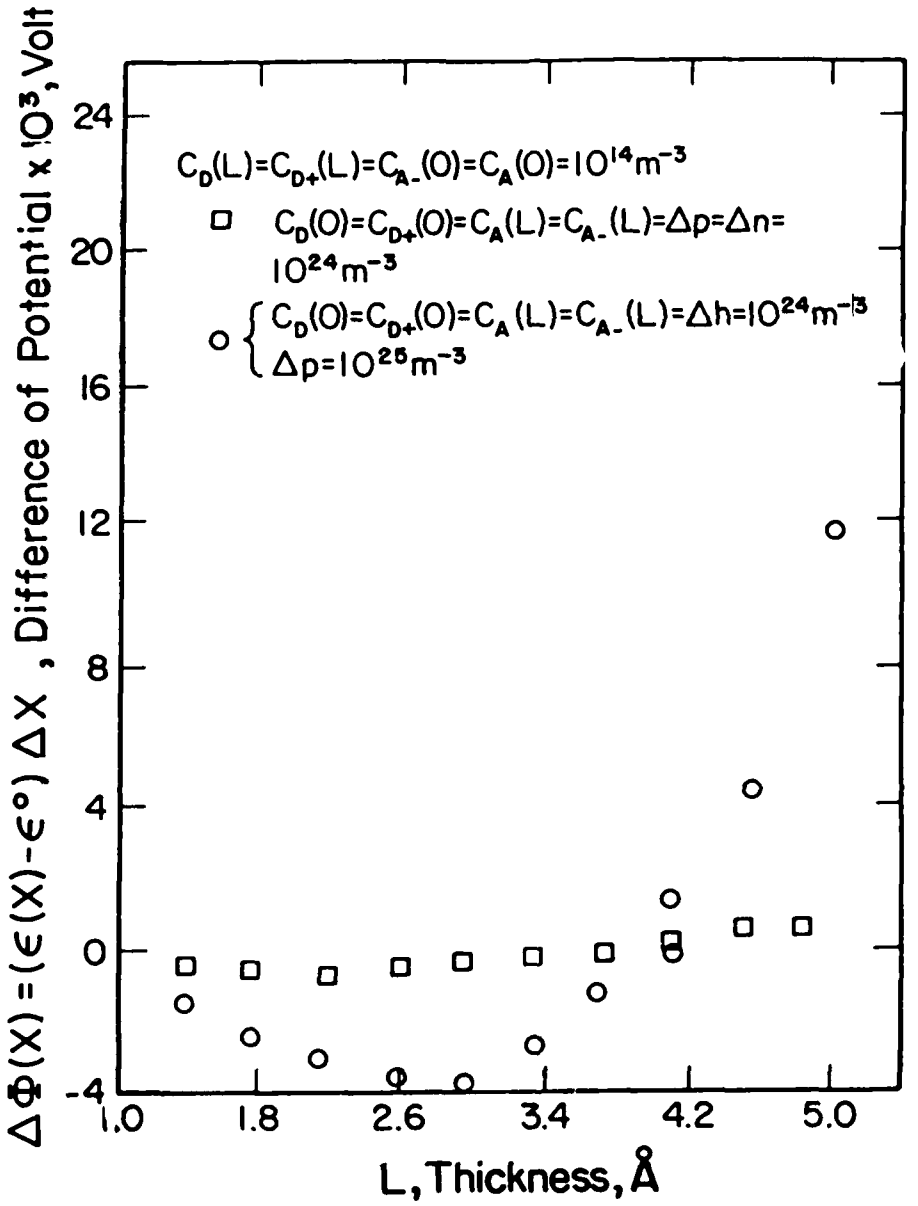

Figure 25. Potential function $\Delta\emptyset(x)$ vs film thickness. Note that the points designed □ obey the electro-neutrality condition.

Sensitivity Study

Because it is difficult to obtain information on the concentration of the different charged species within a growing oxide film and at the two interfaces, a sensitivity study was carried out to determine how the calculated space charge depends upon the concentrations of various species in the film. The various cases considered are as follows:

Anion- and Cation-Defect Film

In this case, the film is supposed to contain all six charged species ($V_{O}^{\cdot\cdot}$, $V_{O}^{\cdot}$, $V_{MX}^{\prime}$, $V_{M(X-1)}^{\prime\prime}$, $e^{\prime}$, $\dot{h}$) and the concentration of each species in turn at each boundary is varied over a wide range (Figures 26 to 29).

Anion-Defect Film

These films are considered to not contain cation or ionized cation defects. The sensitivity of the calculated space charge to variations in the concentrations of anion vacancies at the metal/film and film/solution interfaces was investigated (Figures 30 and 31).

Cation-Defect Film

In this case, the anodic film is considered to be free of anion vacancies, and the response of the space charge to variations in the concentrations of cation vacancies at the two interfaces was determined (Figures 32 and 33).

The electrical neutrality condition can be expressed by the following equation:

$$-2C_{D}(0) + 2C_{A}(L) - C_{D+}(0) + C_{A-}(L) - \Delta n + \Delta P \tilde{\gtrless} C$$

If the equality above is not observed, because one or more of the concentrations of vacancies becomes greater than the other, the strength field through the film does not remain constant or close to constant, but changes abruptly. Thus space charge becomes important when electrical neutrality of the film is not observed. These results are evidenced from Figures 26 to 33.

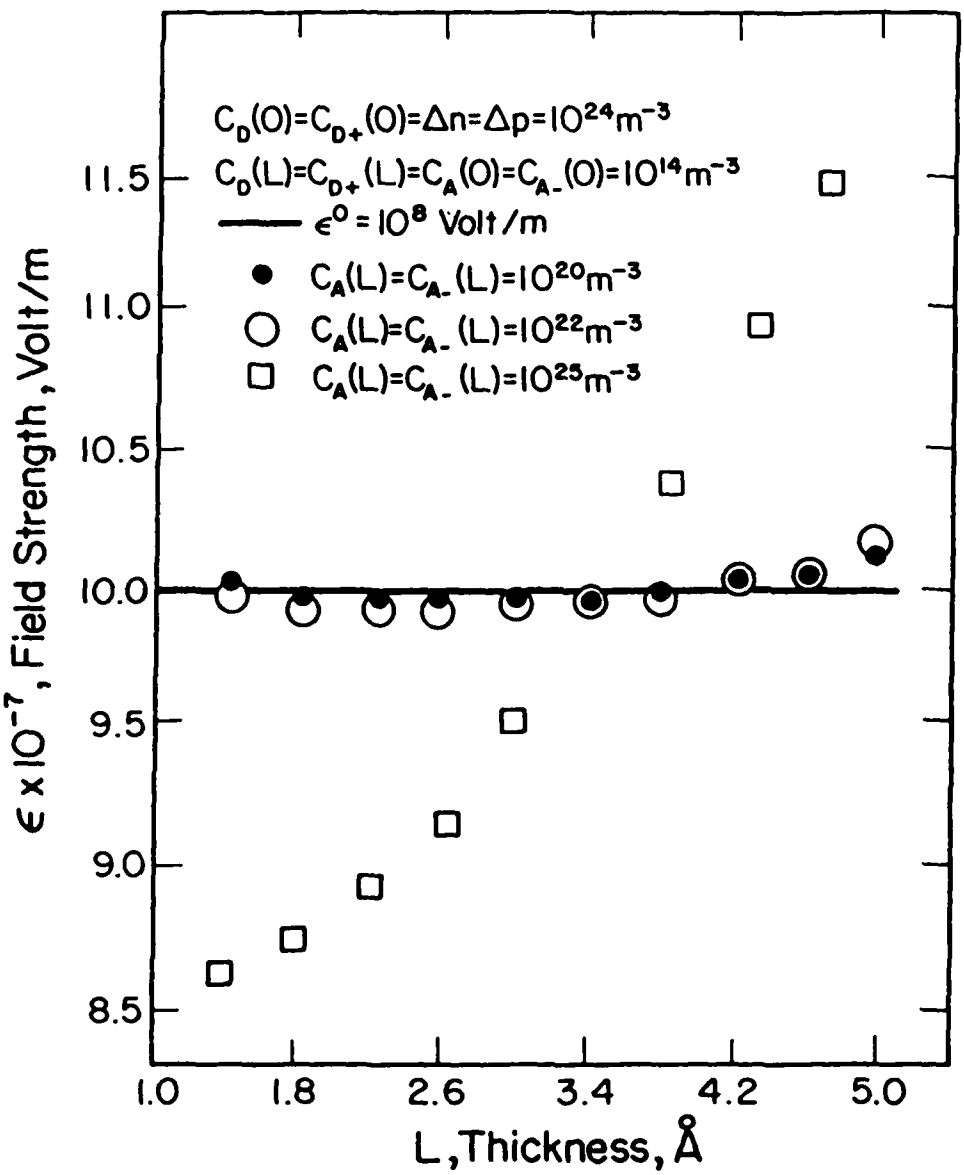

Figure 26. Calculated electric field strength versus film thickness. Increasing deviation from electrical neutrality (● < ◯ < □).

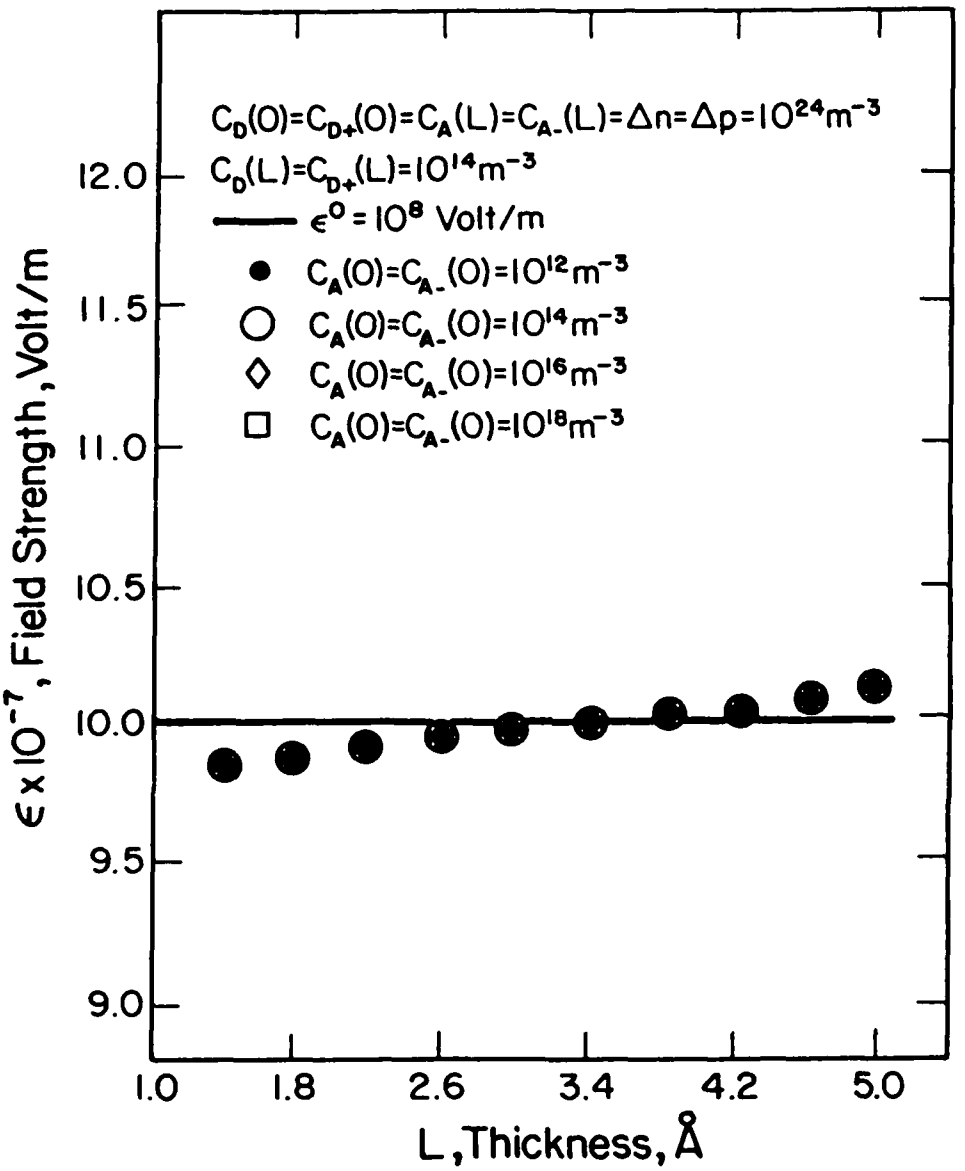

Figure 27. Calculated electric field strength versus film thickness. Note that in this case the anion and ionized-anion vacancy concentrations at the film/solution interface are varied. In all cases, the deviation from neutrality is negligibly small.

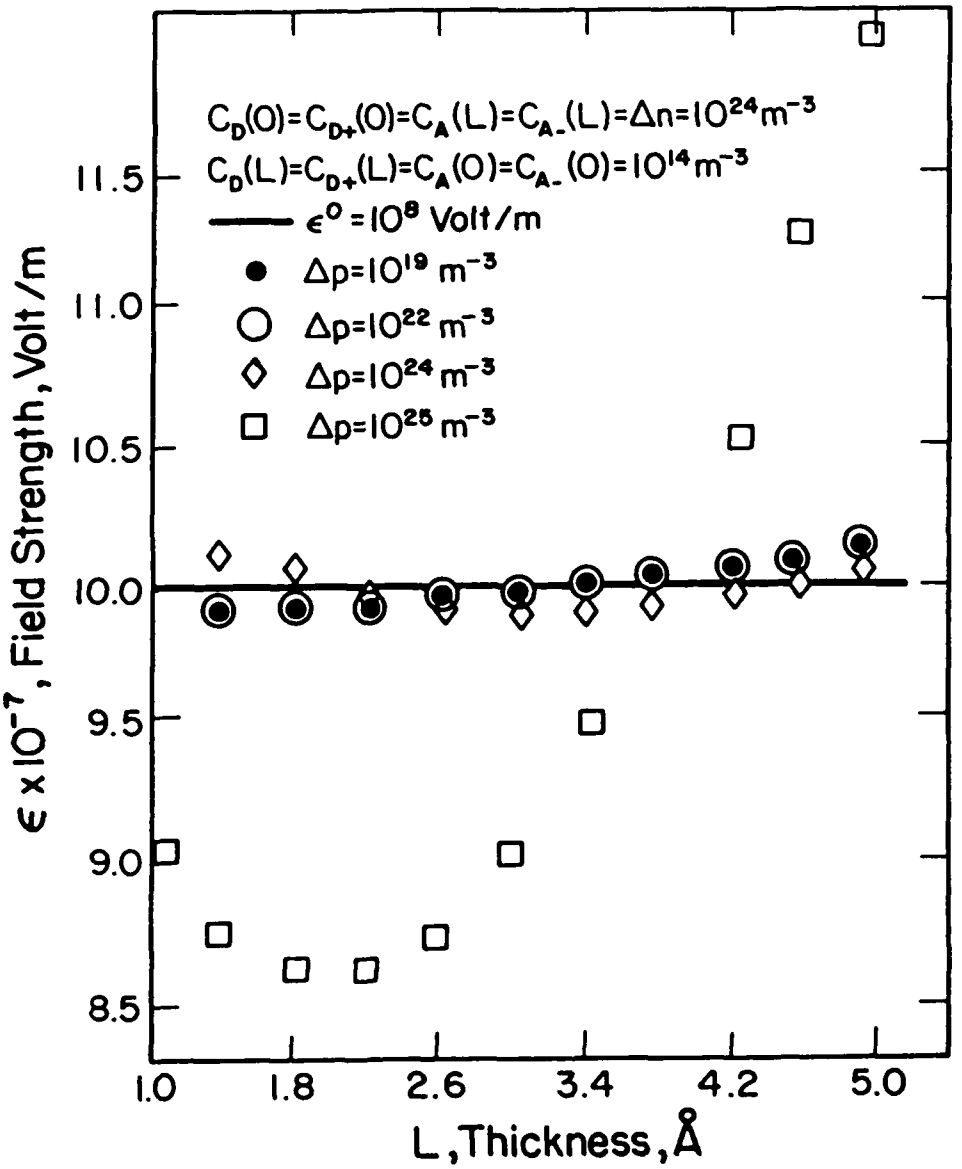

Figure 28. Calculated field strength versus thickness. Note that in this case, the concentration of positive holes Δp is varied.

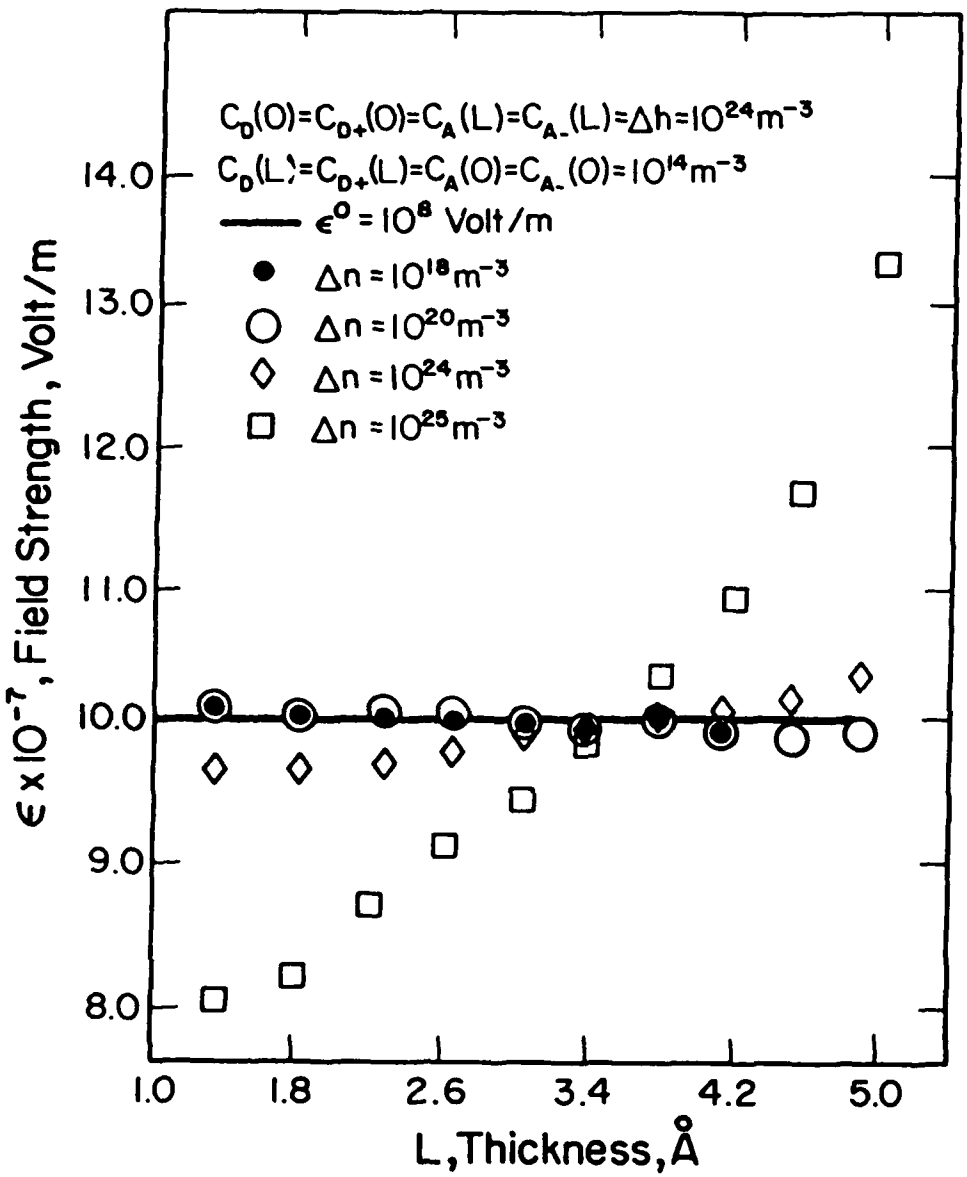

Figure 29. Calculated electric field strength versus film thickness. In this case the concentration of electrons, Δn, is varied.

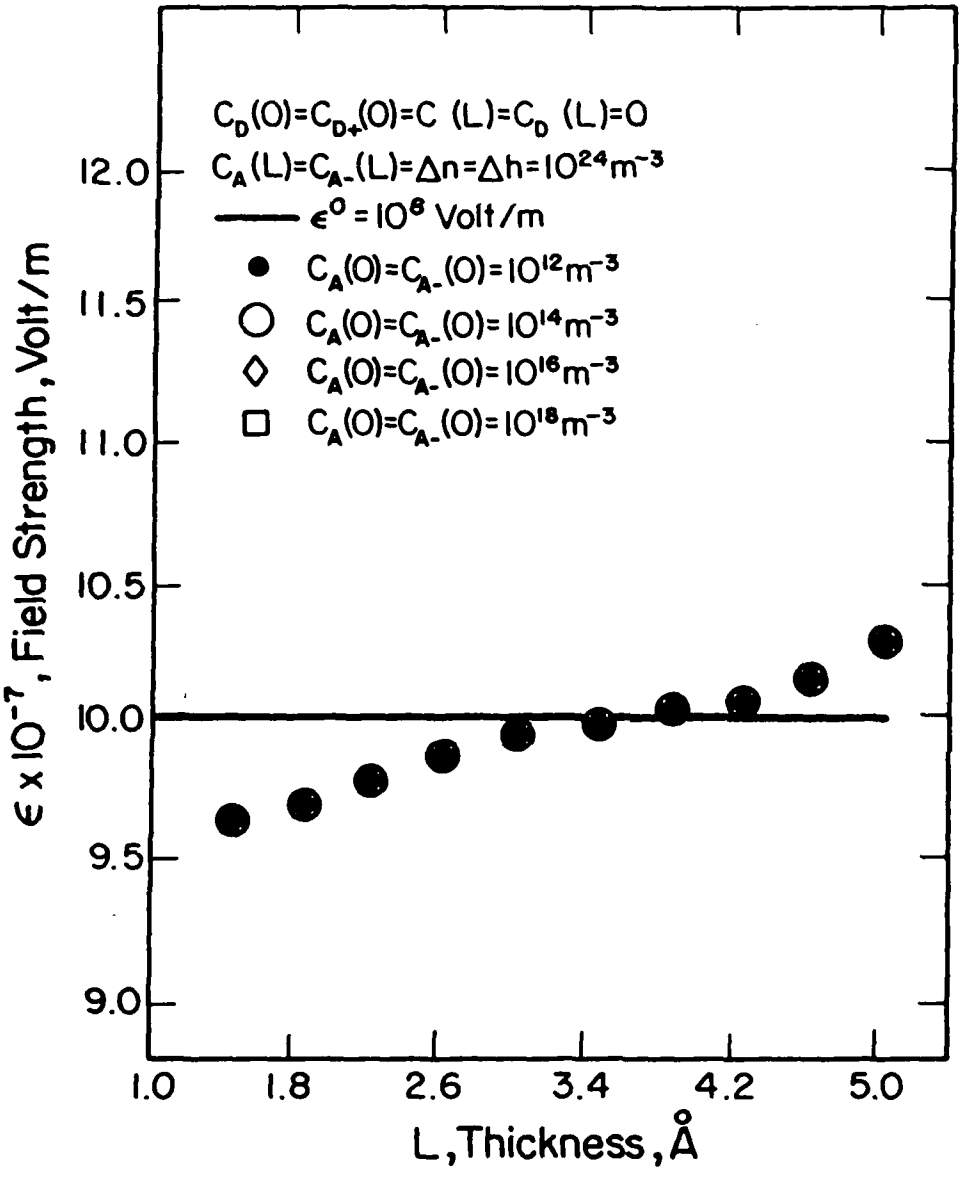

Figure 30. Calculated electric field strength versus film thickness. Note that in this case the anion and ionized-anion vacancy concentration at the film/solution interface are varied and the concentration of cation vacancy at interfaces is null. In all cases the deviation from electro-neutrality is small.

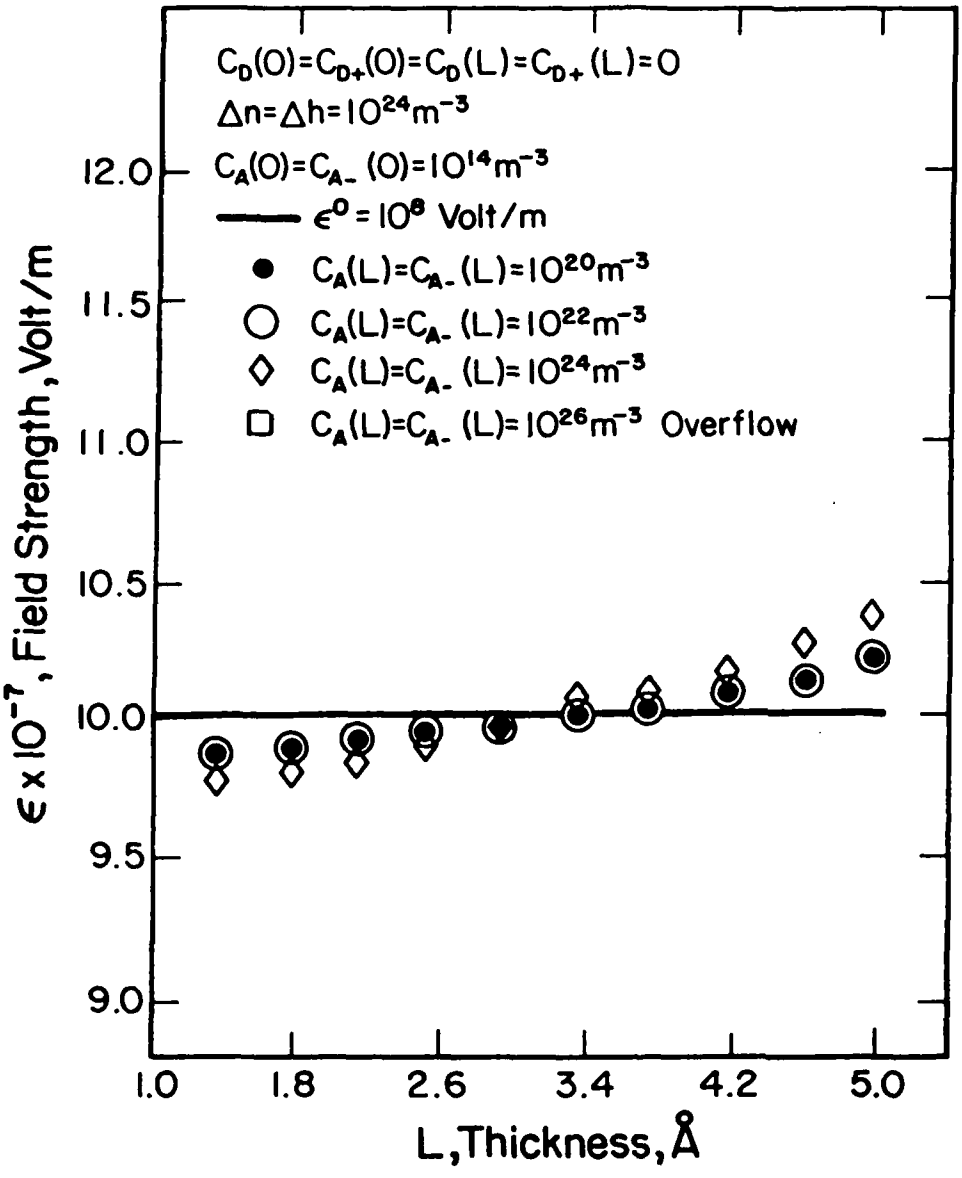

Figure 31. Calculated electric field strength versus film thickness. Note that in this case the anion and ionized-anion vacancy concentration at the metal/film interface is varied and the concentration of cation vacancy at interfaces is null. In all cases the deviation from electro-neutrality is small.

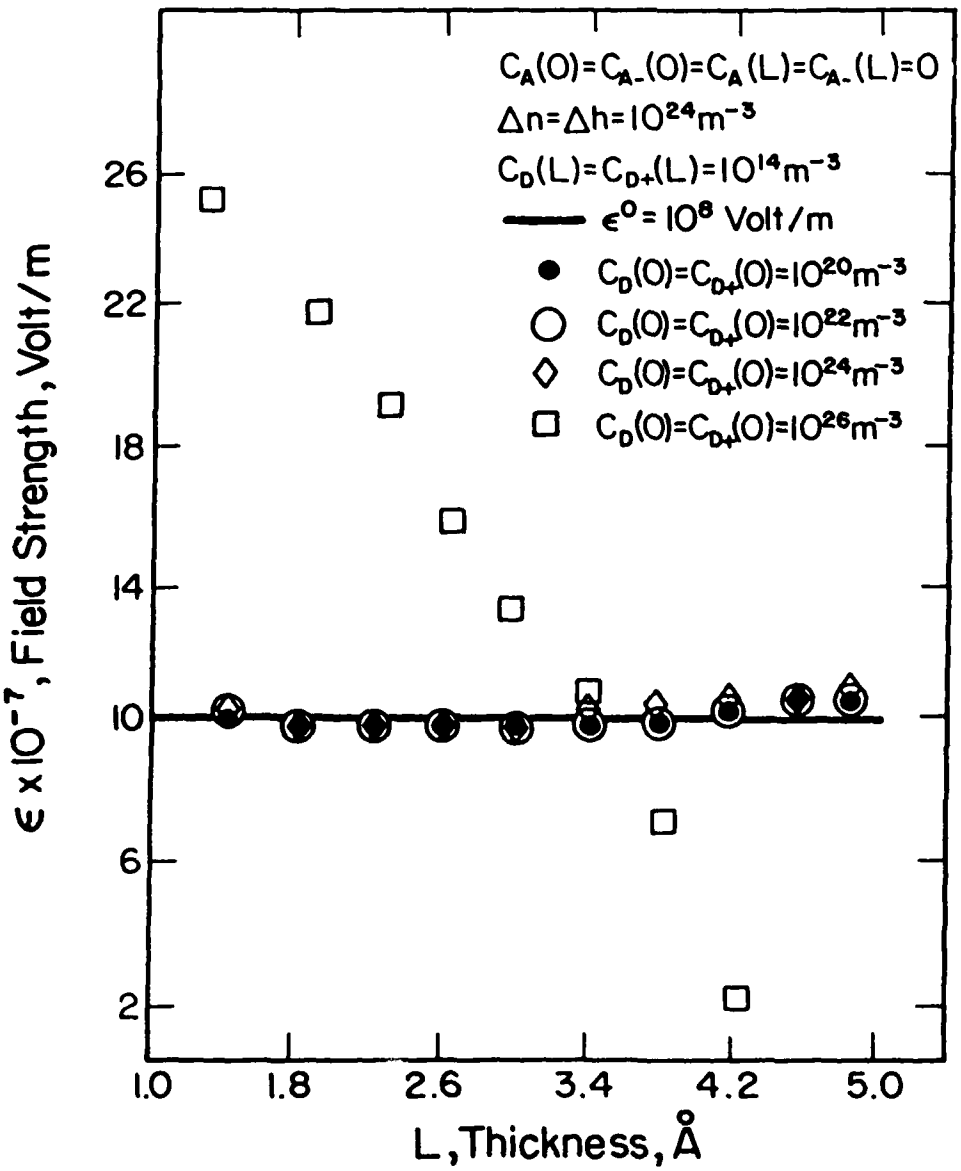

Figure 32. Calculated electric field strength versus film thickness. Note that in this case the cation and ionized-cation vacancies concentrations at the metal/film interface are varied; and the concentration of ion vacancy is null. In all cases the deviation from electro-neutrality is negligibly small.

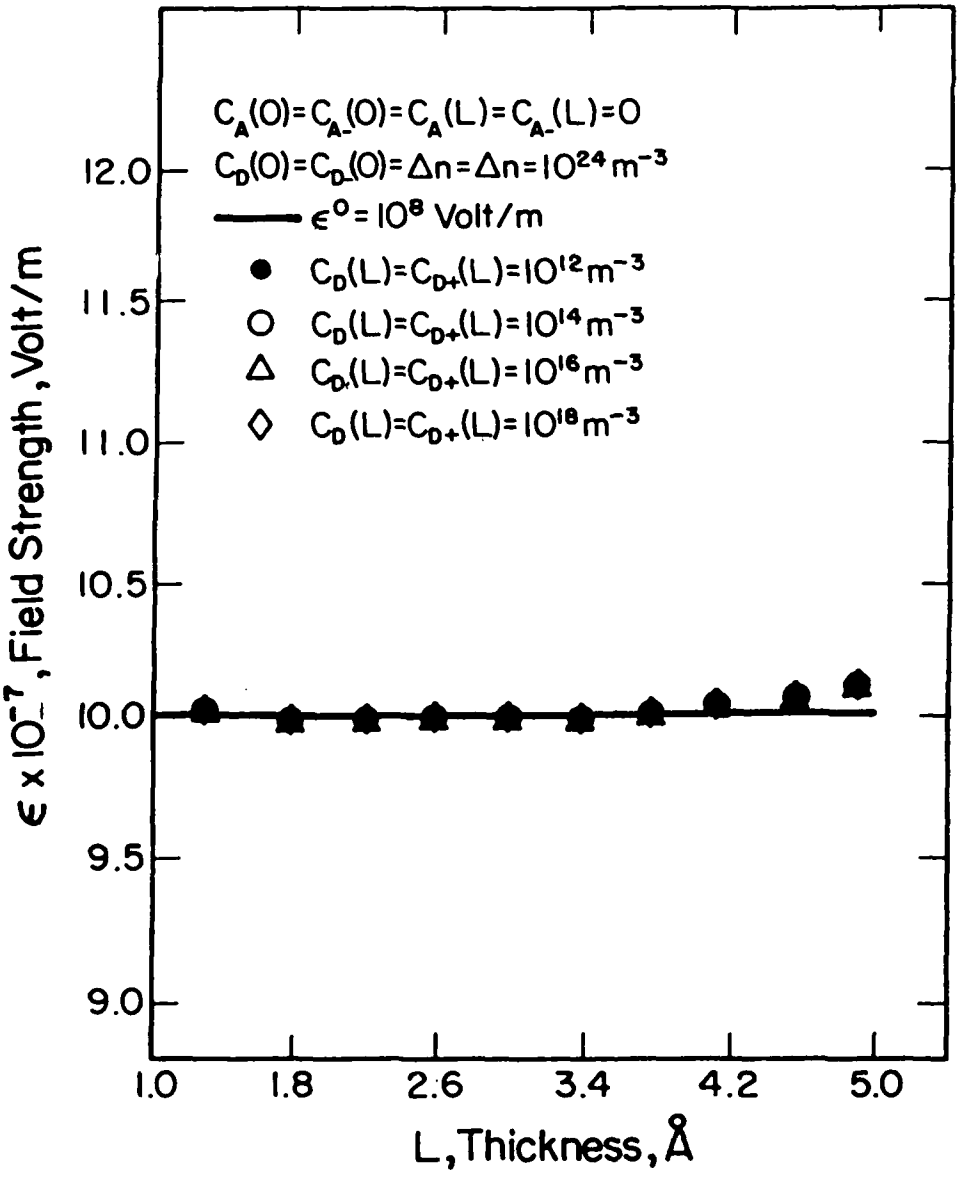

Figure 33. Calculated electric field strength versus film thickness. Note that in this case the cation and ionized-cation vacancies concentrations at the film/solution interfaces are varied; and the concentration of ion vacancy is null. In all cases the deviation from the electro-neutrality is negligibly small.

It is important to note that in this first order model no attempt has been to relate the concentrations of various species using equilibrium or equilibrium statistics. For example, a more realistic treatment would ire that the concentrations of electrons and holes within the conduction valence bands, respectively, be related to the concentrations of donors acceptors by the Fermi-Dirac distribution function, or at least by zman statistics for wide band-gap films.

ussion

The present work involves the calculation of space charge within an anodic n based on a model that involves six non-diffusing species. The culations assume a steady-state charge distribution within a film of stant thickness. Accordingly, a growing film is best viewed as a sequence steady-state steps in which the film thickness increases with time. The w presented here is that of one such step.

This model is different from that developed by Hamilton and Miley (4) for iting thickness growth, which is based on the assumption that space charge ses the bulk concentration of the rate limiting spaces to vary onentially with film thickness. In the present case, the defect centrations (donors and acceptors) vary according to Fick's second law and electrons and holes are assumed to be in e.ectrostatic equilibrium. The centrations of these latter species will vary exponentially with distance y if the potential, $\emptyset$, is a linear function of x. Clearly, this occurs y in the absence of space charge. Exact solutions for concentrations of rged acceptors and donors through the film have been obtained from Fick's ond law under steady-state conditions, and a numerical approximation hnique yields solutions for the dependence of the space charge on film ckness. The space charge is calculated subject to the constraint imposed the Poisson-Boltzman equation. However, the film as a whole must also be ctrically neutral, although to our knowledge this condition is seldom, if r, recognized in space charge computations. In this particular case, the ctroneutrality condition has been applied ex situ, although in later work will use this condition to fix the concentration of one of the charge riers at a boundary.

Sensitivity studies were carried out in order to determine how the ntial through the film can be affected by the boundary conditions assumed he model. For all the cases studied, the space charge through film was found to be important only when the electrical neutrality ition is not satisfied. However, electrical neutrality is a physical irement of anodic passive films. Accordingly, for steady state itions, it is apparent that space charge in the film is possibly not rtant, at least when six charged species are included, as in the model idered here. It is important to note that the boundary conditions (i.e. entrations of the various species at x=0 and x=L) were varied over emely wide ranges; ranges that should include the concentrations of the ies at the boundaries in real films. It is believed that these ulations help to clarify the controversy which exists about the importance pace charge in passive films (7). Unfortunately, comparable experimental do not at present exist, and the experimental difficulties involved in rately measuring the potential drop across a passive film have not been come. However, it might also be argued that the steady-state constraint o simplistic, and that the lack of space charge computed is in fact an fact of the model. In order to extend these calculations to include the species under nonsteady-state conditions it will be necessary to also ider the generation and consumption of charged species within the film as ıction of time and distance.

REAKDOWN OF PASSIVE FILMS

duction

he point defect model that was previously developed (1,2) provided a stic description of the breakdown of passive films in solutions ining aggressive anions (e.g. Cl^-) in terms of the accumalation of cation cies at the metal/film interface to form a void (cation vacacancy ısate) of sufficient size that mechanical collapse ensues to nucleate a The enhanced flux of cation vacancies across the film, which results in accumulation at the metal/film interface, is considered to be due to the key pair reaction and the adsorption of anions (e.g. Cl^-) from solution nion vacancies ($V_{O}^{\cdot\cdot}$) at the film/solution interface.

this analysis, the point defect model is expanded to account for the
of minor alloying elements, such as molybdenum, on the anodic breakdown
ive films on metal surfaces. This topic is important, since minor
ıg elements such as Mo and W are added to stainless steels to improve
esistance to pitting corrosion, particularly in chloride-containing
ments. For example, the addition of ∿2% Mo to Type 304 SS results in
16SS, which is frequently used for seawater service.

tical Basis

a previous study, Chao et al.(1,2) proposed a model for the growth and
wn of passive films which yields analytical expressions for the
al breakdown potential and the incubation time. The model involves (as
t approach) transport of anions (oxygen anions) and cations (metal ions)
ir respective vacancies. Furthermore, the model considers that anions
e from the film/solution (f/s) interface to the metal/film (m/f)
ace and subsequently result in film thickening at that location. On the
hand, cation diffusion, while not excluded, results only in dissolution
t in the growth of the primary passive film. This model has
sfully accounted for a number of previously unexplained experimental
ations (1). One consequence of the diffusion of metal cations from the
to the (f/s) interface is that metal vancancies (or "metal Holes") are
d at the metal/film interface. These metal "holes" will tend to
ge into the bulk at the metal due to the movement of cations from the
into the film, and hence to "disappear". However, when the cation
ion rate (i.e., the metal "hole" production rate) is higher than the
f "metal hole" submergence into the bulk, the metal holes will start
up, and hence will form a void at the metal/film interface (this is the
s of pit incubation). When the void grows to a certain critical size,
ssive film suffers local collapse which then marks the end of the pit
tion period. Subsequently, the collapsed site dissolves much faster
ny other place on the surface thereby leading to pit growth.

cording to this argument, the criterion for pit initiation can be
sed as follows:

AD-A154 685 THE DEVELOPMENT AND EVALUATION OF POINT DEFECT MODELS FOR THE GROWTH OF P.. (U) OHIO STATE UNIV COLUMBUS FONTANA CORROSION CENTER D D MACDONALD ET AL. 2/2

UNCLASSIFIED 30 APR 85 FCC-4445-4 N00014-82-K-0265 F/G 20/2 NL

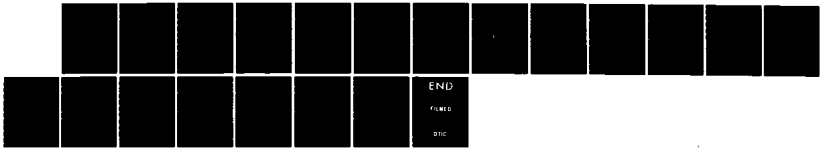

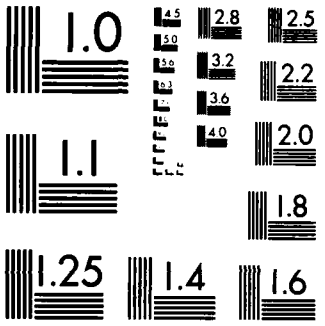

$$(J_{ca} - J_m)(t - \delta) > \xi \tag{36}$$

Where J_{ca} is the cation diffusion rate in the film, J_m is the rate of submergence of the metal hole into the bulk metal, t is the time required for metal holes to accumulate to a critical amount, ξ, (i.e., t is the incubation time) and δ is a constant.

From the first order point defect model developed earlier in this report, and considering that the electric field strength within the film is constant, Fick's first law for the quasi-steady state may be solved to yield the following expression for J_{ca} (see also Refs. 1 and 2):

$$J_{ca} = \chi k D_{V_{M^{\chi'}}} \frac{C_{V_{M^{\chi'}}}(m/f)\exp(-\chi kL) - C_{V_{M^{\chi'}}}(f/s)}{\exp(-\chi kL) - 1}$$

where χ is the charge on the cation, $k = F\epsilon/RT$, ϵ is the field strength through the film, F is Faraday's constant, R is the gas constant, T is temperature, L is the film thickness, $D_{V_{M^{\chi'}}}$ is the diffusivity of the cation vacancy, $C_{V_{M^{\chi'}}}(m/f)$ and $C_{V_{M^{\chi'}}}(f/s)$ are the concentrations of cation vacancies at the metal/film and film/solution interfaces, respectively.

As previously shown (1,2) it is possible to obtain an expression for J_{ca} as follows:

$$J_{ca} = J^{\circ}\mu^{-(\chi/2)} \exp\left(\frac{\chi F\alpha V_{app}}{2RT}\right)\left[a_{Cl^-}\right]^{(\chi/2)}$$

where

$$J^{\circ} = \chi k D_{V_{M^{\chi'}}} \left(\frac{n_v}{\Omega}\right)^{[1+(\chi/2)]} \cdot \exp(-\Delta G_s^{\circ}/RT)$$

$$\mu = \left(\frac{n_v}{\Omega}\right) \exp\left(\frac{\Delta G^\circ_{(A-1)} - F\beta \cdot pH - F\emptyset^\circ(f/s)}{RT}\right)$$

n_v = Avogadro's number

Ω = molecular volume of cations in the film

ΔG°_s = change in standard Gibbs energy for the Schottky-pair reaction

$\Delta G^\circ_{(A-1)}$ = change in the standard Gibbs energy for the reaction:

$$V_{O}^{\cdot\cdot} + Cl^-(aq.) \rightleftharpoons Cl_O^{\cdot}$$

$\emptyset^\circ(f/s)$ = potential drop across the film/solution interface in the absence of an applied voltage and for pH = 0

a_{Cl^-} = activity of chloride ions in solution

α, β = constants

V_{app} = applied potential

The critical pitting potential, V_c, is given by the Equation (36) which leads to

$$J_m = J^\circ \mu^{-(\chi/2)} \exp\left(\frac{F\alpha V_c}{2RT}\right)\left[a_{Cl^-}\right]^{(\chi/2)}$$

Therefore

$$V_c = \frac{4.606RT}{\chi F\alpha} \log \frac{J_m}{J^\circ \mu^{-(\chi/2)}} - \frac{2.303RT}{\alpha F} \log\left[a_{Cl^-}\right] \qquad (37)$$

and the incubation time, t_{ind}, is a function of breakdown overpotential. Mathematically, this can be expressed as

$$t_{ind} = \xi' \left[\exp\left(\frac{\chi F\alpha \Delta V}{2RT}\right) - 1\right]^{-1} + \tau$$

where

$$\xi' = \frac{\xi}{J^{\circ}_{\mu}{}^{-(\chi/2)}\left[a_{Cl^-}\right]^{(\chi/2)}\exp\left[\frac{\chi F\alpha V_c}{2RT}\right]}$$

These expressions have been shown to successfully represent the experimental data for the breakdown of passive films on iron in halide-containing solutions (2).

Solute/Vacancy Interaction Model

It is well known that minor alloying elements can have a profound effect on the susceptibility of a metal or alloy to localized corrosion, including pitting. In this section we propose a solute/vacancy interaction model (SVIM) to account for this phenomenon. The SVIM is develped from the point defect model which was originally proposed to account for the growth and breakdown of passive films.

The basis of the SVIM is that minor alloying elements, which exist in the passive film in a higher oxidation state than the host cation, can interact electrostatically with cation vacancies as described by the following equilibrium:

$$A^{m+} + qV_{M}{}^{\chi'} \underset{}{\overset{K_n}{\rightleftharpoons}} \left[A^{\bullet}\left(V_{M}{}^{\chi'}\right)_q\right]$$

where

$$K_n = \frac{\left[A^{\bullet}\left(V_{M}{}^{\chi'}\right)_q\right]}{\left[A^{m+}\right]\left[V_{M}{}^{\chi'}\right]^q} = \frac{[P]}{[A][V]^q}$$

The complex, P, and the solute, A, are both considered to be fixed in space, and only the cation vacancy, V, is assumed to move through the film from the film/solution interface to the metal/film interface.

Assume that, in the absence of A, the concentration of cation vacancies at positon, x, is n_v. The concentration at the point x after complex formation is given by $(n_v - q[P])$. The conditon for breakdown is still given by

$$(J_{ca} - J_m)_{x=L}(t - \delta) > \xi$$

in which the flux J_{ca} corresponds to that for the uncomplexed vacancies. When no complex formation takes place

$$J_{ca}\Big)_{x=L} = -D\left(\frac{\partial n_v}{\partial x}\right) + Dkn_v(-e\chi) \tag{38}$$

but when complexes exist, the flux the equation must be modified to read

$$J_{ca}\Big)_{L} = -D\,\frac{\partial(n_v - q[P])}{\partial x} + Dk(-e\chi)(n_v - q[P]) \tag{39}$$

where

$$[P] = K_n\left(n_A - [P]\right)\left(n_v - q[P]\right)^q \tag{40}$$

and where n_A is the stoichiometric concentration of solute in the film Equation (39) can be writen as follows

$$J_{ca}\Big)_{L} = -D^*\,\frac{\partial n_v}{\partial x} + D^*k^*(-e\chi)n_v$$

where D^* and k^* are modified to reflect the presence of [p]. These functions must be calculated for specific values of q, i.e., for various complex configurations. In this work, only q = 1, q = 2, and q = 3 are considered. For q = 1 two real roots exist such that

$$k^* = \frac{K\left[1 - \frac{\alpha}{2n_v} \pm \frac{1}{n_v}\left(\frac{\alpha^2}{4} - n_A n_v\right)^{1/2}\right]}{\frac{1}{2}\left[1 \pm \left(\frac{\alpha}{2} - n_A\right) / \left(\frac{\alpha^2}{4} - n_A n_v\right)^{1/2}\right]}$$

$$D^* = D\left[\frac{1}{2} \pm \frac{1}{2}\left(\frac{\alpha^2}{4} - n_A n_v\right)^{-1/2}\left(\frac{\alpha}{2} - n_A\right)\right]$$

where

$$\alpha = n_A + \frac{1}{K_n^{(1)}} + n_v$$

$$k^* = F\varepsilon^*/RT$$

The formulations for q = 2 and q = 3 are given in the appendix. Only the real roots that produce positive values for D* and k* are considered.

In order to quantify the effect of the solute on the pitting characteristics of an alloy, it is necessary to compute the changes in the breakdown potential and induction time as a function of solute (molybdenum) concentration. The appropriate functions are therefore given by:

$$V_c(X_{Mo}) - V_c(X_{Mo}=0) = \left(\frac{4.606RT}{\chi F\alpha}\right)\log\left(\frac{kD}{k^*D^*}\right) \tag{41}$$

$$\frac{t_{ind}\left(X_{Mo}\right)}{t_{ind}\left(X_{Mo}=0\right)} \frac{\left[\xi + \delta J^{\circ}\mu^{-(\chi/2)}[Cl^-]^{(\chi/2)} \exp\left(\frac{\chi F\alpha V_c}{2RT}\right)\right]J^{\circ}}{J^{\circ}\left[\xi + \delta J^{\circ}\mu^{-(\chi/2)}[Cl^-]^{(\chi/2)} \exp\left(\frac{\chi F\alpha V_c}{2RT}\right)\right]} \tag{42}$$

This last equation can be simplified by noting that for $\delta \longrightarrow 0$

$$\frac{t_{ind}(X_{Mo})}{t_{ind}(X_{Mo}=0)} \approx \frac{kD}{k^*D^*} \tag{43}$$

A computational algorithm was developed for an Apple IIe microcomputer in order to obtain the difference in breakdown potential (Equation 41) and the ratio of incubation time (Equation 42) for different concentrations of molybdenum when q was assigned values of 1 to 3.

Results and Discussion

In order to compute the effect of the solute on the pitting potential and induction time, it is necessary to specify values for the various parameters in Equations (41) and (42). The parameters of interest include n_v (concentration of vacancies), n_A (concentration of solute), and K_n (equilibrium constant). In these initial calculations, we have chosen q=1 and the parameters K_n and n_v are selected in order to obtain agreement in the first experimental point in the plot of V_c vs molybdenum content for 18% Cr ferritic steel given by Lizlov and Bond (24) (Figure 34). This graph displays the breakdown potential versus concentration of molybdenum for pitting of 18Cr-%Mo in 1 M NaCl at 25°C. Two sets of parameters resulted:

$$n_v = 4 \times 10^{20}/cm^3 \; ; \quad K_n = 10^{-4}$$

$$n_v = 4 \times 10^{19}/cm^3 \; ; \quad K_n = 10^{-17}$$

Using these values, it was possible to calculate the pitting potential (Fig. 34) and ratio of incubation times (Fig. 35) as a function of percent molybdenum in the alloy. The generally-good agreement between the calculated and experimental breakdown potentials at the higher molybdenum contents is most encouraging, even though the "best" values for q, n_v, and K_n are so poorly-defined.

A sensitivity study was carried out in order to assess the importance of each of the parameters in determining the breakdown potential and incubation time according to the SVIM. Figure 36 shows the importance that the value of K_n can have in determing the pitting potential as a function of molybdenum content, while Figure 37 displays the influence of the concentration of vacancies on the pitting potential and incubation time. The stoichiometry assumed for the complex also exerts a strong influence over the passivity

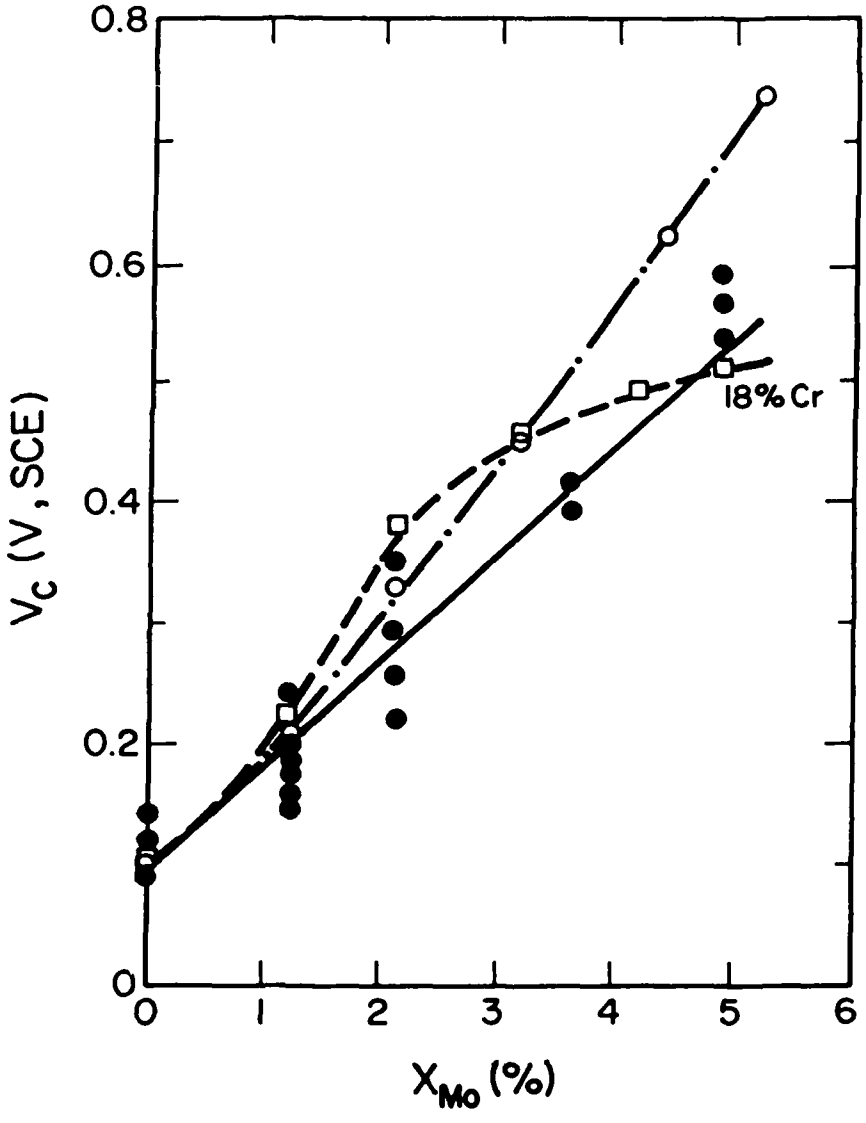

Figure 34. Pitting potentials versus % molybdenum in 18%-Cr ferritic stainless steel. (● experimental work in 1 M NaCl solution at 25°C (24). Theoretical results $q=1$; $n_v = 4\times10^{20}cm^{-3}$, $K_n=10^{-4}cm^3$ (○); $n_v=4\times10^{19}cm^{-3}$, $K_n=10^{-17}cm^3$ (□).

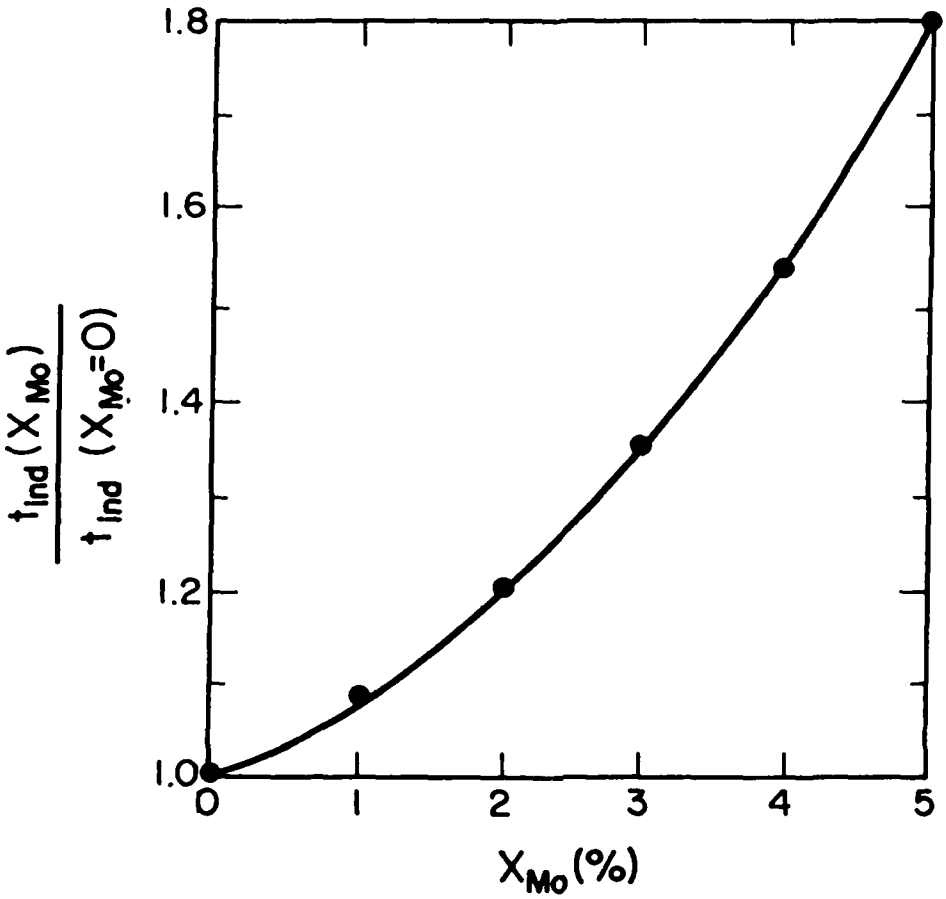

Figure 35. Effect of Molybdenum on induction time for pit-initiation according to the solute vacancy interaction model (SVIM). q=1, $n_v=4x10^{20}cm^{-3}$, $K_n=10^{-4}cm^3$).

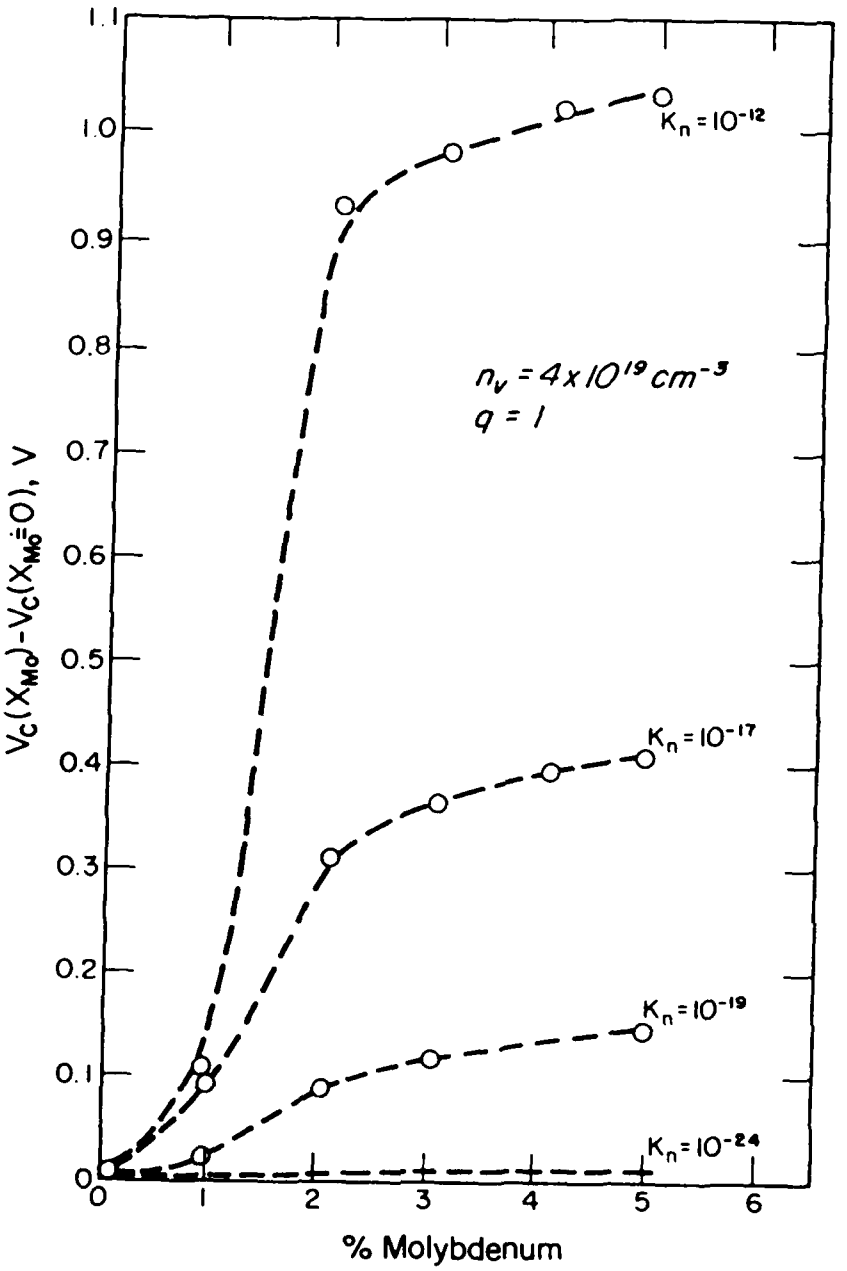

Figure 36. Influence of K_n on the pitting potential as a function of % molybdenum.

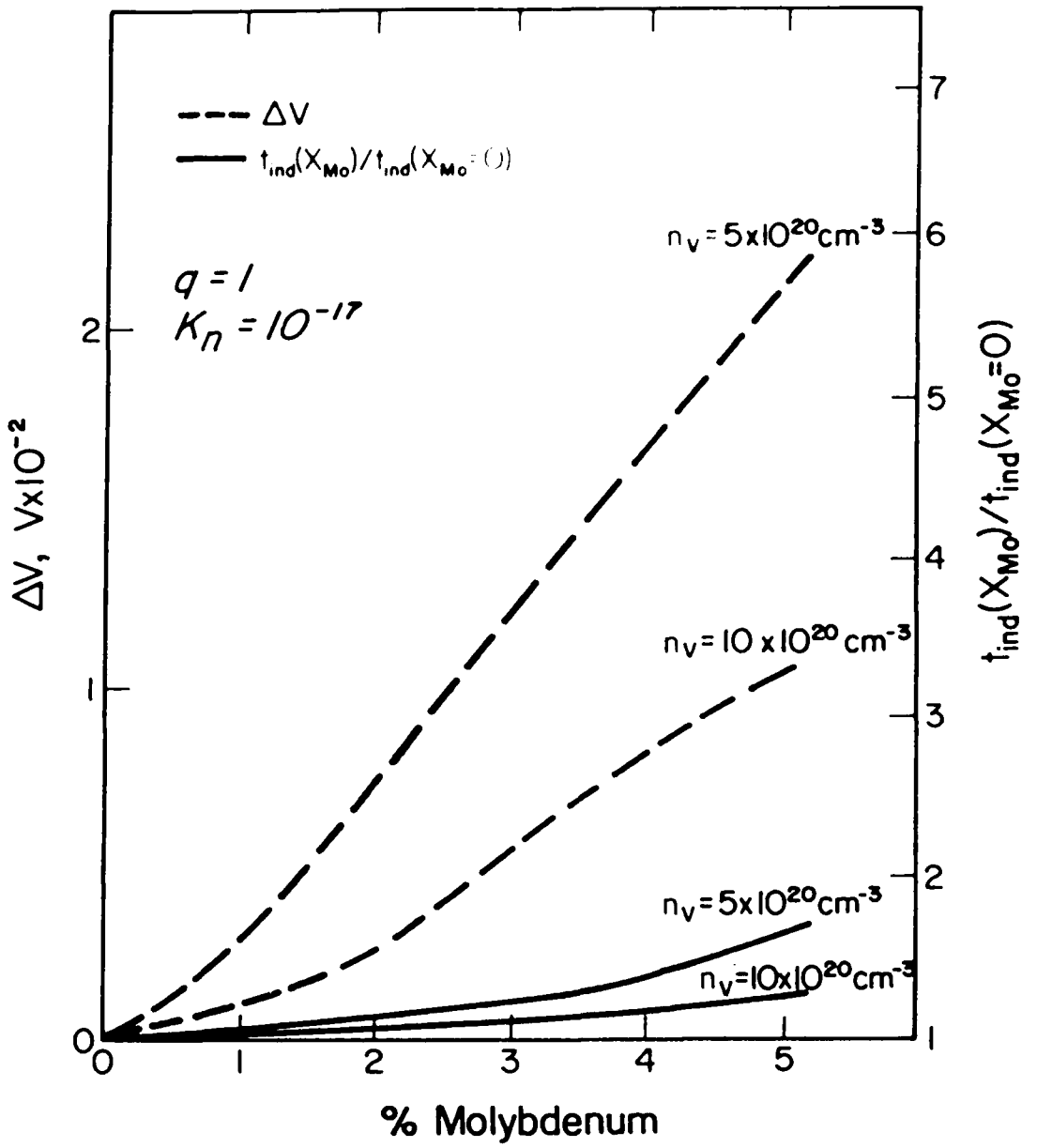

Figure 37. Influence of the concentration of cations vacancies on pitting potential and incubation times as a function of molybdenum content. $\Delta V = V_c(X_{Mo}) - V_c(X_{Mo}=0)$.

breakdown parameters, as shown by the data plotted in Figure 38. Clearly, in order to apply this model to the prediction of the effect of minor alloying elements on the pitting characteristics of steels, it will be necessary to generate more quantitative data. This task represents a major challenge in the future development of the model.

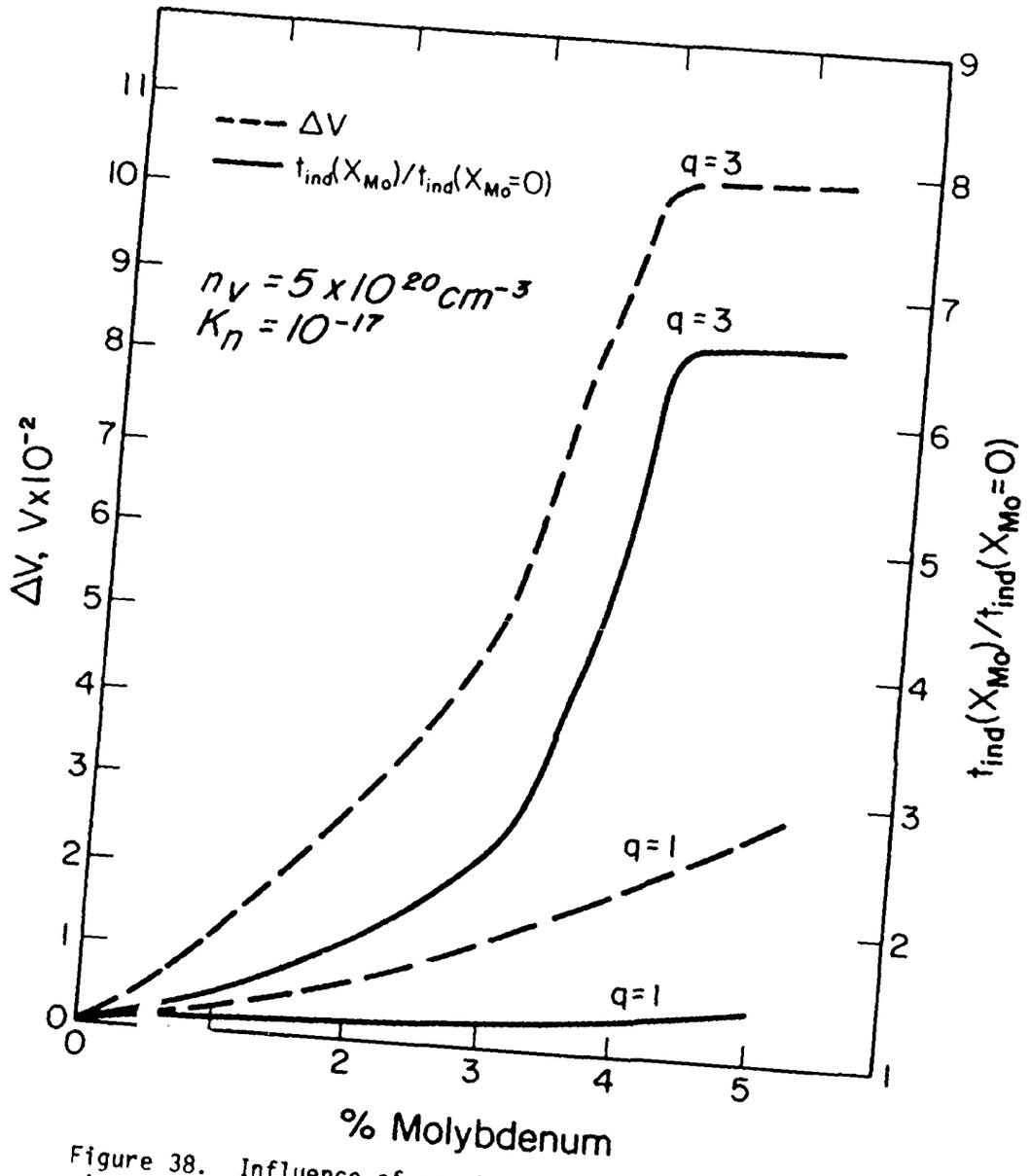

Figure 38. Influence of complex stoichiometry (q) on the pitting potential and incubation time as function of molybdenum content. $\Delta V = V_c(X_{Mo}) - V_c(X_{Mo}=0)$.

REFERENCES

1. C.Y. Chao, L.F. Lin, and D.D. Macdonald, J. Electrochem. Soc. 128 1187-1198 (1981).

2 L.F. Lin, C.Y. Chao, and D.D. Macdonald, J. Electrochem. Soc., 128, 1194 (1981).

3. C.Y. Chao, L.F. Lin, and D.D. Macdonald, J. Electrochem. Soc., 129, 1874 (1982).

4. R.Y. Liang, B.G. Pound, and D.D. Macdonald, "The Development and Evaluation of Point Defect Models for the Growth of Passive Films on Single Crystal, Polycrystalline, and Amorphous Metal Surfaces," Annual Report to the Office of Naval Research, (Feb., 1983).

5. M.J. Madou and M.C.H. McKubre, J. Electrochem. Soc., 130, 1056 (1983).

6. C.Y. Chao, Z. Szklarska-Smialowska, and D.D. Macdonald, J. Electroanal. Chem. 131, 279 (1982).

7. A.T. Fromhold, Jr., Theory of Metal Oxidation, Vol II - Space Charge, North Holland

8. J.F. Wolf, L-S. R. Yeh, and A. Damjanovic, Electrochim. Acta, 26, 811 (1981).

9. G. Fueillade and R. Jacoud, Electrochim. Acta, 14, 1297 (1969).

10. S.R. Morrison, Electrochemistry at Semiconductor and Oxidized Metal Electrodes, Plenum Press, New York (1980).

11. D.C. Silverman, Corosion, 37, 546 (1981).

12. M.C.H. McKubre and D.D. Macdonald, J. Energy, 5, 368 (1981).

13. Ru-Yu Liang, Kuan-Shaur Lei, B.G. Pound, D.D. Macdonald, Non-Technical Report to Office of Naval Research (September 1982).

14. B.G. Pound and D.D. Macdonald, Progress Report to ONR, FCC4445-3 (Sept. 1, 1983).

15. B. MacDougall, D.F. Mitchell, G.I. Sproule, and M.J. Graham, J. Electrochem. Soc. 130, 543 (1983).

16. H.P. Leckie, J. Electrochem. Soc. 117, 1152 (1970).

17. R.L. Horst and G.C. English, Materials Performance, 19, 13 (1980).

18. C.Y. Chao, S. Smialowska, and D.D. Macdonald, J. Electroanal. Soc. 131, 289 (1982).

19. M.C.H. McKubre and D.D. Macdonald, 15th Intersociety Energy Conversion Engineering Conference, 1207, Aug (1980).

20. O. Stasin and J. Teitous, Amm. Physics 1, 261 (1947).

21. A.B. Lidiard, Phil. Mag. 46 (379) 815 (1955); 46 (382), 1218 (1955).

22. Z. Szklarska-Smialowska and W. Kozlowski, Electrochemical and Ellipsometric Investigatons of Passive films formed on Iron in Borate Solutions, J. Electrochem. Soc., 234, February (1984).

23. Norio Sato and Tetsoyi Noda, Migration in Anodic Barrier Oxide Films on Iron in Acid Phosphate Solutions, Electrochimica Acta, 22, August (1975).

24. E.A. Lizlovs and A.P. Bond, J. Electrochem. Soc., 122, 720 (1975).

APPENDIX

CALCULATION OF BREAKDOWN PARAMETERS FOR q = 2 and 3

The general equation that needs to be solved for all values of q is (Eq 34)

$$J_{ca}\Big)_L = - \frac{D\,\partial[n_v - q(P)]}{\partial x} + D\,k(-e\chi)\left(n_v - q[P]\right)$$

where (Eq. 40)

$$[P] = K_n \left[n_A [P]\right] \left[n_v - q[P]\right]^q$$

P is a function of n_A, n_v, K_n and q. n_v, n_A and K_n are constants and q takes the values of 1 to 3. Equation 40 was previously solved for q = 1; here we present the solutions for q=2 and q=3.

q=2

From Equation 40 with q=2 a cubic equation in P is obtained as follows

$$P^3 + P^2\left(-n_A - n_v\right) + P\left(n_v + n_A + n_v^2/4 - (1/4K_n\right) - n_A n_v^2/4 = 0$$

The solutions for this case are then developed by first considering

$$A_1 = -n_A - n_v$$
$$A_2 = n_v n_a + (n_v^2)/4 - 1/(4K_n)$$
$$A_3 = -n_A\, n_v^2/4$$

$$Q = 3A_2 - A_1^2$$

$$R = \left(9A_1A_2 - 27A_3 - 2A_1^3 \right)/54$$

$$D = Q^3 + R^2$$

Thus, the roots are expressed as

$$P = S + T - A_1/3$$

where

$$S = \left(R + [Q^3+R^2]^{1/2} \right)^{1/3}$$

$$T = \left(R - [Q^3+R^2]^{1/2} \right)^{1/3}$$

if D<0 three real roots are obtained

$$P = 2\sqrt{-Q} \cdot \cos(\theta/3) - A_1/3$$

$$P = 2\sqrt{-Q} \cdot \cos(\theta/3+120) - A_1/3$$

$$P = 2\sqrt{-Q} \cdot \cos(\theta/3+240) - A_1/3$$

where $\theta = \text{arc} \cdot \cos(-R/(-Q^3)^{1/2})$

$$P = K_n (n_A-P) (n_v-3P)^3$$

<u>q-3</u>

For the case where q = 3, Equation 35 can be written as follows:

$$P^4+P^3 \left(-n_A-n_v\right) +P^2 \left(n_v^2/3+n_A \cdot n_v \right) +P \left(-n_A \cdot n_v^2/3-1/27K_n-n_v^3/27 \right) +n_v \cdot n_A/27=0$$

Defining

$$B_1 = n_A-n_v$$

$$B_2 = n_v^2/3 + n_An_v$$

$$B_3 = -n_A n_v^{\,2}/3 - 1/27\ K_n - n_v^{\,3}/27$$

$$B_4 = n_v^{\,3} n_A/27$$

and noting that the fourth order equation in P can be reduced to a third order expression by the following substitutions

$$A_1 = -B_2$$

$$A_2 = B_1 B_3 - 4B_4$$

$$A_3 = 4B_2 B_4 - B_3^{\,2} - B_1^{\,2} B_4$$

As for the previous case (q=2) it is possible to obtain a solution for P. Let

$$M = S + T = A_1/3$$

where

$$R = \left(B_1^{\,2}/4 - B_2 + M\right)^{1/2}$$

If $R \neq 0$

$$D = \left[3B_1^{\,2}/4 - R^2 - 2B_2 + \left(4B_1 B_2 - 8B_3 - B_1^{\,3}\right)/4R\right]^{1/2}$$

$$E = \left[3B_1^{\,2}/4 - R^2 - 2B_2 - \left(4B_1 B_2 - 8B_3 - B_1^{\,3}\right)/4R\right]^{1/2}$$

If R=0

$$D = \left[3B_1^{\,2}/4 - 2B_2 + 2\left(M^2 - 4B_4\right)^{1/2}\right]^{1/2}$$

$$E = \left[3B_1^{\,2}/4 - 2B_2 - 2\left(M^2 - 4B_4\right)^{1/2}\right]^{1/2}$$

Thus, the four roots are given by

$$P = -B_1/4 + R/2 + D/2$$

$$P = B_1/4 + R/2 - D/2$$

$$P = -B_1/4 - R/2 + E/2$$

$$P = -B_1/4 - R/2 - E/2$$

Once values are obtained for [P], for q=2 and q=3, it is possible to write

$$[P] = f(n_v)$$

but n_v is a function of the position, x. Accordingly,

$$\frac{\partial[P]}{\partial x} = \frac{\partial[P]}{\partial n_v} \cdot \frac{\partial n_v}{\partial x}$$

Let

$$PP = \frac{\partial[P]}{\partial n_v}$$

Therefore, we can write

$$\frac{\partial[P]}{\partial x} = PP \cdot \frac{\partial n_v}{\partial x}$$

where the expression PP is obtained from the solution for [P].

Fick's first law can then be written as follows

$$J_{ca}\Big)_L = - D \left[1 - PP\right] \cdot \frac{\partial n_v}{\partial x} + D\, k(-eX)(n_v - q[P])$$

where PP and [P] are known functions. Letting

$$D^* = D \cdot [1-PP]$$

and

$$k^* = k \cdot (1-q[P]/n_v) \quad /[1-PP]$$

we obtain

$$J_{ca} = - D^* \partial n_v/\partial x + D^*k^* (-eXn_v)$$

END

FILMED

7-85

DTIC